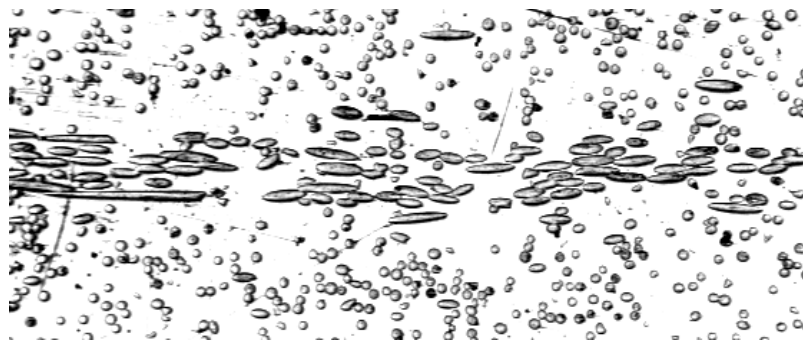


Residual stresses in short fibre reinforced injection moulded plates



J. H. D. Voerman

August 1996

WB - OK - 39

University of Twente
Department of Mechanical Engineering
Chair of Design in Plastics

Residual stresses in short fibre reinforced injection moulded plates

J. H. D. Voerman

August 1996

WB - OK - 39

Cover illustration: Cross section of a fibre reinforced injection moulded plate, transverse to flow direction.

UNIVERSITY OF TWENTE

Department of Mechanical Engineering

Chair of Design in Plastics

Examination committee	
Chairman:	prof. P. C. Powell
Mentor:	ir. M. P. I. M. Eijpe
	prof. dr. ir. J. Huetink
	dr. ir. R. Akkerman
	ir. H. G. Vlogman (DSM)

Research topic:	Residual stresses in short fibre reinforced injection moulded plates	
By:	J. H. D. Voerman	
	report nr. : OK - 39	date : August 14 th 1996

Summary

Residual stresses arise in a product during almost every manufacturing process. After manufacturing residual stresses remain in the product and can induce unexpected effects. When residual stresses are large they can influence product strength and shape (warpage) considerably. So an appropriate prediction of residual stresses could help to optimise product design.

For fibre reinforced injection mouldings very little is known about the residual stresses that remain after processing. In literature several effects that contribute to residual stresses are reported. Most important stress effects are thermally induced stresses at solidification, flow induced stresses and stress effects due to a change in material properties across the thickness. Because of the severe change in material properties across the thickness of a fibre reinforced injection moulded product, it is expected that the major part of the stresses are built up by the latter. In this report a model is introduced to predict these thermal residual stresses in plates of this type of products and verify them with experiment. The model is based on the Classical Laminate Theory.

For the prediction of the material properties models were used that have been introduced previously by several authors. The predictions of the material properties were compared with experiment. For the determination of the material stiffness a combination of layer removal and three point bending was used. This method was first verified with well defined laminate material. The prediction of the material properties appeared to be in good agreement with the practical results. It turned out that the material properties are dominated by the orientation of the fibres. Therefore the fibre orientation across the thickness must be known very well to make a good prediction of the material properties across the thickness. It is tried to predict this fibre orientation with a computer simulation, but the fibre orientation prediction appeared to be unreliable in comparison to the fibre orientation that was measured and could not be used.

With a modified layer removal method the residual stresses were measured in plates with a high fibre content. The resulting stress profile across thickness appeared to be in accordance with the theoretical prediction. Up to one third of the documented failure stress was measured in the material. This means that in this type of material residual stresses cannot easily be neglected with product design.

It is concluded that a good first approximation of residual stresses is given with the model that was introduced. This means that the change in fibre orientation is the main cause of residual stresses in the material. With the product shape and the right choice of the location for injection the resulting fibre orientation in the product can be influenced. Residual stresses can so be minimised or applied in such a way that material strength can even be improved and warpage minimised.

For future work the practical layer removal method has to be refined to get more accurate measurement results. The model to predict the stresses can then better be verified and refined.

Preface

As a final part of my study of Mechanical Engineering at the University of Twente I have done my graduation project of which this report is the result. Since September 1995 I have been trying to catch that invisible quantity: residual stress. The subject of this project follows on a series of projects carried out in the field of residual stresses in composite laminates. I have worked at a part of the puzzle in this field. With this report I hope that I have been able to contribute to the research for residual stresses at our Chair of Plastics Design.

I wish to thank everybody who has given me the time, advise and support to bring this project to the end, especially during the hard times. In particular I want to thank my mentor ir. Michiel Eijpe who provided me with the means and the good support to carry out this project. Finally I wish to thank the members of my examination committee for their contribution to my graduation.

Enschede, July 1996

Rik Voerman

Table of Contents

1. INTRODUCTION.....	2
1.1 RESIDUAL STRESSES.....	2
1.2 INJECTION MOULDING	2
1.3 SHORT FIBRE REINFORCEMENTS.....	3
1.4 PLATES.....	3
1.5 AIM OF THE PROJECT	3
2. RESIDUAL STRESSES	5
2.1 THE CAUSES OF RESIDUAL STRESSES IN INJECTION MOULDED PRODUCTS.....	5
2.1.1 <i>Thermally induced stresses at solidification</i>	5
2.1.2 <i>Flow induced stresses</i>	6
2.1.3 <i>Stress effects due to a change in material properties across the thickness</i>	7
2.1.4 <i>Microscopic stresses</i>	9
2.1.5 <i>Other stress effects</i>	9
2.2 THE CONSEQUENCES OF RESIDUAL STRESSES	9
2.3 STRESS RELAXATION.....	9
2.4 NARROWED AIM OF THE PROJECT	10
3. THEORETICAL MODELLING	11
3.1 MODELS TO CALCULATE THE MATERIAL PROPERTIES.....	12
3.1.1 <i>The model of Advani and Tucker in combination with the model of Halpin and Tsai</i>	12
3.1.2 <i>The modified Rule of Mixtures</i>	16
3.1.3 <i>Physical non-linearity</i>	17
3.1.4 <i>Concluding remarks</i>	18
3.2 THE CLASSICAL LAMINATE THEORY.....	18
3.2.1 <i>Stress-strain</i>	18
3.2.2 <i>Thermal residual stresses</i>	19
3.2.3 <i>Concluding remarks</i>	20
3.3 THE ENERGY APPROACH FOR NON-SYMMETRIC LAMINATES.....	20
3.3.1 <i>Geometrical non-linearity</i>	21
3.3.2 <i>Solving the energy equation</i>	21
3.4 THE LAYER REMOVAL METHOD.....	21
3.4.1 <i>Calculation of residual stresses using the Layer Removal results</i>	22
3.4.2 <i>Calculation of the moments for every layer</i>	23
3.4.3 <i>Fit of the moments as a function of thickness</i>	24
4. THE TEST MATERIAL	26
4.1 GEOMETRY OF THE PLATES	26
4.2 MATERIAL CHARACTERISATION	27
4.3 PROCESSING CONDITIONS OF THE PLATES.....	28
5. DETERMINATION OF THE MATERIAL PROPERTIES (RECOVERED).....	29
5.1 FIBRE ORIENTATION	29
5.1.1 <i>Cmold computer simulation model</i>	29
5.1.2 <i>Interpretation of the Cmold simulation</i>	29
5.1.3 <i>Experimental fibre orientation</i>	30
5.1.4 <i>Discussion of the fibre orientation results</i>	30
5.2 MATERIAL STIFFNESS.....	32
5.2.1 <i>Specimen preparation</i>	32
5.2.2 <i>Description of the tensile test</i>	33
5.2.3 <i>Description of the three point bending test</i>	33
5.2.4 <i>Calculation of the modulus in the several layers of the plate from the bending test</i>	34
5.2.5 <i>Validation of the three point bending method</i>	35
5.2.6 <i>Analysis of sensitivity for the used material constants</i>	36
5.2.7 <i>Discussion of the material stiffness results</i>	37
5.3 THERMAL EXPANSION	38

5.3.1	<i>Specimen preparation</i>	38
5.3.2	<i>Description of the experiment</i>	39
5.3.3	<i>Theoretical calculation</i>	39
5.3.4	<i>Discussion of the thermal expansion results</i>	40
5.4	STRESS FREE TEMPERATURE.....	42
5.4.1	<i>Description of the experiment</i>	42
5.4.2	<i>Discussion of the stress free temperature results</i>	43
6.	EXPERIMENTAL DETERMINATION OF RESIDUAL STRESSES.....	48
6.1	DESCRIPTION OF THE EXPERIMENT	48
6.1.1	<i>Specimen Preparation</i>	48
6.1.2	<i>Removal of a layer</i>	49
6.1.3	<i>Dimensions measurement</i>	50
6.1.4	<i>Curvature scanning</i>	50
6.1.5	<i>Curvature determination</i>	51
6.1.6	<i>Strain measurement</i>	53
6.1.7	<i>Calculation of the stresses from the moments</i>	53
6.2	VALIDATION OF THE MEASUREMENTS	55
6.2.1	<i>In-plane symmetry</i>	55
6.2.2	<i>Twisting curvature</i>	56
6.2.3	<i>Symmetry in thickness direction</i>	57
6.2.4	<i>Effects of the coating</i>	58
6.2.5	<i>Time and temperature effects</i>	58
6.3	DISCUSSION OF THE LAYER REMOVAL RESULTS	60
6.3.1	<i>Comparison of the curvatures from the different processing conditions</i>	60
6.3.2	<i>Experimental stresses</i>	62
6.3.3	<i>Theoretical stresses</i>	64
6.3.4	<i>Comparison of theory and experiment</i>	66
7.	CONCLUSIONS AND DISCUSSION.....	69
7.1	CONCLUSIONS	69
7.1.1	<i>Determination of the material properties</i>	69
7.1.2	<i>Experimental determination of residual stresses</i>	70
7.1.3	<i>Theoretical stress prediction</i>	70
7.2	PRACTICAL CONSIDERATION	70
7.3	RECOMMENDATIONS	71
	LITERATURE	73
	APPENDICES: Table of contents	

List of symbols

α_1, α_2	thermal expansion coefficient in main and transverse direction respectively
β	constant in the fibre length factor of the Cox model
γ	shear strain
ε^o	mid-plane strain
ε	strain
ϕ^o	angle between local main direction (direction of most of the fibres) and the global x-axis
$\eta(o)$	fibre orientation factor
$\eta(l)$	fibre length factor
κ	curvature
ν	Poisson's ratio
$\psi(p)$	probability distribution function
ρ	density
σ	normal stress
τ	shear stress
a	constant in the displacement field and in the compliance
a	orientation tensor of the Advani-Tucker model
[a]	part of the compliance matrix in the Classical Laminate Theory
A	cross sectional area
[A]	part of the matrix used in the Classical Laminate Theory
b	width, constant in the displacement field and in the compliance
[b]	part of the compliance matrix in the Classical Laminate Theory
[B]	part of the matrix used in the Classical Laminate Theory
B ₁ -B ₅	constants in the Advani-Tucker model
C ₁	fibre-fibre interaction coefficient
d	fibre diameter
[d]	part of the compliance matrix in the Classical Laminate Theory
D(t)	time dependant compliance
[D]	part of the matrix used in the Classical Laminate Theory
E	Young's modulus
F	loading force
G	shear modulus
K _{β_i}	correction function for fibre orientation measurements
f	Hermans factor
ℓ	fibre length
l _{ec}	critical fibre length
L	support span
M	moment
p	number of layers
p	unit vector
r	radius
t	time
T	temperature
T	material property tensor

T_c	crystallisation temperature
T_g	glass transition temperature
T_m	melt temperature
u	displacement in x direction
v	displacement in y direction
V_f	fibre volume fraction
w	displacement in z direction
W	energy
W_f	fibre weight fraction
Q_{ij}, Q_{ijkl}	the elements of the stiffness matrix and tensor respectively
x, y, z	co-ordinates

subscripts:

1, 2, 3	main (fibre) and transverse direction, or the element number of a vector
x, y, z	global flow direction and transverse to global flow direction
f	concerning the fibres
m	concerning the matrix
n	concerning layer number n

notations:

$[]$	a matrix
$\langle \rangle$	orientation average according to Advani-Tucker
*	rotated matrix from main fibre to flow direction
bold	a tensor or vector

1. Introduction

Up to now very little is known about residual stresses in short fibre reinforced injection moulded products. It is known that material can fail unexpectedly and therefore in designing the dimensions of a product safety factors are used. This ensures that the product will not fail, but material and weight could have been saved if more was known about the material behaviour. From previous work it was concluded that residual stresses can be large for fibre reinforced materials. Therefore it is expected that this is also the case for injection moulded fibre reinforced products. This report deals with the prediction and measurement of residual stresses in fibre reinforced injection mouldings.

In this chapter the terms residual stresses, injection moulding and short fibre material will be explained first. Then the goal of this report is discussed.

1.1 Residual stresses

When a product is loaded with a force a stress is induced in the product. Generally it is assumed that this stress becomes zero when no external load is applied. For many products this is not true. During manufacturing the material is deformed plastically, heated, etc. and all these modifications lead to a change in the stress state of the material. It can mean that stresses reside in the product also when the loading deformations are removed again. These stresses are called residual stresses. Residual stresses can be very large. They can even become larger than the material strength so that the material fails without any externally applied load (e.g. cracks).

1.2 Injection moulding

Injection moulding is a production technique that is frequently used for processing of plastics. At the beginning of a cycle the material is heated up above its melting point, generally between 150 and 350 °C. This heating is combined with high pressures and shear flow. When enough material is ready to fill a cavity (mould) with the required product shape, the material is injected into the mould with high pressures and high flow rates. The material is then cooled in the mould until the shape of the product becomes stable. During this cooling the material shrinks and therefore a second pressure is used during the so-called packing stage to fill the mould with extra material. This second pressure is generally very high (in the order of 10^8 Pa). When the product has cooled enough the mould is opened so that the product can be ejected. The process is now repeated. Figure 1-1 shows the injection moulding set-up schematically.

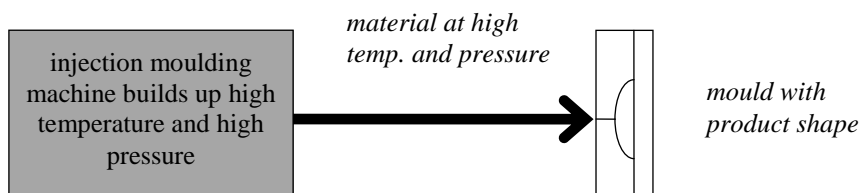


Figure 1-1: Schematical injection moulding set-up.

In this report the flat plate that is obtained in the mould is considered in more detail. It will become clear that flow effects, temperature history and pressure history are important factors when material properties of the product are considered.

1.3 Short fibre reinforcements

Fibres are thin 'hair-like' fibrils generally made of glass, carbon, kevlar etc. The mechanical stiffness of these fibres is found to be larger than the stiffness of most plastics. Combination of both the plastic and the fibres can improve the material properties of the plastic considerably. In a lot of products these material improvements are welcome. They can result in stiffer, lighter or stronger products.

In most production techniques long fibres are used (from 10 mm up to 'continuous'), but during the injection moulding process the material must be able to flow. Therefore fibres have to be short with injection moulding, typically 0.2 mm.

1.4 Plates

In this report only flat plates are considered. Flat plates have a simple geometry which means that modelling and measurements can be performed without geometrical complications. Another reason is that flat plates can be made with different processing techniques and therefore a better comparison can be made with results of other products.

1.5 Aim of the project

The aim of the project in the broadest sense is:

Model and measure the residual stresses in short fibre reinforced injection moulded plates.

To achieve this, the project can be divided into the following questions of investigation:

1. What is known about residual stresses in injection moulded products and what stress effect is expected to be dominant in fibre reinforced ones? In chapter two a survey is discussed about the different effects that cause residual stresses. This results in a narrower description of the projects aim.
2. How can the material properties be modelled? For the modelling and measurement of residual stresses some material properties have to be known. Documented models to predict these properties are discussed in chapter three.
3. How can the stress in a plate be modelled? In the second half of chapter three it is tried to describe the stress-strain state of a plate when the stress build-up mechanism and the material properties are known.
4. Are the models for material characterisation (i.e. the parameters in the stress predictions) accurate? With several experiments the predicted material properties are verified in chapter five.
5. Is the stress prediction in accordance with the theoretical predictions? In chapter six the experiment is discussed to determine the residual stresses in a plate. The results of the experiments are compared to the theoretical predictions.

2. Residual stresses

In this chapter it is tried to get insight in the existence of residual stresses for injection moulded products. The central question will be: What is known about residual stresses in injection moulded products and what stress effect is expected to be dominant in fibre reinforced products? A survey will be given about different effects that have been reported in literature and it will be concluded with a narrowed focus of this report.

2.1 The causes of residual stresses in injection moulded products

Residual stresses are caused by a lot of different effects. In injection moulded products the most important effects can be divided in three categories. During high flow speeds stresses are induced due to flow effects. Inhomogeneous cooling results in stresses due to shrinkage effects. A change in material orientation across the thickness induces stresses during cooling after the material has frozen in. These three effects are explained in more detail in the following subsections.

2.1.1 Thermally induced stresses at solidification

Stresses are thermally induced when a product is cooled inhomogeneously and the material solidifies in the meantime. At high cooling rates of the product, the product contains a temperature gradient, so that differences in density are present. Figure 2-1 shows a schematic cross section of a squared product during solidification.

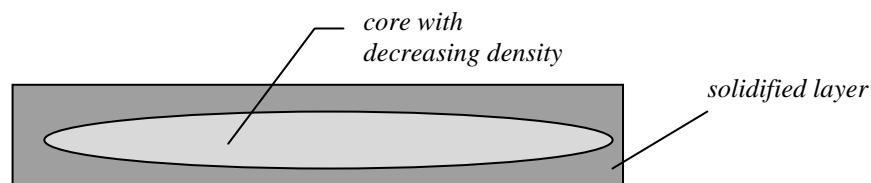


Figure 2-1: Schematic cross section of a plate during solidification.

First the surface of the product is cooled and the core shrinks later, when no material can flow into the mould anymore. This results in a parabolic stress profile, being compressive in the surface and tensile in the core (often observed as 'sink marks'). The pressures that occur during cooling are also frozen in. They have an opposite influence on the stresses in the skin layer, so that the stress in the skin layer can become positive again. A typical thermally induced stress profile is given in Figure 2-2.

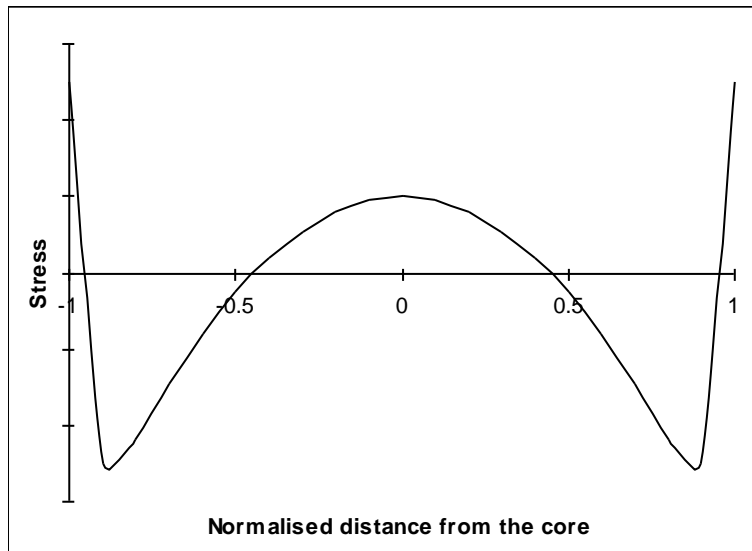


Figure 2-2: Typical thermally induced stress profile.

During the process of changing pressure and temperature little flow occurs. This flow induces some extra molecular orientation, but this effect is of minor importance. Thermally induced stresses are dependent on the cooling rate.

2.1.2 Flow induced stresses

Generally a product is injection moulded in a short time, in the order of one second. During this process the material is subject to high pressures and high deformation rates with respect to the relaxation time of the material. This means that there is not enough time to let the stresses relax. The stresses that arise can be divided in:

- elongational stresses in the flow front (fountain region) and near changes in the flow path width
- shear stresses at some distance behind the flow front and during the packing stage when back-flow occurs
- first and second normal stress differences due to visco-elastic behaviour of the melt

All these stresses generally freeze in very soon because of the high cooling speed of the product. They remain partially in the product when the material temperature drops below the glass transition temperature T_g (when considering amorphous material). Stress relaxation is very slow below this temperature.

Polymer material consists of large molecular chains which are straightened by loads during flow (molecular orientation). This molecular orientation induce the so-called entropy elastic stresses. According to statistic theory the stretched molecule chains want to form a 'random coil'. In this contracted state the molecules have maximal entropy. When molecule chains are stretched the entropy is lowered and so the chains are not in their preferential conformation anymore. The oriented molecule chains will always try to return to the random state during their rapid thermal vibrations. This results in a certain stress.

When the material contains fibres, also the fibres will orient in a similar way (fibre orientation) causing material anisotropy. This induces another important stress effect that will be discussed in subsection 2.1.3.

Here it is explained how orientation is induced according to the flow model that is generally used for injection moulding. The material orientation concerns the molecules as well as the fibres.

At the skin of the product a layer is formed in which the so-called fountain flow has induced a certain material orientation. This orientation is usually random or slightly oriented in flow direction.

Between the core and skin layers a frozen layer is created during injection. At the flow side of this layer the mentioned shear stresses are predominant. These shear stresses cause alignment of the material in the flow direction to a high extend. During injection the frozen layer grows in thickness so that the thickness of this layer is related to the duration of the injection.

The third layer that can be discerned is the core region. A schematic example of the regions is shown in Figure 2-3.

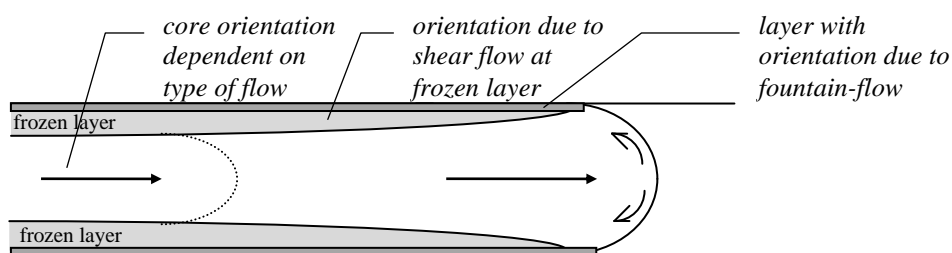


Figure 2-3: Surface layer, frozen (shear) layer and core layer with different material orientations due to flow effects.

In the core the orientation is mainly dependant on the type of flow [25]. When the flow is divergent the fibres will align transverse to the flow direction. When the flow is convergent or elongational the fibres will align in flow direction. From this it can be deduced that a pin-point injection always has fibres transverse to the flow in the core [25]. A film-gate is generally designed for a flat flow front. When the die has been designed badly, flow will not become parallel, but slightly divergent or convergent. This has a considerable influence on the fibre orientation in the core. So for parallel flow the fibre orientation is very dependent on geometry.

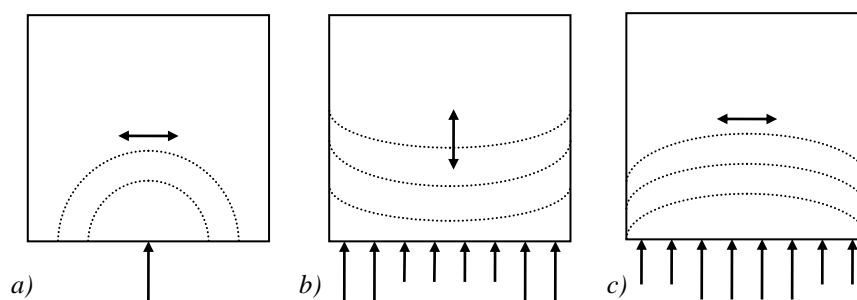


Figure 2-4: Fibre orientation in the core region of squared plates schematically: a) for radial flow, b) for badly designed film gate (convergent) and c) for badly designed film gate (divergent). The melt front advancement is indicated with the dashed lines; the doubled arrows indicate the main direction of the fibre orientation.

2.1.3 Stress effects due to a change in material properties across the thickness

The previous subsection showed that in injection mouldings the material orientation is depth dependant, because the different flow effects induce a changing material orientation

across the thickness. Therefore the product has a considerable change in thermal expansion across the thickness and so a stress is induced during cooling (in this report these stresses are called thermal residual stresses). This effect is illustrated in Figure 2-5. In first approximation an injection moulded plate can be considered as a four layer cross ply symmetric laminate. In fibre direction of the outer layers the thermal expansion in the outer layers is much smaller than in the core layers. So the outer layers would shrink less during cooling when slip existed between the layers. But because the layers are connected to each other, slip is prevented and the shrinkage of each layer is equal. This effect induces residual stresses in the laminate.

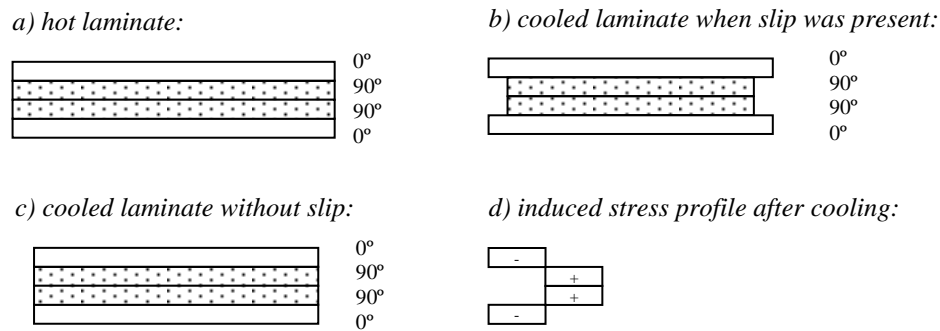


Figure 2-5: Stresses in a $(0/90)_s$ laminate due to different material properties in each layer. Different layers tend to shrink with a different amount (b), but they prevent each other because no slip is present between the layers (c). This induces a stress profile (d).

When the laminate would be non-symmetric, the stress profile would induce an internal bending moment in the laminate resulting in a curved shape. The amount of stresses is also dependent on the modulus of elasticity in the different layers over the thickness. In contrast with the other stress effects this type of stresses is independent on the cooling trajectory as long as stress relaxation is negligible. Eijpe [11, 12] showed that these stresses are predominant in compression moulded composites with continuous fibres. Also other authors calculated residual stresses only on the basis of this phenomena and neglected the previously discussed stress effects.

The thermal residual stress is built up from a certain temperature, below which the material does not flow anymore. This is called the *stress free temperature*, because often the other stresses are neglected or are assumed to compensate temperature dependant effects.

The stress free temperature is roughly assumed to be the crystallisation temperature T_c for semi-crystalline materials [21] and the glass transition temperature T_g for amorphous materials.

The different material properties are caused by two orientation effects:

1. molecular orientation: In orientation direction the molecule chains behave different than in transverse direction. This leads to a higher stiffness, a higher thermal conductivity and a lower thermal expansion in orientation direction.
2. fibre orientation: Generally the fibres possess material properties that are considerably different from the matrix, and so the material becomes highly an-isotropic because of fibre orientation.

Generally the fibre orientation is mainly responsible for the anisotropy (Hindle, [15]) and in first instance molecular orientation can be neglected in fibre reinforced materials.

The fibre orientation across the thickness can be described with several models. In chapter three these models will be discussed. because the fibre orientation is very important two effects need to be mentioned. In the above discussion it is assumed that the fibre density

and the fibre length is uniform across the thickness. This is not exactly the case. The fibre density is somewhat lower near the frozen layer [4] due to flow effects. Furthermore the fibre length is dependent on the amount of shear loading. In regions with high shear flow fibre breakage will be more present which results in shorter fibres. Related to the other effects these two effects are of minor importance and will be neglected in the rest of this report.

2.1.4 Microscopic stresses

Up to now only macroscopic stresses have been discussed. Also microscopic stresses are present in fibre reinforced material. These stresses are mainly induced by a difference in thermal expansion coefficient between the fibres and the matrix. This results in compressive stresses in the fibres and tensile stresses in the matrix on a microscopic scale. These stresses are not further discussed in this report.

2.1.5 Other stress effects

The previously discussed stresses are present in all injection moulded products. It has been shown for continuous fibre reinforced plastics that thermal residual stresses are predominant. But still there are other effects that can influence the residual stress considerably like chemically induced stresses in thermosets. In this case the stresses are induced by the difference in volume before and after curing. In this report these stresses are not discussed in more detail because a thermoplastic resin is used.

2.2 The consequences of residual stresses

Residual stresses exist in a lot of materials. Especially in injection moulded products residual stresses are unavoidable. When a product with residual stresses is loaded, the stress builds up cumulatively with the residual stress.

When the total stress becomes higher than the maximum strength of the material, the material will fail. Thus the material will fail sooner under loading when residual stresses are present and both the loading and residual stresses have the same sign. When their signs are opposite, the residual stress can compensate the loading stress partially, which results in a seemingly stronger material.

Another result of residual stresses is warpage. When a residual stress distribution is not symmetric around the mid-plane of the product, the product will deform out of plane. Up to now it is very difficult to predict the amount of deformation in short fibre reinforced products because very little is known about the residual stresses in injection moulded short fibre reinforced thermoplastics. In this report the first steps are made to predict the residual stress in fibre reinforced injection mouldings.

2.3 Stress relaxation

Because the molecules are not linked to each other like in thermosets, in a thermoplastic stresses can relax by movement of local chain segments. For a given material it is difficult to predict how much the stresses will diminish. Usually stress relaxes according to a logarithmic function. Above T_g , when molecule chains can move freely, stress relaxation is much more present than below T_g . Hindle and co-workers [15] concluded that stress relaxation is much smaller in reinforced than in the un-reinforced material. This can be explained by the fact that the fibres prevent the local matrix material movements.

2.4 Narrowed aim of the project

In the area of non-reinforced injection mouldings the insight in stress build up is increasing at the moment, but the residual stresses are still difficult to predict. About the stress built up in fibre reinforced injection mouldings very little is known. Considering what has been published on the subject of residual stresses in fibre reinforced and non-reinforced injection moulded products, it can be expected that for injection moulded thermoplastics with a high fibre content:

- a change in thermal expansion across the thickness is generally present and induces large stresses
- compared to these stresses other effects that are responsible for stresses in non-fibre reinforced thermoplastics are of minor importance and can be neglected in first instance
- a plate can be successfully modelled by laminate analogy
- relaxation is much smaller than in non-fibre reinforced thermoplastics

Therefore the residual stresses will be modelled with a laminate model. The considered laminate is formed by a number of layers that have material properties depending on the fibre orientation at that place of the product.

With a computer simulation it is tried to get insight in the fibre orientation distribution.

For a practical determination of the stresses the modified layer removal method will be used. This method was used previously for the determination of stresses in compression moulded composite plates [11, 12] which were known to be the type of stresses discussed above. The model will then be compared with the practical results.

3. Theoretical modelling

As discussed in chapter 2 the fibre orientation varies across the thickness of an injection moulded plate. The fibres have a significant influence on the material properties and hence the material properties will vary across the thickness as well. The first main question in this chapter is: How can the material properties be modelled? To model the plate the material is considered as a stack of plies. All plies have material properties that are constant throughout the thickness of each ply. To calculate thermal residual stresses the mechanical and thermal properties in each layer are needed. The models that have been published to calculate these material properties are discussed in the first section of this chapter.

The second question is: How can the stress in a plate be modelled? On the basis of the material properties thermal residual stresses can be calculated. For symmetric layered composite materials the residual stresses can be calculated using the Classical Laminate Theory (CLT). This model is introduced in section 3.2.

For non-symmetric layered composite materials that have large deflections an error is introduced when using the CLT because of geometric non-linearity. Therefore an energy approach is introduced. By minimising the potential energy the thermal residual stresses can be calculated. This model is discussed in section 3.3.

Finally a modified layer removal method is discussed, with which the residual stresses can be determined experimentally.

Figure 3-1 illustrates the way the residual stresses will be determined with the different models. It is indicated which values are needed after every step in the model. At the right the sections are given in which the models are introduced with small fonts. The large fonts indicate in which chapter the results are discussed.

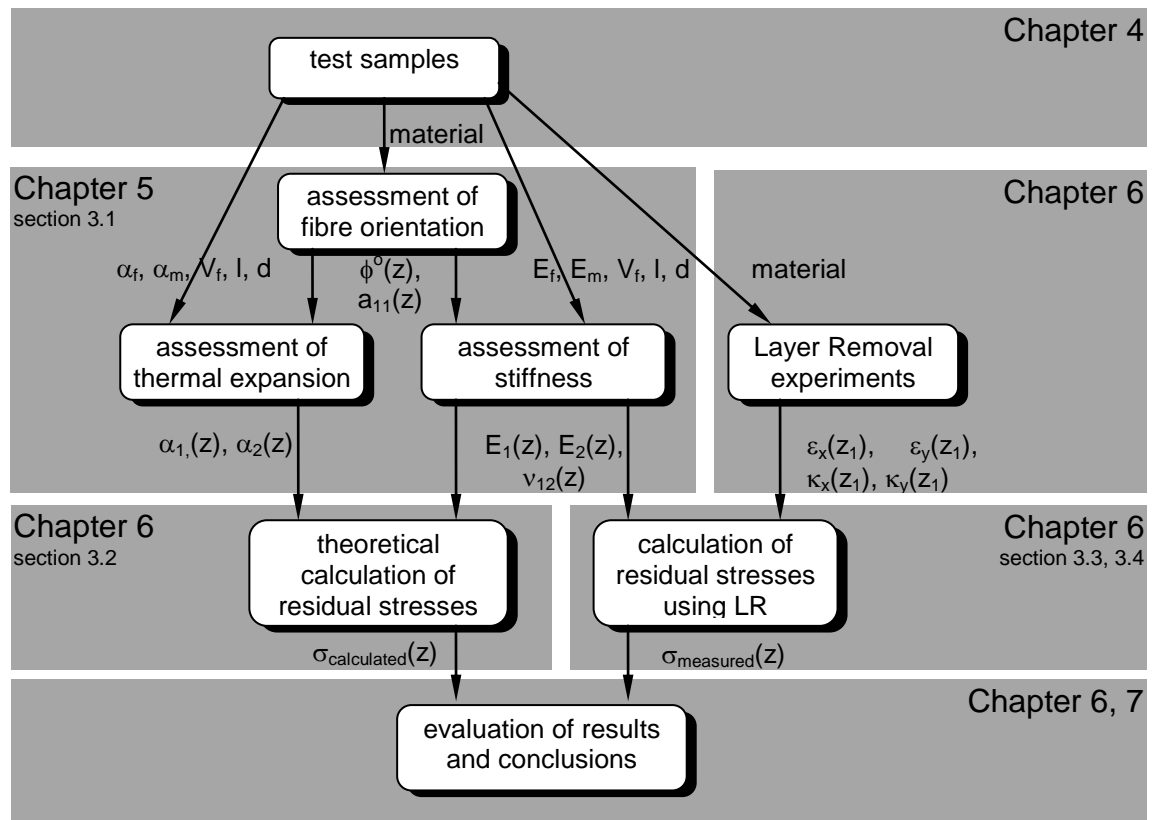


Figure 3-1: The different steps in the project. The grey boxes indicate the chapters in which the results are presented. With small fonts the section of this chapter in which the models are discussed are given.

3.1 Models to calculate the material properties

For a specific layer in the plate the material properties need to be estimated as a function of:

- the fibre orientation
- the average fibre length to thickness ratio; l/d
- the material properties of the matrix
- the material properties of the fibres
- the fibre volume fraction; V_f

In literature there are two important models that have been used to calculate these properties. In subsection 3.1.1 the model of Advani and Tucker in combination with the model of Halpin and Tsai is introduced. The subsequent subsection discusses the model according to Cox.

3.1.1 The model of Advani and Tucker in combination with the model of Halpin and Tsai

Advani and Tucker introduced a model to describe the fibre orientation [5]. With this model the material properties can be calculated when the material properties of the fibres and the matrix are known.

3.1.1.1 Description of the fibre orientation

To describe the fibre orientation Advani and Tucker used an orientation tensor. To build this tensor a vector of unity \mathbf{p} is introduced, together with a probability distribution function $\psi(\mathbf{p})$. The vector can describe the direction of a fibre and the function represents the chance that a fibre is oriented in that direction. The components of the vector can be given in spherical co-ordinates as shown in Figure 3-2:

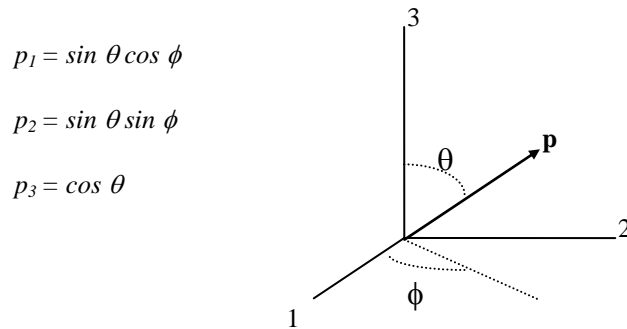


Figure 3-2: Sphere co-ordinates to describe the orientation of one fibre.

The probability distribution function $\psi(\mathbf{p})$ must satisfy a few physical properties. It should be periodical and no difference should be made between a rotation of 0 and π radians:

$$\psi(\theta, \phi) = \psi(\pi - \theta, \phi + \pi) \quad \text{Eq. 3-1}$$

Also, the function should describe all the fibres (normalisation condition), so:

$$\oint \psi(\mathbf{p}) d\mathbf{p} = 1 \quad \text{Eq. 3-2}$$

A set of orientation tensors can be defined by forming the dyadic products of the vector $[\mathbf{p}]$ and next the integration of these tensors with the distribution function in all possible directions. The fourth order tensor can be written as:

$$a_{ijkl} = \oint p_i p_j p_k p_l \psi(\mathbf{p}) d\mathbf{p} \quad \text{Eq. 3-3}$$

where a_{ijkl} are the orientation tensor elements and p_i, p_j, p_k, p_l are the elements of the vector $[\mathbf{p}]$.

The orientation tensor is symmetric, so:

$$a_{ijkl} = a_{jikl} = a_{kijl} = a_{lijk} = a_{klji} \quad \text{Eq. 3-4}$$

and the trace should be one because of the normalisation condition:

$$a_{iiii} = 1 \quad \text{Eq. 3-5}$$

Note that the Hermans factor f , which is used often in literature, can be assessed with the equation for planar conditions:

$$f = 2 \cdot a_{ij} a_{ji} - 1 \quad \text{Eq. 3-6}$$

As a definition, the Hermans factor is 0 for random and 1 for complete orientation.

3.1.1.2 Calculation of the material properties

Advani and Tucker used the mentioned model to predict the modulus and other material properties. The properties of a composite are taken as an average of the properties in several directions, weighed by the distribution function. This is called *orientation averaging*.

When a tensor is considered with material properties $[T](p)$ the orientation average $[\langle T \rangle]$ becomes:

$$\langle T \rangle = \int T(p) \psi(p) dp \quad \text{Eq. 3-7}$$

For the stiffness tensor Q_{ijkl} this equation can be written as:

$$\langle Q_{ijkl} \rangle = B_1(a_{ijkl}) + B_2(a_{ij}\delta_{kl} + a_{kl}\delta_{ij}) + B_3(a_{ik}\delta_{jl} + a_{il}\delta_{jk} + a_{jl}\delta_{ik} + a_{jk}\delta_{il}) + B_4(\delta_{ij}\delta_{kl}) + B_5(\delta_{ik}\delta_{jl} + \delta_{il}\delta_{jk}) \quad \text{Eq. 3-8}$$

where B_1 through B_5 are constants composed from the elements of the stiffness tensor for completely oriented material (see appendix A) and δ_{ij} the unity tensor.

Now the stiffness tensor is written in contracted notation, where the subscripts 11, 22, 33, 31, 23 and 12 are replaced by 1, 2, 3, 4, 5 and 6. Considering plane stresses [1], [16] the 3x3 stiffness matrix is obtained. This matrix will also be used in section 3.2.

The orientation average of the stiffness matrix for a given layer n , $\langle [Q] \rangle_n$, can now be written as:

$$\begin{bmatrix} \langle Q_{11} \rangle & \langle Q_{12} \rangle & \langle Q_{26} \rangle \\ \langle Q_{12} \rangle & \langle Q_{22} \rangle & \langle Q_{16} \rangle \\ \langle Q_{26} \rangle & \langle Q_{16} \rangle & \langle Q_{66} \rangle \end{bmatrix}_n = \begin{bmatrix} a_{11}Q_{11} + (1-a_{11})Q_{22} & Q_{12} & 0 \\ Q_{12} & a_{11}Q_{22} + (1-a_{11})Q_{11} & 0 \\ 0 & 0 & Q_{66} \end{bmatrix}_n \quad \text{Eq. 3-9}$$

Where Q_{ij} are the elements of the material stiffness matrix in main direction, that is, the direction in which most of the fibres are oriented. For every layer n the stiffness matrix in the main direction can be calculated with:

$$\begin{bmatrix} Q_{11} & Q_{12} & Q_{16} \\ Q_{12} & Q_{22} & Q_{26} \\ Q_{16} & Q_{26} & Q_{66} \end{bmatrix}_n = \begin{bmatrix} \frac{E_1}{(1-\nu_{12}\nu_{21})} & \frac{\nu_{12}E_2}{(1-\nu_{12}\nu_{21})} & 0 \\ \frac{\nu_{12}E_2}{(1-\nu_{12}\nu_{21})} & \frac{E_2}{(1-\nu_{12}\nu_{21})} & 0 \\ 0 & 0 & G_{12} \end{bmatrix}_n \quad Eq. 3-10$$

where E_1 , E_2 , G_{12} , ν_{12} and ν_{21} are the elastic constants in layer n in the main direction.

The orientation averaged stiffness matrix $[\langle Q \rangle]_n$ is valid into main direction. To get the stiffness into the global direction, $[\langle Q^* \rangle]_n$, a transformation of the matrix has to be performed, which is given in appendix A.

3.1.1.3 Calculation of the elastic constants for completely oriented material

Now we have the stiffness matrix in the main direction as a function of the element a_{11} from the orientation tensor and the elastic constants for completely oriented material. These elastic constants can be estimated with different models. The Halpin-Tsai equations were used by Advani-Tucker and others and give a reliable estimate of the effective modulus [6, 7, 8]. For the main direction the stiffness E_1 is calculated as follows:

$$E_1 = \frac{1 + 2\left(\frac{\ell}{d}\right)\eta_{EI}V_f}{1 - \eta_{EI}V_f} E_m \quad \text{with} \quad \eta_{EI} = \frac{\frac{E_f}{E_m} - 1}{\frac{E_f}{E_m} + 2\left(\frac{\ell}{d}\right)} \quad Eq. 3-11$$

As can be seen the fibre length is taken into account by these equations. Note that when the fibre length becomes infinite the equation reduces to the Rule of Mixtures:

$$E_1 = V_f E_f + (1 - V_f) E_m \quad Eq. 3-12$$

The complete set of equations to calculate all elastic constants is given in appendix A, equations 5. The Halpin-Tsai model assumes that all fibres have the same length to thickness ratio (aspect ratio). There is always a distribution of aspect ratio due to breakage during injection moulding (Denault [20]). Doshi and Charrier [19] have found that a distribution of aspect ratio results in a slightly higher modulus than the model predicts, but this difference is of minor importance.

3.1.1.4 Calculation of the thermal expansion

Advani and Tucker stated that other material properties can be calculated in the same way as was done for the material stiffness. For the thermal expansion only a second order tensor is needed. Accordingly the thermal expansion coefficient can be calculated with equation 3-13 for planar problems.

$$\langle \alpha \rangle_1 = \alpha_1 a_{11} + \alpha_2 (1 - a_{11}) \quad \text{Eq. 3-13}$$

$$\langle \alpha \rangle_2 = \alpha_1 a_{22} + \alpha_2 (1 - a_{22})$$

Like with the material stiffness, α_1 and α_2 are the longitudinal and transverse values for complete oriented material. These values can be calculated using the Schapery equations (see appendix A, equations 6). Like with the Halpin-Tsai equations, it has been shown that the Schapery model gives a good approximation of the thermal expansion [12].

In general it has been shown that the Advani - Tucker model gives good results for the material properties discussed above [18, 25].

3.1.2 The modified Rule of Mixtures

The model that was used by Cox and other investigators is an empirical modification of the Rule of Mixtures [2, 4, 20]. The model uses two compensation factors which should correct the influence of fibre orientation and fibre length:

$$E = \eta(o) \cdot \eta(l) \cdot V_f \cdot E_f + (1 - V_f) \cdot E_m \quad \text{Eq. 3-14}$$

Because the fibres are oriented to some extent, the ‘correction factor’ $\eta(o)$ is used. The factor is 1 for fully oriented material in the main direction and 0 transverse to this direction. To compensate for the length of the fibres the factor $\eta(l)$ is used. For infinite fibre length this factor equals one.

Christie [3] concluded that this model gives good results. For the calculation of the transverse modulus of highly oriented material the approximation becomes less accurate. In the following sections the assessment of the two factors is discussed.

3.1.2.1 Calculation of the fibre orientation factor

To assess the orientation factor $\eta(o)$ Krenchel [4], [37] used the following formula:

$$\eta(o) = \frac{1}{\sum_{i=1}^n K_{\beta_i}} \sum_{i=1}^n K_{\beta_i} \cos^4(\beta_i) \quad \text{Eq. 3-15}$$

where β_i is the angle of fibre i , and n the number of fibres that are considered. K_{β_i} is a correction function that depends on the chance to encounter a fibre under angle β_i and the fibre dimensions [37].

3.1.2.2 Calculation of the fibre length factor

To compensate for the fibre length the estimation of the factor $\eta(\ell)$ was introduced by Cox [2]:

$$\eta(\ell) = 1 - \frac{\tanh\left(\frac{\beta\ell}{2}\right)}{\left(\frac{\beta\ell}{2}\right)} \quad \text{Eq. 3-16}$$

where ℓ is the fibre length, which is considered uniform, and

$$\beta = \sqrt{\frac{2\pi G_m}{E_f * A_f * \ln\left(\frac{2r_1}{d}\right)}} \quad \text{Eq. 3-17}$$

with A_f the cross sectional area of a fibre ($A_f = \frac{\pi}{4}d^2$), G_m the shear modulus of the matrix and r_1 the average distance between the fibres. To obtain the ratio r_1/d Eq. 3-8 can be used according to Cox, assuming hexagonal arrangement of the fibres:

$$V_f = \frac{\pi d^2}{2\sqrt{3}r_1^2} \quad \text{Eq. 3-18}$$

Denault [20] and Bader [24] discussed a critical fibre length depending on the strain. For a certain strain fibres that are too short cannot transmit the loads and will be of no use for the material. The fibres that are too short are the ones that are shorter than the critical fibre length:

$$\ell_{ac} = \frac{\varepsilon_c E_f r_f}{\tau} \quad \text{Eq. 3-19}$$

For very small loads the critical fibre length becomes smaller than the fibre thickness d , so that $\eta(0) \eta(\ell) = 1$.

3.1.3 Physical non-linearity

When the elastic properties depend on the amount of load and the material is physically non-linear. The elastic properties can be physically non-linear. In short fibre reinforced plastics physical non-linearity can be divided into two categories. First it is possible that the Young's modulus of the matrix or the reinforcement is not constant over the range that the material is loaded.

Another non-linear effect is that very short fibres are possibly not able to transmit the loads and will not contribute to the reinforcement of the material. This results in a relative lower modulus at higher strains. Bader used the critical length of a fibre, as discussed in the previous section. When a fibre is shorter than the critical fibre length, the fibre is

assumed not to contribute to the stiffness of the material. In theory stiffness is reduced when the material has a wide fibre length distribution, so that a lot of short fibres are present in the material. In this report physical non-linear effects will be neglected because this effect is assumed to be too small to be measured.

3.1.4 Concluding remarks

Two models have been introduced to calculate the material properties. Of both models it has been shown that they can give a good estimate of the material properties, especially at temperatures of 0 - 20°C [3, 22]. This means that the following assumptions made by both of the models are valid:

- molecular orientation of the matrix has no significant influence on the material stiffness (with a sensitivity analysis this can be shown easily because the fibre properties dominate). There are some materials from which the influence of molecular orientation can be measured [16].
- physical non-linearity is neglected and hence the fibre aspect ratio (ℓ/d) is assumed to be uniform. The average of the aspect ratio is used for the calculations. It has been shown that the distribution of the fibre aspect ratio has little influence on the material stiffness.
- the material properties are assumed to be independent on time and temperature.

Apart from the two discussed models other models like the Reuss-Voigt model have been published. Although these models give good results as well, they were of no use in this case because the orientation parameters were unknown in this case.

In this report the Advani-Tucker model in combination with the Halpin-Tsai equations will be used because this model has proven to give reliable results.

3.2 The Classical Laminate Theory

To assess the thermal residual stresses in a layered composite plate the Classical Laminate Theory can be used (Powell [2]). It is supposed that the model can be used also for plates with a continuous change in material properties across the thickness. In that case the material is considered as a layered structure wherein each layer has its own material properties, depending on the average fibre orientation in that layer. With 10-20 layers a good approximation of an injection moulded plate is obtained. This was shown by several authors [8, 9, 16, 17].

3.2.1 Stress-strain

According to Hooke's law the relation between stresses ($\sigma_x, \sigma_y, \tau_{xy}$) and strains ($\epsilon_x, \epsilon_y, \gamma_{xy}$) is given in Eq. 3-1:

$$\begin{bmatrix} \sigma_x \\ \sigma_y \\ \tau_{xy} \end{bmatrix} = [Q] \begin{bmatrix} \epsilon_x \\ \epsilon_y \\ \gamma_{xy} \end{bmatrix} \quad \text{Eq. 3-20}$$

where the subscripts x and y indicate the global x and y directions and [Q] is the stiffness matrix for a single ply. It is assumed that the plate is very thin (thickness \ll length and width) and that there is plane stress (no stress in the z-direction).

For a layer n in a short fibre reinforced material, the stiffness matrix [Q] into a given direction should be replaced by the 'orientation averaged transformed stiffness matrix for layer n', being $[\langle Q^* \rangle]_n$. This matrix was introduced in section 3.1. When for every layer n the matrix $[\langle Q^* \rangle]_n$ is known, the ABD matrix can be calculated from it. This matrix is involved in the following stress-strain relationship for the entire laminate:

$$\begin{bmatrix} N \\ M \end{bmatrix} = \begin{bmatrix} A & B \\ B & D \end{bmatrix} \cdot \begin{bmatrix} \varepsilon^\circ \\ \kappa \end{bmatrix} \quad \text{Eq. 3-21}$$

where [N] and [M] are the resultant forces and moments per unit width acting on the plate respectively and $[\varepsilon^\circ]$ and $[\kappa]$ are the mid-plane strains and curvatures. The formulae to calculate [A], [B] and [D] respectively from $[\langle Q^* \rangle]_n$ are given in appendix A.

3.2.2 Thermal residual stresses

Now the stiffness of the material can be described, the residual stresses can be calculated theoretically, if the thermal expansion is known in every layer and direction and if the temperature is known from which the stresses are built up (the *stress free temperature*). Assuming that the material is symmetric, the following equations result in the thermal stress in each ply:

Calculate the thermal force resultant:

$$[N]_L^T = (\Delta T) \sum_{n=1}^p [Q]_n [\alpha]_n (h_n - h_{n-1}) \quad \text{Eq. 3-22}$$

where h_n is the height of the upper side of the nth ply, p is the number of plies, and ΔT is the difference between the stress free temperature and the actual (room-) temperature. Calculate the mid-plane strain where [a] is the inverse of [A] ([B]=0 because of symmetry assumption):

$$[\varepsilon^\circ]_L^T = [a][N]_L^T \quad \text{Eq. 3-23}$$

Now the thermal residual stress can be calculated in each layer of the product with the stiffness and the difference between mid-plane and thermal strain.

$$[\sigma(z)]_n^T = [Q]_n \cdot \left[[\varepsilon^\circ]_L^T - [\alpha]_n \Delta T \right] \quad \text{Eq. 3-24}$$

It is obvious that we need a good estimate of the material properties to calculate the stresses in the several layers of the material. Therefore attention will be paid in this report to have accurate material properties.

3.2.3 Concluding remarks

Thermal residual stresses in flat plates can be calculated using the Classical Laminate Theory when the material can be considered as a symmetric layered structure. Also plates that were not laminates from origin can be modelled by considering the material with a sufficient amount of layers. For each of these layers the material properties are needed.

It is assumed that the material properties are independent of temperature. It has been shown by Hamberg [12] that temperature dependence of the modulus does not have effect on the results because of the linear elastic reversible behaviour assumptions. So the assumption reduces in: thermal expansion independent of temperature.

Further assumptions that are made by the CLT are:

- the stress-strain relationship is reversible.
- small deformations are assumed and so geometric non-linearity is neglected
- the laminate plies are homogeneous.
- only thermal residual stresses are calculated and other kinds of residual stresses are neglected.
- the plane stress condition is assumed. This means that it is assumed that there are no out-of-plane stresses.

3.3 The energy approach for non-symmetric laminates

When a plate has internal bending moments into two directions (which usually is the case for non-symmetric laminates), the plate tends to curve into two directions. This *anti-clastic* behaviour cannot be modelled properly with the CLT when deformations become large.

Jun and Hong [30, 31] used an energy approach to predict the deformed shape of a non-symmetric laminate. This energy equation can also be used in reverse order. When the deformations are known the resulting moments that are present in the material can be calculated, without knowing the thermal expansion in each layer and without knowing the stress free temperature. Since no external load is applied, the total potential energy W of a laminate, including thermal effects is given by [33]:

$$W = \int_{Volume} \left(\frac{1}{2} Q_{ij} \varepsilon_i \varepsilon_j - Q_{ij} \alpha_i \varepsilon_j \Delta T \right) dVolume \quad Eq. 3-25$$

The second term represents the resultant residual thermal forces and moments. The strains can be substituted in this equation when an appropriate displacement field is known. Jun and Hong used the following equations for this displacement field:

$$\begin{aligned} \bar{u}(x, y) &= x \left(a_1 - \frac{a^2}{6} x^2 + a_3 y^2 \right) \\ \bar{v}(x, y) &= y \left(b_1 - \frac{b^2}{6} y^2 + b_3 x^2 \right) \\ \bar{w}(x, y) &= \frac{1}{2} (ax^2 + by^2) \end{aligned} \quad Eq. 3-26$$

Where the constants a and b represent the curvatures into x and y direction respectively, a_1 and b_1 are the mid-plane strains. The strain field can now be assessed when the strain-displacement relations are known.

3.3.1 Geometrical non-linearity

Generally linear mechanics are used. In linear mechanics displacements are proportional to loads. When the out of plane deformations become large, geometrical second order effects are introduced which can not be neglected anymore. In that case the strain-displacement relations obtain an extra second-order term. For flat plates these equations become [14]:

$$\begin{aligned}\varepsilon_x(z) &= \frac{\partial u}{\partial x} + \frac{1}{2} \left(\frac{\partial w}{\partial x} \right)^2 - z \frac{\partial^2 w}{\partial x^2} \\ \varepsilon_y(z) &= \frac{\partial v}{\partial y} + \frac{1}{2} \left(\frac{\partial w}{\partial y} \right)^2 - z \frac{\partial^2 w}{\partial y^2} \\ \varepsilon_{xy}(z) &= \frac{\partial u}{\partial x} + \frac{1}{2} \left(\frac{\partial u}{\partial y} + \frac{\partial v}{\partial x} + \frac{\partial w}{\partial x} \frac{\partial w}{\partial y} \right) - z \frac{\partial^2 w}{\partial x \partial y}\end{aligned}\tag{Eq. 3-27}$$

3.3.2 Solving the energy equation

To solve the energy equation the displacement field should be substituted in the strain-displacement equations. This results in:

$$\begin{aligned}\varepsilon_x(z) &= a_1 + a_3 y^2 - z a \\ \varepsilon_y(z) &= b_1 + b_3 x^2 - z b \\ \varepsilon_{xy}(z) &= \left(a_3 + b_3 + \frac{ab}{2} \right) xy\end{aligned}\tag{Eq. 3-28}$$

Now the unknowns in the energy equation can be solved by minimising the potential energy. In general form when a_i are the n constants from the displacement field (in this case a , b , a_1 , b_1 , a_3 , b_3), the problem can be solved using:

$$\frac{\partial W}{\partial a_i}(a_i, L) = 0; \quad \text{for } i = 1, \dots, n; \quad L = \text{constant}\tag{Eq. 3-29}$$

This is a system of 6 non-linear algebraic equations. The system can be solved for 6 unknowns. These unknowns can be the resultant thermal residual moments and/or several constants from the displacement field. The system can be solved by using a Newton-Raphson procedure. For a stable solution $\delta^2 W$ has to be positive and definite.

3.4 The Layer Removal method

If a product contains residual stresses, equilibrium is disturbed when some material is removed. As a result the material will deform so that equilibrium can re-establish. Several methods have been introduced using this principle. For example hole drilling was used in certain cases. With this method a hole is drilled in stressed material. The deformed shape

of the hole after drilling can be determined with a strain gauge around the hole. This strain is a measure of the internal stress.

Another method of getting deformation as a cause of removing material is the Layer Removal method. When a layer is removed from the surface of a flat plate, the material will ‘curl up’ if compressive stresses exist in the surface of the material. From the resultant curvatures and strains the residual stresses can be obtained. The following subsections give a detailed description for the calculation of residual stresses with the layer removal method. This method was first used in metals by Treuting and Read [13] and has been investigated for the use on reinforced plastics by Eijpe and co-workers [10, 11, 12, 41]. They showed that experiments on long fibre reinforced thermoplastic laminates give reliable results. One of the goals of this report is use this method on short fibre reinforced injection moulded materials as well.

3.4.1 Calculation of residual stresses using the Layer Removal results

To recover the residual stress profile in a plate several layers have to be removed. After each layer removal the deformation and dimensions of the plate are measured. These are the strains and curvatures in x and y directions and the new thickness. Figure 3-3 illustrates the co-ordinate definition of the problem.

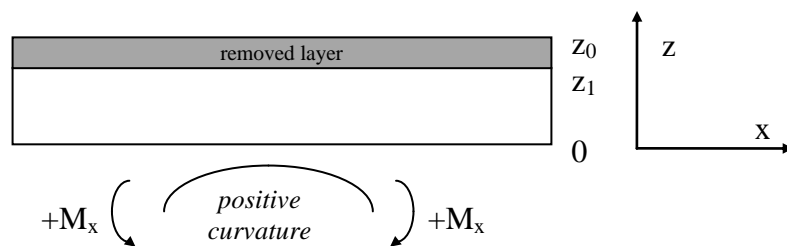


Figure 3-3: Co-ordinates definition used with the Layer Removal calculations The y direction is perpendicular to the plane of reading.

When the material stiffness is known the internal bending moment can then be calculated. Up to now this was done with the CLT [10, 11, 12]. For a cross-ply laminate (where $B_{16} = D_{16} = 0$) the moment in x-direction is:

$$M_x(z_1) = B_{11}(z_1)\epsilon_x^0(z_1) + B_{12}(z_1)\epsilon_y^0(z_1) + D_{11}(z_1)\kappa_x(z_1) + D_{12}(z_1)\kappa_y(z_1) \quad Eq. 3-30$$

Here z_1 is the new plate thickness after layer removal. The B and D components are dependant of z_1 because whenever a layer is removed, a new laminate is created which has his own ABD matrix. These constants can be calculated using the formulae in appendix A and the theory discussed in section 3.2. For our case of an unbalanced non-symmetric cross ply the in-plane strains and curvatures in both directions have to be measured.

For large deformation this equation is not valid anymore. Therefore the moments in x and y direction have to be calculated using the energy equation, as discussed in section 3.3. The moments M_x and M_y are calculated for every removed layer. This results in two moment profiles as a function of the upper surface z_1 . The moment profiles have to be fitted to get a continuous function. This function can then be substituted in the relation introduced by Treuting and Read [13]:

$$\sigma_x(z_1) = \frac{2}{z_1} \frac{dM_x(z_1)}{dz_1} + 2 \frac{M_x(z_1)}{z_1^2} - 4 \int_{z_1}^{z_0} \frac{M_x(z)}{z^3} dz \quad \text{Eq. 3-31}$$

that results in a stress profile across the thickness.

This equation is based on mechanics, and has been derived from the equation:

$$M_x(z_1) = \int_0^{z_1} \sigma_x \left(z + \frac{z_1}{2} \right) dz \quad \text{Eq. 3-32}$$

that is the mechanics equation to obtain the moments around the centre of the plate.

The stress calculation is visualised schematically in Figure 3-4.

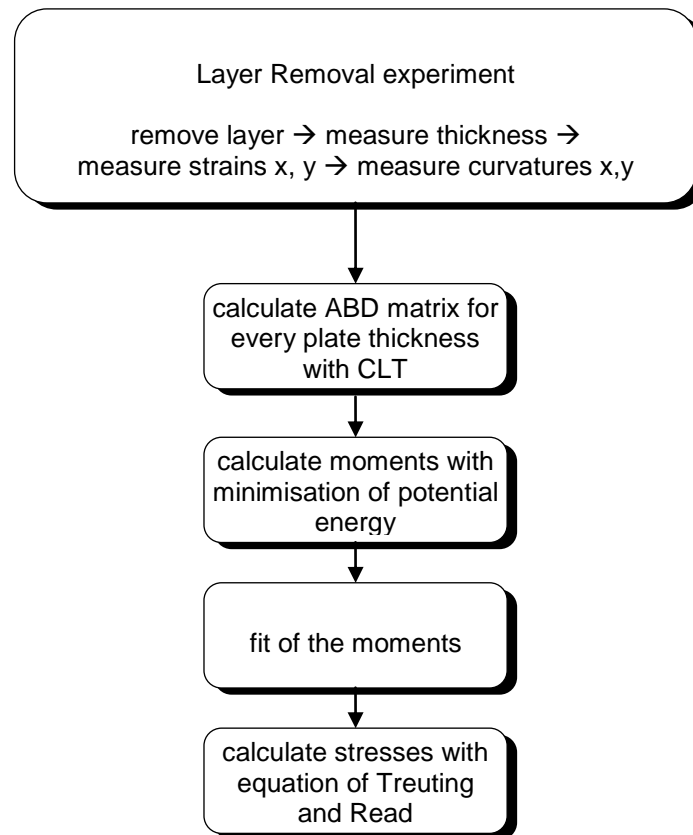


Figure 3-4: The calculation steps for the layer removal experiment schematically.

3.4.2 Calculation of the moments for every layer

To calculate the moments from the measured geometry the CLT was used in previous work [10, 11, 12, 41]. As mentioned previously a refinement of this equation is introduced with minimisation of the potential energy.

The equation needs the following input for the moments calculations:

- the measured curvatures and strains
- the geometry and the thickness after each layer removal
- when rewriting the energy equation the elements of the CLT ABD matrix are again introduced in the equation. The values for the ABD elements are recalculated for every plate thickness.

Now the equation has the following six unknowns:

- the in plane moments in x and y direction (M_x, M_y)
- the in plane forces in x and y direction (N_x, N_y)
- the shear related con
- stants (a_3, b_3)

These variables can be solved by differentiating the energy equation with respect to the six displacement parameters being equal to zero. This results in six equations from which the six unknowns can be obtained after substituting the known values.

3.4.3 Fit of the moments as a function of thickness

When the moments for every layer have been calculated, the stress profile can be obtained from this information with equation 3-30. To solve this equation a description of the moments being a function from the thickness is needed. This is done by a fit on the moments.

- the function should result in a symmetrical stress profile (not a symmetrical moments profile), so the derivative of the stress profile with respect to the thickness in the middle of the plate must be zero.
- the resultant force should be zero, that is the surface under the stress graph should be zero

There is no reason to assume any shape of the moment lines. Beside that we would introduce extra theoretical information in the experiment, we do not even have a theoretical description for the shape of this line. Therefore several fit techniques were compared.

The fitting techniques that are considered are:

1. polynomials; to fit the moments a polynomial function of the form: $f(z) = \sum_{i=0}^n a_i z^i$ was used on the entire domain, where n is the order of the polynomial and a_i are constants. In the graphs polynomials of several orders are plot.
 2. splines; splines were used by Klarenbeek [41] to recover stresses from unfilled material using the layer removal technique. This fit uses B-splines as trial functions. The graph is divided into a given number of intervals. The splines have a local support depending on the size of the intervals. Therefore a local error will not be transferred throughout the complete domain. A higher resolution is obtained by using smaller intervals. This technique is used in combination with the zero stress condition and the stress symmetry condition.
 3. moving window using polynomials; to fit the moments a polynomial function of order n is used within a certain window of the moments data. The window width is the number of data points that is used within the window. These points are fit with a polynomial and then the window is shifted. The fit applies to the middle window point.
- Each technique uses its own set of functions that is fitted using the least squares method. Note that the R^2 value of this method is not the only aspect of the fit that should be considered. The fit should also not oscillate between the data points, but give good detail. A third restriction is that the fitting line should be within the error of the data point.

4. The test material

In this chapter the plates are described that were used for the measurements that are discussed in this report and the theoretical stress prediction of the material. The plates have been injection moulded at the university of Aalborg, Denmark, December 1990.

First the dimensions and mould geometry of the plates are given. Then the material properties are presented and finally the processing conditions of the several samples are tabulated.

4.1 Geometry of the plates

The used samples are film gated square plates with dimensions $110 \times 110 \times 2 \text{ mm}^3$ injected with a coat hanger die according to the Figure 4-1. All samples were taken out of the middle of the plate as indicated.

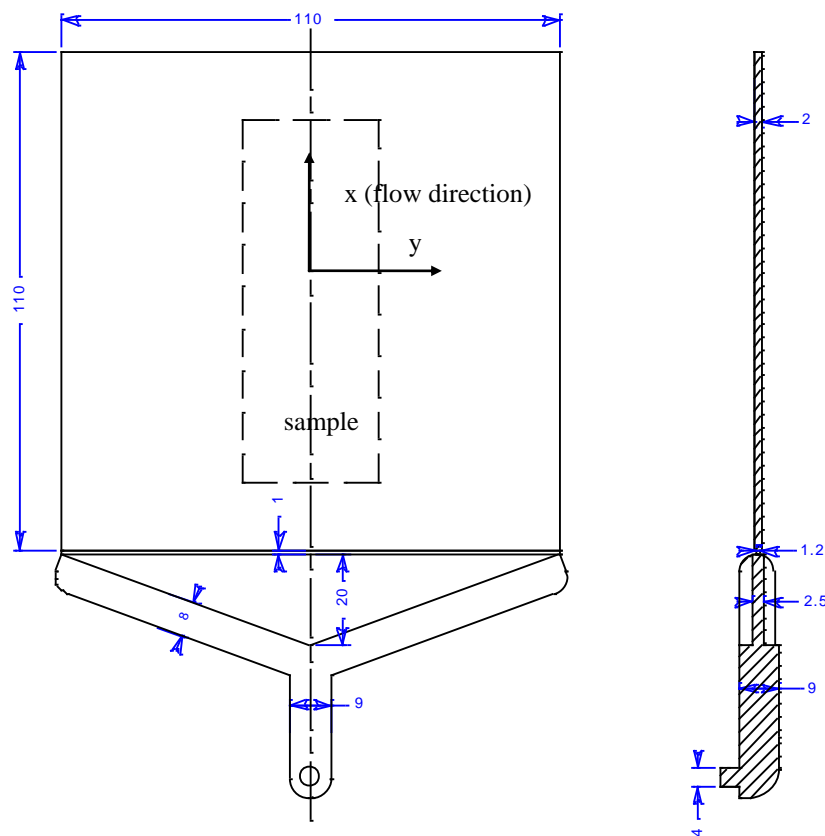


Figure 4-1: Injection geometry schematically; dimensions in mm.

4.2 Material characterisation

The material that has been used is 40% glass reinforced Poly Phenylene Sulphide (PPS) provided by PHILLIPS (trade name: PPS RYTON R4 XT HV). The material is known for its good dimensional stability, good temperature resistance and good flame resistance. The semi-crystalline matrix material is constructed from aromatic rings and sulphur,

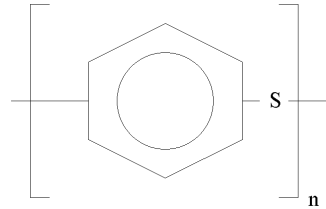


Figure 4-2: Chemical structure of the matrix material.

resulting

in the structure depicted in Figure 4-2.

The most important material properties are given in Table 4-I:

	<i>symbol</i>	<i>unit</i>	<i>fibres</i>	<i>matrix</i>
material			glass	PPS
tensile modulus ¹	E_f, E_m	MPa	76000	4100
shear modulus ¹	G_f, G_m	MPa	29670	1500
Poisson's ratio ¹	ν_{12}		0.22	0.43
thermal expansion coefficient ¹	α_f, α_m	K ⁻¹	5.0E-6	5.13E-5
density ¹	ρ_f, ρ_m	kg/m ³	2.560	1.383
average fibre length	ℓ	mm	0.194 [0.20]	-
average fibre diameter	d	mm	0.10 [0.020]	-
fibre weight fraction	W_f		0.427 [0.40]	-
melt temperature	T_m	°C	-	285
crystallisation temperature	T_c	°C	-	130
glass transition temperature	T_g	°C	-	88

1) values at room temperature

Table 4-I: Material properties of PPS GF40 [26, 27, 37, 38]. Values between [] are the documented values, they have been replaced by measured values.

These values are given for the granulate in general. For a specific product some properties may be different. The material properties may be slightly different for different batches. Particularly the fibre length may change because of fibre breakage during processing. For the used plates the fibre length distribution, the fibre thickness and the weight fraction W_f were measured. These values are used in the table and the documented values are put between brackets. In these measurements it was found that the fibre length distribution was not very sensitive to the used processing conditions. Because the measurements were done on exactly the same plates, the measured values will be used in this report.

It can be concluded from the given material properties that the aspect ratio $\ell/d = 19$ and the fibre volume fraction $V_f = 0.287$. These values will be used frequently in this report.

The crystallinity of the matrix depends on the mould temperature mainly. This has been investigated by Brady [26]. According to this information the crystallinity is about 50% at a mould temperature of 140 °C. This is close to maximum crystallinity, which is about 62%.

To anneal the material a temperature of 204°C was chosen by several authors, often during two hours. Higher temperatures around the melt temperature are not to be recommended, because the material slowly cross-links around this temperature. Most of the crystallisation occurs during the first ten minutes at 200°C.

For this material the modulus is not affected so much by the crystallinity. The change in the flexural modulus in the most extreme cases (maximum crystallinity of 60% and minimum of 5%) is only 3.5% [26].

For the tensile strength of the material a value of 121 MPa is given [27]. This is an indication of the tensile strength, because it is supplied only as an average of injection moulded test pieces, and therefore are not accurate, like many other material properties. The actual material properties are dependant on fibre orientation.

4.3 Processing conditions of the plates

Three series of different processing conditions have been investigated. The sample numbers are the numbers used by the university of Aalborg. The plates were injection moulded in December 1990.

<i>series number</i>	<i>melt temperature [°C]</i>	<i>mould temperature [°C]</i>	<i>injection time [s]</i>	<i>second pressure [MPa]</i>
2	320	140	2	40
5	340	140	1	20
8	360	140	3	60

Table 4-II: Processing conditions of the tested samples

Of every processing condition five plates were available for testing.

5. Determination of the material properties (recovered)

5.1 Fibre orientation

5.1.1 Cmolde computer simulation model

being a combination of the two. The equations for these closure approximations are given in Appendix A.

Finally, to solve the equation of change a boundary condition is needed. This 'inlet boundary condition for alignment' has been set to one during the simulations, which means that the fibres are assumed to be aligned in the flow direction at the skin and random in the core at the film-gate. All (other) parameters needed in the calculations can be found in appendix B where the used files are listed for a particular processing condition. Note that during injection the ram-speed profile recommended by Cmolde has been used.

Finally the following assumptions are made by Cmolde:

in practice the fibres influence the flow of the material during injection. This fibre-flow coupling is not taken into account by the model used by Cmolde.

the fibre orientation in the skin is not calculated because fountain flow effects are present in this region, and no fountain flow model has been implemented in Cmolde.

the a_{33} element of the orientation tensor is assumed to be constant at a value of 0.005. This is an empirical average for planar orientation and is not calculated by Cmolde.

flow perpendicular to the plane is neglected

inertia effects are neglected

5.1.2 Interpretation of the Cmolde simulation

Only the fibre orientation in the centre of the x-y plane of the plate is considered (so typically for $x = 0$ and $y = 0$). The plate geometry is symmetrical, so that it is assumed that the fibre orientation of the plate is symmetric around this centre point. This means that the fibre average orientation should be 90° (or 180° theoretically in this centre point of the plate). Also in all measurements reported in this chapter the plate was assumed to be symmetrical in all three directions (flow (x) -, and transverse (y)- and out-of-plane (z) direction).

The orientation data around the centre of the plate are obtained from the computer simulation by taking an average of the values from 6 mesh-elements after the packing stage. These elements are within a 1.25 mm square in the centre of the plate. It was chosen to use more than one element, because there were slight differences in the fibre orientation results for each element.

An example of the fibre orientation simulation is given in Figure 5-1.

LINK Excel.Sheet.5 \\\\UTWOU5\\VOERMAN\\rik\\orienta.xls
simulatie!R25C1:R35C7 \a \p ____

Figure 5-1: (left:) Fibre orientation in the core of the plate as simulated by Cmolde for process condition number two. (right:) Melt front advancement for process condition number two. A line indicates the shape of the flow front at a certain time instant.

Table 5-1: Simulated orientation for each processing condition . The orientation tensor element a_{11} and the angle of the fibre main direction with the global y axis is given.

In Table 5-1 the average orientation angle with the y axis and the average of the orientation average of the six elements from the Advani-Tucker tensor are listed. According to the simulation the fibre main direction is close to 90° as expected.

It can be seen that closer to the surface the simulated main direction of the fibres becomes larger than 90° , up to a difference of 16° in the outer layer. It is supposed that this effect is caused by the cooling of the plate, which is not completely symmetrical. Cooling channels are located transverse to polymer flow direction. This may result in a difference in temperature that induces a difference in thickness of the frozen layer.

5.1.3 Experimental fibre orientation

The fibre orientation results of Cmolde can be compared with other values, obtained from the University of Aalborg, Denmark. There the a_{11} element of the orientation tensor in several points across the thickness of the plates were measured. In the out-of-plane direction an average of $a_{33}=0.05$ was measured. The results were reported in [37]. In Aalborg also the fibre orientation was calculated using another software package, Moldflow.

When the fibre orientation was measured the sign of the angles of the fibres with the cross section could not be assessed. Therefore the symmetry assumption was necessary to be able to measure the fibre orientation.

5.1.4 Discussion of the fibre orientation results

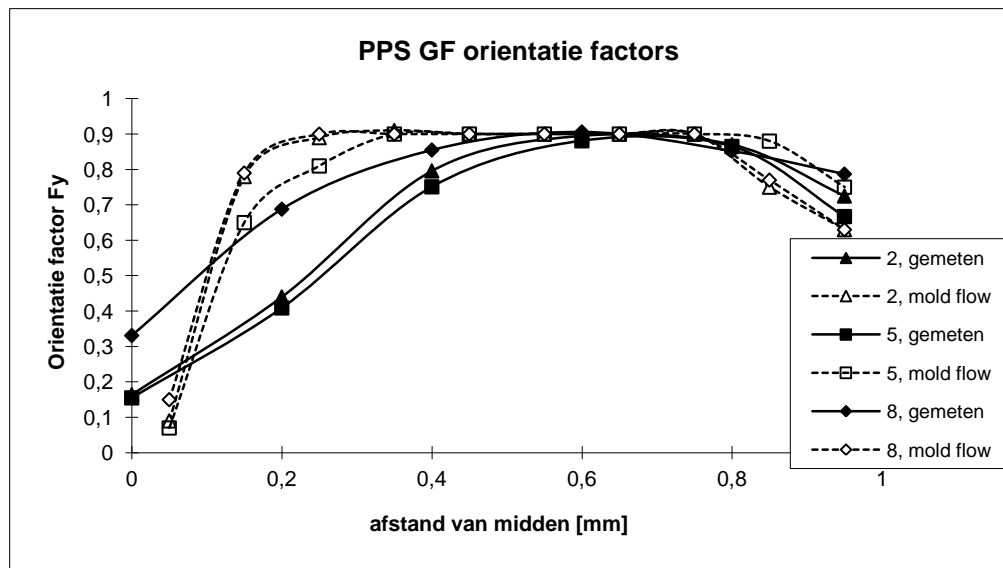


Figure 5-2: Fibre orientation across the thickness for process condition number two as a result of the measurements and the computer simulations using Moldflow and Cmolde.

Figure 5-2 illustrates the orientation tensor element a_{11} drawn against the normalised distance from the core. The results from the measurements, the Moldflow simulation and

the C mold simulation are compared for processing condition 2. The other processing conditions that were considered resulted in similar graphs, as can be found in appendix B. The data points in the graphs are connected with a line to indicate the trend of the fibre orientation.

From the fibre orientation analysis it can be concluded that Moldflow as well as C mold do not calculate an accurate fibre orientation. The fibre orientation across the thickness can be divided into three regions:

in the surface region no model has been implemented to calculate the orientation. This region is generally small.

in the shear flow region fibre orientation is approximated best by the simulation programs, but C mold predicts too low a fibre orientation here. Also the borders of this region are not calculated accurately. The explanation for this may be that no fibre-flow coupling is modelled (i.e. it is assumed that the fibres do not influence the material flow during injection).

in the core region the fibre orientation tends to drop and become transverse according to the measurements. This indicates a diverging flow in the core during injection. The C mold simulation predicts a slightly converging flow instead, resulting in fibre orientation that is more into flow direction. Apparently the melt front advancement is not predicted correctly. Especially in this case where the film gate produces an almost flat flow front, small errors in the flow front advancement prediction have a significant influence on the fibre orientation in the core.

Other facts that can be observed from the simulation results are:

immediately after filling of the mould the simulated fibre orientation is more into flow direction. During the packing stage the fibre orientation becomes more random.

for the used geometry the fibre orientation is constant in the centre region and therefore experiments can be done with specimens taken from this region. From the simulation results (Figure 5-1) it can be concluded that specimens should not be longer than 90 mm into flow direction and not wider than 40 or 50 mm into transverse sections.

according to the simulation the assumption that the fibre orientation is symmetric around the centre of the plate (i.e. around the x as well as the y axis) is acceptable because the simulated fibre main direction was close to 90°. Therefore this assumption is used during the experiments discussed in the following paragraphs.

Material properties calculated by C mold are based on the fibre orientation. Because the fibre orientation prediction of C mold is not accurate in this case, the material properties calculated by C mold are of no use.

For the calculations in the rest of this report that are based on the fibre orientations the measured fibre orientations are used because they seem to be most reliable. The measured fibre orientations across the thickness are given in Figure 5-3 for each processing condition.

LINK Excel.Sheet.5 ":///UTWOU5\\VOERMAN\\rik\\orienta.xls"
"orientation![orienta.xls]orientation Chart 2" \a \p ____

Figure 5-3: Fibre orientation for every processing condition across the thickness, as measured in Aalborg, Denmark. The measured points are connected with lines to indicate the trend.

5.2 Material stiffness

Because of the changing fibre orientation in the thickness of the plate, the modulus is not constant through the thickness. The modulus can be calculated theoretically in the center of the plate using the known fibre orientation and the models discussed in section 3.1 of this report. To verify these values the modulus was measured using three point bending. First a tensile test was done (subsection 5.2.2) that results in an average modulus over the cross section of the specimen. After that the specimen was used for a three-point bending test (subsection 5.2.3). The bending test was done several times, each time after removing a layer. From the tests the modulus profile in the original specimen was then obtained. The theoretical profile can be compared to the profile that was obtained with the three point bending test. The tensile stiffness can be compared with the average stiffness obtained from the three point bending test and the theoretically calculated stiffness. Figure 5-4 illustrates the different steps to obtain the modulus for one specimen. In all cases only the modulus in flow direction is considered.

—

Figure 5_4: Stiffness measurements schematically. The tensile and bending measurements were done with the same specimen.

5.2.1 Specimen preparation

For both the tensile and the three point bending tests the same specimens were used. Specimens of 10 mm wide were cut out of the middle of the plate with the length parallel to the flow direction. For the tensile test the specimens were kept at full length (110 mm) to have a better clamping of the specimen. For the three point bending test 15 mm was cut at both free edges. The specimens were cut carefully with a liquid cooled diamond saw. The cooling liquid that was used is based on water.

During the experiments the temperature was kept at a temperature of 22(3) C.

For both the tensile and bending measurements a Zwick type 1445 testing machine was used.

For the tensile test a strain gauge into loading direction was applied. The properties of this strain gauges are listed in Table 5-2

strain gauge GFLA 6-350-50
length 6 mm
width 2.7 mm
electrical resistance 350 (1.0 (
gauge factor 2.14

Table 5-2: Strain gauge used for tensile test.

Before the gauges were mounted (with CN adhesive of Tokyo Sokki Kenkyujo Co.) the surface was carefully treated in the following way:

roughen with sandpaper P 300

clean with ethyl alcohol

clean with M-Prep conditioner A, a water based acidic surface cleaner

clean with M-Prep neutraliser 5A, a water-based alkaline surface cleaner

The strain gauge was connected in a bridge of whetstone configuration, with a dummy gauge. The strain can be calculated with:

— EMBED Equation.2 — Eq. — STYLEREf 1 \n _5_- SEQ Eq. * ARABIC
4

5.2.2 Description of the tensile test

For the tensile test it was tried to meet the ASTM D 3039 (Standard test method for tensile properties of fibre-resin composites). Contrarily to the standard, aluminium tabs were not used. Also the specimen dimensions were slightly different from the standard. The testing speed that has been chosen is 0.16 mm/min, which results in a strain rate of 0.000041 mm/mm.s. (clamping distance: 65 mm).

Plates of 10 mm wide and 110 mm long were cut out of the injection moulded plates in the middle. The thickness and the width were measured in the middle and 25 mm from the middle into both directions. Then a strain gauge was applied in the middle of the plate, as described in the previous subsection, to measure the strain during tensile testing.

The plates were clamped in all four possible positions, to minimise errors. After clamping the plate was first loaded up to the maximum load. Then three times the plates were tested. So 12 tensile values for every plate were obtained, from which the average was taken.

5.2.3 Description of the three point bending test

After the tensile test the same specimen was used for a three point bending test. It was tried to meet the ASTM D 790M standard (Standard test methods for Flexural properties of non-reinforced and reinforced plastics and electrical insulating materials), method I, as much as possible. This test set-up is drawn schematically in Figure 5-5.

—

Figure 5-5; Three point bending test, method I, schematically.

The plates were tested three times and then a layer of about 0.1 mm was removed. For this layer removal a two point cutter was used with a diameter of 75 mm. The rotation speed was 1400 rpm, the feed rate was 80 mm/min. After removing a layer the plates were kept untouched for 12 to 18 minutes and then the thickness was measured and the next bending tests were done.

The dimension that are recommended by the ASTM standard could not be met completely. There were restrictions in the plate dimensions, because only a plate length of 75 mm can be milled. Also the support span L of the plate has been kept the same for every plate thickness to maintain accuracy. For this reason the span to thickness ratio could not always be 60 as is recommend in the standard. Also the radii of the supports and the cross head nose were slightly different from the standard because the required ones were not available.

In 5-3 the geometry and test parameters for the used bending test are listed.

plate length 80 mm
plate width b 10 mm
support span L 60 mm
nose radius 5 mm
support radius 2 mm
cross-head motion 1 mm/min
max. deflection depth w 1 mm

Table 5-3: Test parameters for the three point bending test.

With these values the maximum strain rate in the outer fibres is 0.000027 up to 0.000055 mm/mm. s., which is of the same order as the tensile strain rate. The maximum strain in the outer fibres is 0.33 %. Because the width of the plate is only 10 mm, the extra stiffening effect of the transverse curvature occurring after milling can be neglected.

The results of these tests were used to recover the average modulus for every layer, as is described in the following subsection.

5.2.4 Calculation of the modulus in the several layers of the plate from the bending test

For bending of composite beams equation 5-5 represents the stiffness relation between force and deflection [16, 32, 33, 34, 35]:

_EMBED Equation.2 ____ Eq. _STYLEREF 1 \n _5_- _SEQ Eq. * ARABIC
5

With EI the bending stiffness, being b/d_{11} (width divided by first element of CLT bending compliance matrix) for composite beams and A the cross sectional area.

The second term is usually neglected, but in composite beams this term can have a significant value. From the bending test in every layer the ratio F/w was obtained by fitting the load-deflection curve. After calculating the d_{11n} for every layer n, containing the stiffness in main direction, (E_{11n}) symbolically, a set of equations is obtained, with the stiffnesses in main direction as the unknowns. In these equations the other material constants $(E_{22}, (I_2 \text{ and } G_{12}))$ are needed. The values for these constants were taken from measurements previously done (see Table 5-4). The set of equations is then solved

resulting in a modulus profile across thickness. Appendix E contains the listings of the Mathematica 2.2.3 software program that has been used to solve the problem.

	Carbon/PEI ¹	PPS GF40 ²	Halpin-Tsai for PPS GF40
modulus transverse direction [MPa] E22	7849	8010	8093
Poisson's ratio (12	0.32	0.418	0.37
shear modulus [MPa] G12	4550	3050	2551

¹ results obtained from other tests at the University of Twente

² results obtained from tests at the University of Aalborg, [36]

Table 5-4: Material constants as used in the calculations for the Carbon-PEI laminates and the Glass filled PPS.

Beside the measured values also the material constants for PPS GF40 are calculated using the Halpin-Tsai equations. These calculations are based on the measured fibre orientations from section 5.1 and the material properties presented in chapter 4.

5.2.5 Validation of the three point bending method

To verify this bending test procedure, first a bending test on a 12 ply unidirectional and a (04, 904)s cross-ply of Carbon-PEI specimen was made. It was chosen to use this material because its material properties have appeared to be well defined. Because the laminates are compression moulded from unidirectional prepreg material the fibre orientation is accurately known.

The long sides of the specimen were cut parallel to the fibre (main) direction. The same geometry was used as for the injection moulded specimens. *_ REF _Ref358533208 ** MERGEFORMAT *_Figure 5-6_* shows the results of the three point bending tests for the Carbon-PEI laminates. More detailed information can be found in appendix C.

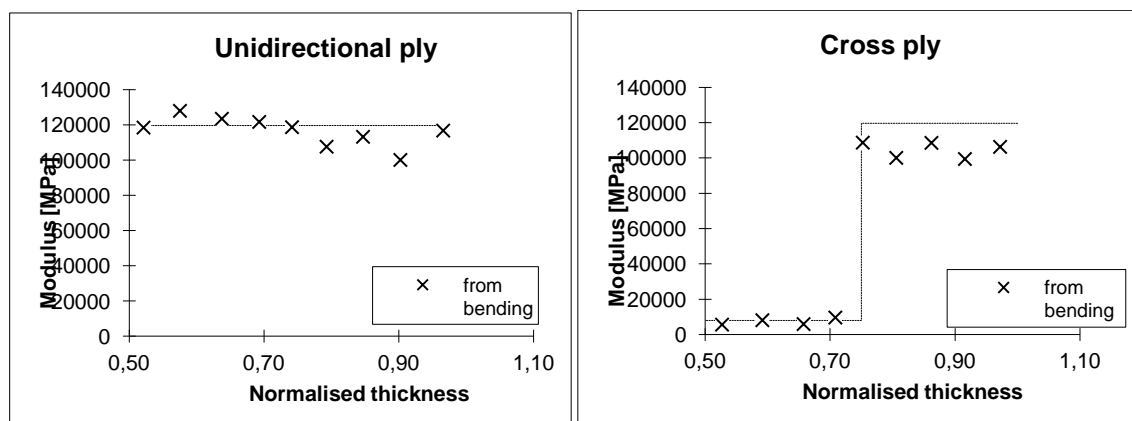


Figure 5-6: Measured and expected stiffness of 12 layer unidirectional and cross-ply Carbon/PEI laminates.

The expected stiffness is the stiffness that was measured previously in the unidirectional laminate. The graphs show scatter of the points around the expected values. This scatter may be caused by the bad packing of the fibres. The fibres are assumed to be well aligned, but the stacking of the fibres is not constant. This can be seen very well when a cross section of the material is put under the microscope. There are zones with extra matrix

material in between the original plies. Another effect that may cause errors is that the fibres in the milled surface are loaded with a compressive stress. This may result in local buckling or breaking out of the fibres.

To compare the bending test results the average of the bending test is calculated with:

$$E_{avg} = \frac{1}{n} \sum_{i=1}^n E_i \quad (5.6)$$

with f_i the thickness of each layer, and n the number of layers. The average of the tensile tests is the stiffness measured with the tensile tests, averaged for all four clamping modes. The results of these tests are listed in Table 5-5, including the values that are expected. For the unidirectional laminate the expected value is the one that was previously measured by M. Eijpe, with exactly the same laminate. The expected value for the cross-ply laminate is the half of the longitudinal plus the transverse modulus measured previously with the unidirectional laminate. Another error that is introduced is caused by the milling process. The milling process did not result in a constant thickness. Clamping problems of the plate caused a slightly varying thickness of up to 0.05 mm. This influences the stiffness of the plate considerably and also contributes to a measurement error. The size of this error is difficult to predict, because of the complicity of the calculations.

Comparison of average modulus				
	UD	error	CP	error
from tensile test	119700	-	62300	-
from expected values	119880	0,2%	63775	2,4%
from bending test	116512	-2,7%	59441	-4,6%

(1) results from other tensile tests at University of Twente, at a strain rate of 0.00022 m/ms

Table 5-5: Average modulus for the tensile test, bending test and the values obtained from other experiments for a unidirectional and a cross-ply laminate of Carbon-PEI. The error with the tensile results is also listed.

The tensile tests result in values that were expected from previous tests. This means that the material behaves as expected and that there are no irregularities in the material. The bending test results give a lower material stiffness of up to 5 %. Maybe this can be explained by the fact that in bending the specimen is partially loaded in compression. The compressive modulus is generally lower than the tensile modulus and so the specimen stiffness decreases. Particularly at the surface the fibres that are loaded in compression may even buckle out of the surface, which results in an even lower stiffness. But this effect was expected and so the results are in good agreement with the 'expected values'.

5.2.6 Analysis of sensitivity for the used material constants

For the bending test calculation previously measured values were assumed for the shear modulus, the poisons ratio and the transverse modulus. To analyse the sensitivity of the calculation to these values, calculations were done with different values for G_{xy} , ν_{xy} and E_{yy} . Each variable has been changed separately, so second order effects have not been analysed. The variables were changed from the values listed in Table 5-4 to 2000 MPa,

0.3 and 5000 MPa respectively. The calculation is done for comparison with specimen 5/28. The calculated errors are listed in Table 5-6.

thickness [mm]	1.900	1.735	1.635	1.535	1.440	1.345	1.240
error for $G_{xy} = 2000$ MPa [%]	0.7	0.5	0.4	0.3	0.1	0.0	-0.2
error for $(xy = 0.3$ [%]	0.0	0.0	0.0	0.0	0.0	0.0	-4.6
error for $E_{yy} = 5000$ MPa [%]	0.0	0.0	0.0	0.0	0.0	0.0	-4.6

Table 5-6: Error in the calculated material stiffness E_{xx} for every layer of specimen 5/28, for a different G_{xy} , (xy) and E_{yy} .

In the table it can be seen that the calculations are not sensitive to improper values of the considered material constants. So the accuracy of the material constants that are used in the calculations is sufficient to achieve an accurate value for the material stiffness E_{xx} .

5.2.7 Discussion of the material stiffness results

For the injection moulded plates the test circumstances were kept identical with the Carbon/PEI tests. For every processing condition one specimen was used to do a tensile and a bending test consecutively. The results of these tests are listed in appendix C.

The tensile tests resulted in good values. The force-deflection curve was a straight line, as can be seen in the R^2 values for each fit of the tensile test. These values can be found in appendix C.

A typical example of the stiffness profile obtained by the three point bending tests is drawn in Figure 5-7. The figure also shows the material stiffness calculated with the Halpin-Tsai equations and the fibre orientation information of section 5.1. The measured points are connected with lines to make the graph better readable.

LINK Excel.Sheet.5 ":///UTWOU5\\VOERMAN\\rik\\modulus.xls"
 "grafieken![modulus.xls]grafieken Chart 2" \a \p ____

Figure 5-7: Stiffness profile as a function of the normalised distance from the core for process condition 2 into flow direction. The dashed line represents the interpolation between the stiffness based on the fibre orientation.

From the PPS GF40 measurements it can be seen that there surely is a change in modulus across thickness, which was already predicted by the change in fibre orientation. From the bending data two local maxima can be discerned. This was not expected when we look at the fibre orientation measurements only. These local maxima are found for every processing condition in the same regions at a distance of 0.4 and 0.9 from the core.

Comparison of the average modulus

	2/21	error	5/28	error	8/18	error
from tensile test	14851	-	14370	-	14899	-
from tensile test (1)	14916	0,4%	14138	-1,6%	15258	2,4%
from bending test	14743	-0,7%	13850	-3,6%	14264	-4,3%
from orientation	15650	5,4%	11110	-22,7%	11110	-25,4%

(1) results from tensile tests as reported in 'Fiberorientering, Malemaethode, databehandling og anvendelse' or. denmark

	14241	12767	14308
--	-------	-------	-------

Table 5-7: Average modulus into flow direction as measured with the tensile test, three point bending test and according to theory for the specimens of every processing condition.

As was done for the measurements for Carbon/PEI laminates the average was taken from the tensile tests and the bending tests. These are listed in Table 5-7.

As with the results from the Carbon/PEI laminates the bending tests averages result in a lower material stiffness than obtained from the tensile test. The table also shows the results of the tensile test performed previously in Aalborg, Denmark, with identical plates. There is only a small error between the tensile results.

Using the fibre orientation as discussed in section 5.1 and the material properties from chapter 4 the average stiffness was also calculated. The influence of molecular orientation on the matrix stiffness is not considered. The stiffness is then calculated with the models of Halpin - Tsai and Advani - Tucker, as discussed in chapter 3.

The average modulus for each processing condition is considerably different. Processing condition 8 has a significant different modulus, caused by the significant difference in fibre orientation.

For every processing condition the expected average stiffness based on the fibre orientation is up to 9 % higher than measured. This error is most likely caused by the inaccuracy in the measured orientation data.

5.3 Thermal expansion

In the centre of the plate the thermal expansion can be calculated using the measured fibre orientation and the material properties of the matrix and the fibres separately. To verify the results of these calculations the thermal expansion was measured in flow and transverse directions for the plates of every process condition. This thermal expansion is an 'average across thickness' because the strains were only measured at the surface, and so no change in thermal expansion across the thickness could be measured. The values obtained from both theory and experiment are compared in this section.

5.3.1 Specimen preparation

For the measurement of the thermal expansion, from every processing condition one specimen was cut to be measured. The specimens were taken out as plotted in figure 4-1. The dimensions of the specimens are 80 mm x 30 mm, the same as used in the layer removal measurements described in chapter 6.

High temperature strain gauges (Table 5-8) were applied in the middle of the plate into flow and transverse direction. The strain gauges were mounted with a high temperature epoxy based adhesive (M-Bond 610).

strain gauge ZFLA 6-350
length 6 mm
width 2.7 mm
electrical resistance 350 (1.0 (
gauge factor 2.03

Table 5-8: Strain gauge used for the thermal expansion experiment.

Because theoretically the strain gauges would cross each other, the strain gauges were shifted up to 3 mm into flow direction. The surface preparation of the specimens was performed as for the tensile test (section 5.2).

To cure the used adhesive the specimen has to be heated at 150°C and 230°C consecutively, both during two hours. Because of this thermal history, the crystallisation of the material should have reached its maximum of 60%. As mentioned in chapter 4 the crystallinity of the material is expected to be around 50% before heating, so the crystallinity of the material should have increased.

5.3.2 Description of the experiment

After the specimen preparation the specimens were placed in an oven (Instron A74-37) and connected to a whetstone bridge as described in section 5.2.1. A quartz bar with negligible thermal expansion was used for the dummy strain-gauges.

The specimens were heated and cooled one time. Then the measurements were done by raising the temperature carefully up to 180°C three times. A typical heating and cooling cycle during which the measurements were done is shown in Figure 5-8.

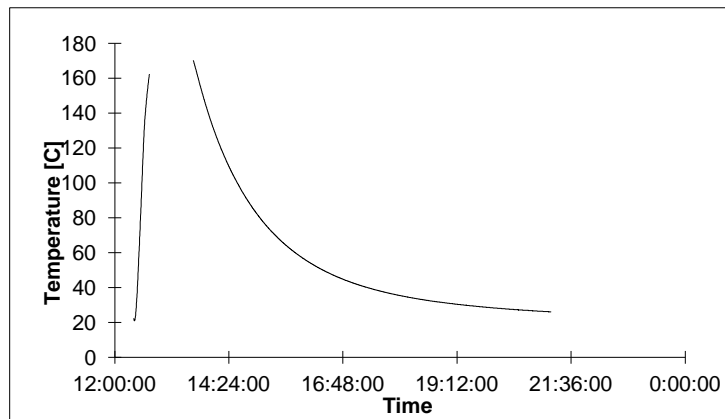


Figure 5-8: Heating (left line) and cooling line (right curve) of a specimen (8/14).

During the measurements the time, the temperature at both sides of the specimen and the strains into both directions were monitored with a computer. From the obtained data the strain is plotted against the temperature. The resulting graph is then approximated with a straight line using the least squares method. So the thermal strain ($\epsilon(T)$) is obtained as a function of temperature. The linear thermal expansion coefficient can then be obtained by taking the first derivative according to equation 5.3-1:

$$\epsilon(T) = \int \alpha(T) dT \quad \text{Eq. 5.3-1}$$

As an indication of the accuracy of the fitted line the R² value is used. Because the measurements indicated a change in thermal expansion at the glass transition temperature, the thermal expansion was determined below this temperature and above separately.

5.3.3 Theoretical calculation

Based on the fibre orientation the thermal expansion can be calculated across the thickness. With the Schapery equations and the measured Advani-Tucker orientation tensor elements (section 5.1) the thermal expansion was calculated for every processing

condition. The models that have been used have been discussed in chapter three. The resulting graph for one processing condition is plotted in Figure 5-9.

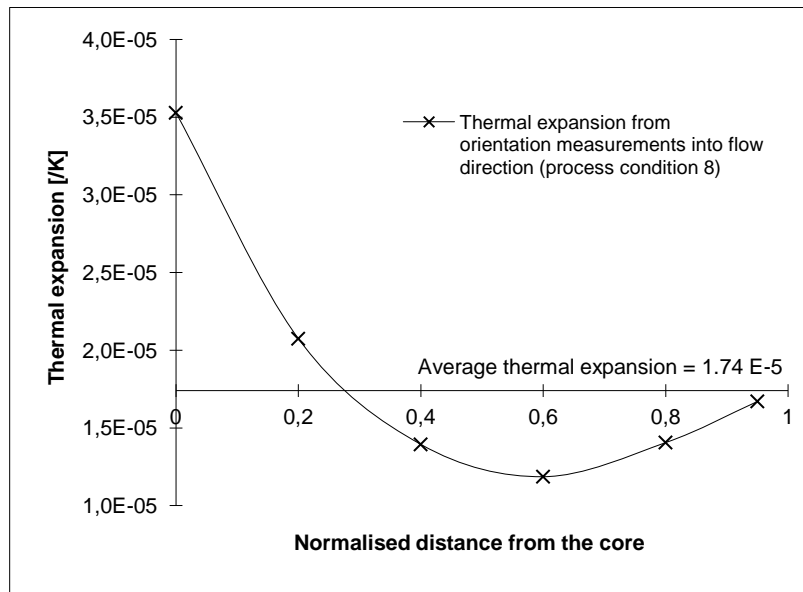


Figure 5-9: Thermal expansion across thickness of process condition 8 into flow direction, calculated from the measured orientation with the Schapery equation.

To obtain the average thermal expansion the average was calculated by taking the integral of the graph, divided by the thickness as was done for the material stiffness in section 5.2.

5.3.4 Discussion of the thermal expansion results

Figure 5-10 shows a typical example of the measured strain versus temperature.

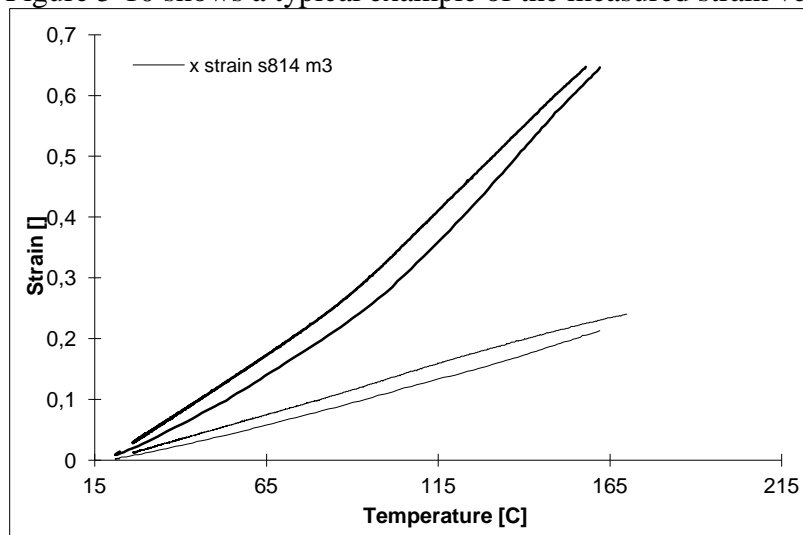


Figure 5-10: Thermal expansion of specimen 8/14 into flow direction (x) and transverse direction (y). The lower lines are measured during heating, the upper during cooling. Into transverse direction the change in thermal expansion at T_g (88(C)) can be seen.

From this graph it can be seen that the thermal strains are lower during heating than during cooling. This effect is caused by the heating speed that was too high. In that case there is a considerable difference in temperature between the surface and the core of the

plate. The expansion of the core and so the total expansion is smaller than was expected from the measured temperature at the surface resulting in a lower thermal expansion. During cooling the change in temperature is not constant, but is typically slower than during heating. Therefore the results obtained during cooling are used in this report. Into transverse direction there is an obvious change in thermal expansion above the glass transition temperature T_g . This indicates that the material still contains a considerable amount of amorphous material, like expected. The determined thermal expansion coefficients and the fit errors are given in appendix C. An average of these values is summarised in Table 5-9. The table contains also the average thermal expansion theoretically calculated from the orientation data below T_g and the error with experiment.

	<i>flow- direction</i>	<i>diff.</i>	<i>transverse dir.</i>	<i>diff.</i>
<i>Sample 2/22</i>				
from experiment under T_g	1,76E-05	-	3,62E-05	-
from experiment above T_g	1,86E-05	5%	5,04E-05	39%
from orientation under T_g (1)	2,08E-05	18%	3,80E-05	5%
<i>Sample 5/26</i>				
from experiment under T_g	1,77E-05	-	-	-
from experiment above T_g	1,87E-05	6%	-	-
from orientation under T_g (1)	2,19E-05	24%	3,69E-05	-
<i>Sample 8/14</i>				
from experiment under T_g	1,60E-05	-	3,75E-05	-
from experiment above T_g	1,63E-05	2%	5,52E-05	47%
from orientation under T_g (1)	1,74E-05	9%	4,14E-05	10%

(1) the average thermal expansion was calculated using the Schapery equations and the supplied orientation values

Table 5-9: Average thermal expansion from the experiment during cooling and from the measured orientation into both directions. The thermal expansion from the orientation is below T_g . The experimental expansion is measured below and above T_g .

In transverse direction the change in thermal expansion at T_g is considerable. Apparently the matrix has a much higher thermal expansion above T_g .

In flow direction the expansion is dominated by the fibres, because they are oriented in the flow direction mainly. There is almost no difference between the thermal expansion below T_g and above. The theoretical prediction is for both directions too high. The differences may be caused by:

bad modelling; the generalisation of Advani and Tucker that their model can be used to calculate the thermal expansion in combination with the Schapery equations may not be correct. The thermal expansion of a composite depends not only on the thermal expansion of the matrix and the fibres, but also on the material stiffnesses (as can also be seen in the Schapery equations). The model does not deal with this effect properly for a distributed fibre orientation.

wrong material data; the glass fibres or the matrix material may have a lower thermal expansion coefficient than documented. For the matrix material a variation in thermal expansion can be expected because of molecular orientation. This variation was not modelled.

As expected the specimen of processing condition 8 has a measurable different thermal expansion from the other processing conditions. This indicates that the measured fibre orientation is in good accordance with the results. The same was found with the material stiffness measurements in section 5.2.

5.4 Stress free temperature

To calculate the thermal residual stresses, the temperature from which the stresses are built up has to be known. For an unfilled amorphous material the glass transition temperature is generally considered as the stress free temperature. For a crystalline material this is the crystallisation temperature.

The material used in this report (PPS) is semi-crystalline and therefore the determination of the stress free temperature is complicated. The matrix consists of two phases, a crystalline and an amorphous phase. Both phases are present for approximately 50%. Hence the stress free temperature may be in between the crystallisation and the glass temperatures.

Chapman and co-workers [42] also studied the stress build-up of continuous fibre reinforced laminates with a semi crystalline matrix. For unidirectional plies they used the melt temperature as the temperature from which stresses build up in fibre direction. Chapman stated that the temperature from which stresses are built up is that temperature at which the elapsed time since solidification equals the relaxation time of the material. When the relaxation time is much larger, the material behaves elastic. When the relaxation time is much smaller the material behaves viscous and stresses will therefore relax. He used this model to predict the temperature for stress build-up in transverse direction for unidirectional plies. The problem with this model is that the relaxation time of the specific matrix material has to be known as a function of temperature.

5.4.1 Description of the experiment

Because there was not enough known about the material behaviour, the stress free temperature could not be predicted. Therefore it was tried to measure the stress free temperature. Specimen 8/18 was used, from which one side had been milled off. During heating of this specimen the resulting curvature should become zero when the stress free temperature is reached.

`_ INCLUDEPICTURE "U:\\rik\\report\\strfree.bmp" * MERGEFORMAT ____`
Figure 5-11: Schematic specimen for the stress free temperature measurement.

Therefore at both sides of the plate strain gauges were applied. During heating at both sides the strains increase because of the thermal expansion. At the same time the thermal stresses will reduce until zero at the stress free temperature. This results in a reduction of the curvature, so that the strains at the surface will change, both in a different way. The specimen is drawn schematically in Figure 5-11.

Resuming for this problem the strain at side 1 will be:

`_ EMBED Equation.2 ____ Eq. _ STYLEREF 1 \n _5_- SEQ Eq. * ARABIC`
`_8_`

with ϵ_0 the initial curvature and $\epsilon(T)$ the curvature at a certain temperature, being equal to ϵ_0 at the initial temperature. Similarly the strain at the other side will be:

9 _ EMBED Equation.2 ____ Eq. _ STYLEREF 1 \n _5_- SEQ Eq. * ARABIC

The stress free temperature is that temperature at which (T is zero. So at that temperature the difference in the strains is:

10 _ EMBED Equation.2 ____ Eq. _ STYLEREF 1 \n _5_- SEQ Eq. * ARABIC

5.4.2 Discussion of the stress free temperature results

During the experiment the specimen did not become flat below the crystallisation temperature T_c . Higher temperatures were needed, but for practical reasons the temperature was kept below 180(C. Possible explanations for this behaviour are: in fibre direction the stress builds up from a temperature higher than T_c (maybe the melt temperature) as was also found by Chapman for continuous fibres.

due to creep in the material after milling the specimen will not become flat again when heated up. To prove this the time between milling and heating should be very short. This is practically impossible because the applied strain gauges have to be cured previously (even at higher temperatures), and at least a period of 24 hours is needed between milling and measuring.

Concluding it can be said that the material behaviour is very complicated. Even if some temperature at which a specimen flattens could be measured, then still this would be an indication. The actual temperature from which stresses had built up may namely be dependant on factors that can not be controlled during the experiment, like the amount of crystallisation and cooling speed. A better method is required to find the stress free temperature.

For this reason it was decided to use the glass transition temperature as a minimum value for the calculations of the stresses. Independent of the stress free temperature the trends of the residual stresses can be compared in a qualitative way with the results of experiments. For a quantitative comparison the values can only be used minima.

Chapter five:

- x
- y
- tensile test
- three point bending test
- bending test
- mill off a layer
- wait 15 minutes
- calculate average stiffness
- calculate stiffness profile from three point bending test
- compare tensile and bending results with theoretical prediction
- calculate average stiffness
- calculate theoretical stiffness profile from
- fibre orientation

6. Experimental determination of residual stresses

In this chapter the layer removal experiments for the determination of the residual stresses in the plate will be described. In section 3.4 the theory of the method has been described. The first section of this chapter explains how the experiments were carried out and how each quantity was measured. Section 6.2 analyses the accuracy of different aspects that might influence the results of the experiment. This analysis is done by comparing the resulting curvatures of the different experiments rather than comparing the stresses.

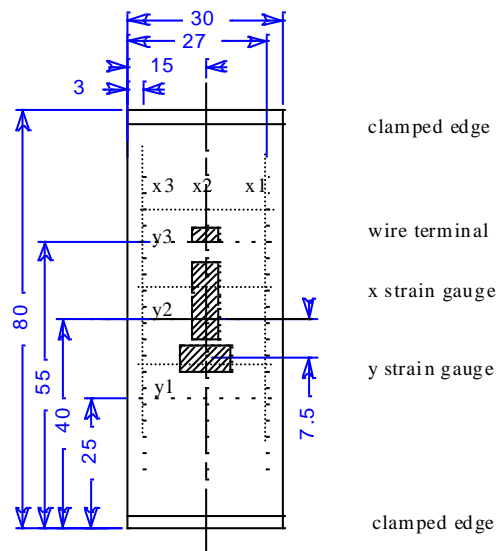
In the last section the stresses are presented that were calculated from the measurements. These are compared with the stresses calculated from theory.

6.1 Description of the experiment

For the determination of the residual stresses layers were removed. This section describes how the specimens were prepared and how the layers were removed. After each layer removal the resulting curvatures and the strains into both directions are needed to calculate the required residual moments. The consecutive sub sections explain how this was done.

6.1.1 Specimen Preparation

The specimens that were used for the measurements were carefully cut out of injection moulded plates, with the long sides parallel to the flow direction. The centre of the plate is the region of interest and so the specimens were cut out of the middle of a plate (see figure 4.1). For cutting the specimens out of the plate a liquid cooled diamond saw was used. This resulted in a nice smooth cutted edge. The dimensions of a specimen are drawn in Figure 6-1.



x1, x2, x3, y1, y2 and y3 are the scan lines.
x2, y2 and y3 cannot be scanned when strain gauges are applied.

Figure 6-1: Dimensions of a specimen and locations of the strain gauges. The dashed lines are the lines over which is scanned.

Because the strains have to be measured in both directions, strain gauges were applied in both flow and transverse direction. The strain gauge in flow direction was similar to the strain gauges used for the tensile tests (subsection 3.2.1). Because of clamping geometry the transverse strain gauge was only 3 mm long, but had the same properties. Mounting of the strain gauges was done in the same way as described for the tensile test (section 5.2).

6.1.2 Removal of a layer

To remove a layer the specimen is clamped in a block while vacuum is applied underneath it. The strain gauges fit precisely in the holes of the vacuum chamber. In Figure 6-2 the clamping is drawn schematically.

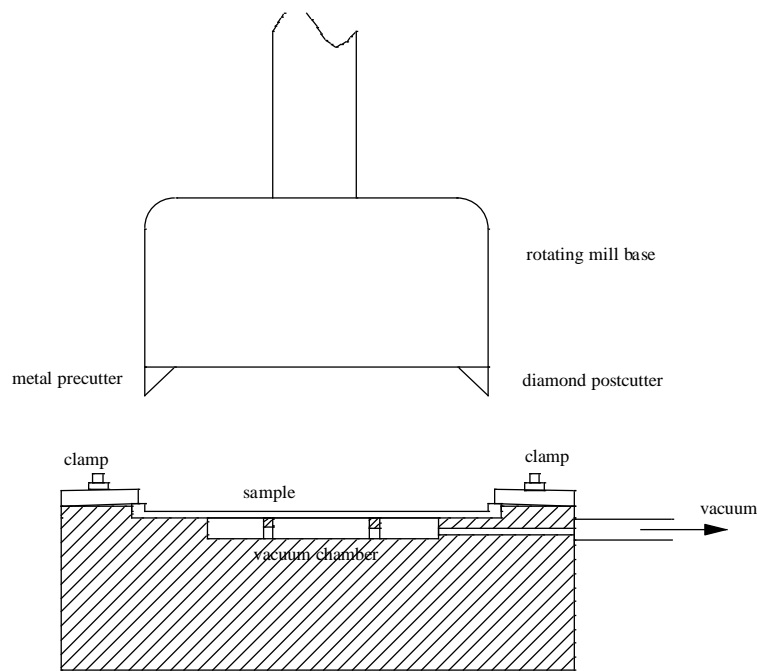


Figure 6-2: Schematic drawing of the clamping of the specimen and the mill. There is room for strain gauges underneath the specimen where vacuum is applied.

To mill off a layer, a rotating mill base containing two cutters moves over the surface at a layer depth of 0.06 mm. The milling process was exactly the same as was used with the bending tests (see section 5.2). One cutter is used for material removal and is made of a special metal alloy. A diamond post-cutter is used for smoothing. The mill base rotates at a speed of 1400 r/min, moving with a feed rate of 80 mm/min. Each specimen was re-used until 15 layers were removed.

It is assumed that the milling process does not affect the residual stresses in the plate. Previous work [10] confirms this assumption.

The temperature of the specimen has a significant influence on the curvature. Because an increase of temperature was observed during milling, the specimens were kept untouched for 15 minutes, before curvature measurements and strain readings were taken. Fifteen minutes was enough, since the strain gauges stabilised after ten minutes.

6.1.3 Dimensions measurement

When a specimen was cut out of a plate, first the thickness, length and width were measured. The width was measured at the three locations, where the y-scanning lines in Figure 6-1 are located. The length was measured at the three places where the x-scanning lines are located. The average of the three values for length and width were used. In all cases the maximum error in these values was 1.5 %.

After these measurements some of the specimens were coated with white spray to optimise the laser beam reflection needed for the curvature measurement, as explained in the next subsection. The thickness of the coating layer was found to be 0.015 mm.

After the removal of each layer the thickness of the plate was measured with a micrometer near the points where the x and y scan lines cross each other, resulting in 9 values.

There were some specimens without strain gauges. For them all these point could be measured. For the specimens with strain gauges the middle three points could not be measured. In most cases the thickness varied up to ± 0.03 mm due to inaccuracy of the milling machine and due to deformation during clamping. For the calculations the average was taken from these points, and then the paint thickness was subtracted.

Because of clamping at the ends of the specimen small rims of material were left over at the specimen. The energy calculations compensate for these stiffening rims. Therefore the width of these rims was measured with an accuracy of 0.05 mm.

6.1.4 Curvature scanning

The curvatures of the specimens are measured on a x-y table using a three point support. The initial curvature that was measured before milling was subtracted from the curvatures that were measured after each milling step. On the table the height of the specimen was scanned using a laser. In the length direction of the specimen 31 points were measured with an interval of 2 mm. In the transverse direction 29 points were measured with an interval of 1 mm. The accuracy of the x/y movement lies within ± 3 micron. The measured data were logged by a computer. The set-up of the measurement system is drawn in Figure 6-3.

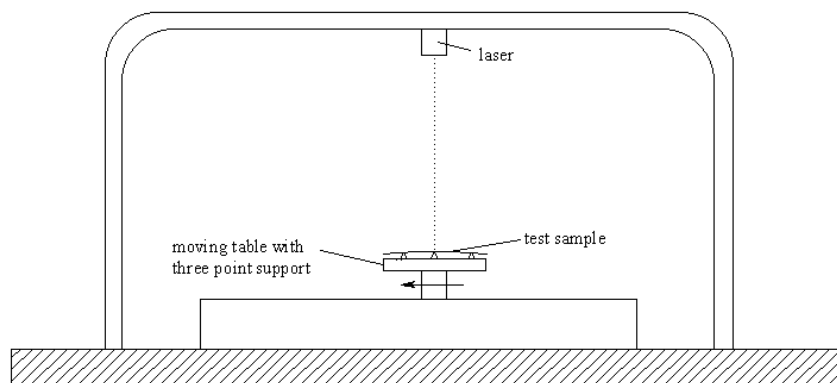


Figure 6-3: The equipment to measure the curvature schematically. The specimen is moving on a three point support while a laser scans the height of the specimen. Data is logged by a computer.

The lines over the specimen that were scanned this way are indicated with dashed lines in Figure 6-1. In both the longitudinal and the transverse direction three lines were scanned for the specimens without strain gauges. For the specimens that had strain gauges only x1, x3 and y1 could be scanned.

The reflection of the laser beam by the specimen has been a problem in the past. This was mainly caused by the transparency of the material matrix and by surface roughness. During the layer removal experiments with the glass filled PPS scanning results appeared to be subject to these effects. Therefore a coating was applied using white spray paint, thus overcoming the reflection problems.

6.1.5 Curvature determination

In theory the deformations of the plates are assumed to be circular, indicated by only one value for every direction, the curvature κ . In previous work by Peeters and Eijpe it was found that the shape of a non-symmetric continuous fibre reinforced laminate is really circular. But for injection moulded plates the fibre orientation may change along the flow-path as well as transverse to it. This means that there may be a change in fibre orientation in scanning direction. This change of fibre orientation may result in a shape that is not completely circular. From the computer simulations (section 1.1) however we have seen that the fibre orientation does not change within the limits of the plate dimensions. In practice this circular shape was found as well. Figure 6-4 illustrates this circular shape. The scale of this figure was increased to make the accuracy visible.

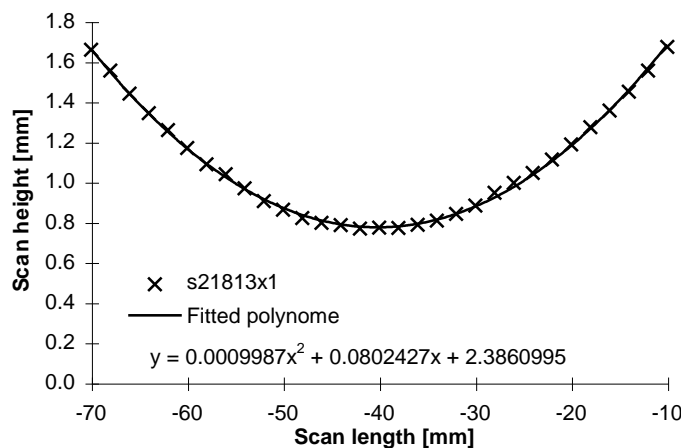


Figure 6-4: Fit of a series into flow direction with a strong curvature (13 layers removed of specimen 2/18). The polynomial fits very well. Note the difference in scale of the axes to improve visibility.

To fit the curvature a (circular) shape function has to be chosen from which the constants can be solved using the least squares method. The curvatures follow then with:

$$\kappa_x = \frac{d^2z}{dx^2}$$

Eq. 6-1

$$\kappa_y = \frac{d^2z}{dy^2}$$

For an infinitesimal scan length a real circular fit and a second order polynomial fit are identical. To verify the accuracy of these functions both fits were performed for every data series and the one with the smallest quadratic error was chosen. The R^2 value was

calculated as a measure of the accuracy for every fit. For the larger curvatures the R^2 value was between 0.920 and 1, which indicates that the fits were accurate.

Also in y direction a good fit was found for the stronger curvatures (Figure 6-5). In the figure we see that the outer points of the series do not fit very well. These outer points were measured very close to the edge of the specimen. To get the curvature in the middle of the plate, eliminating this edge effect, the first and last three points were thrown out from the data series for curve fitting .

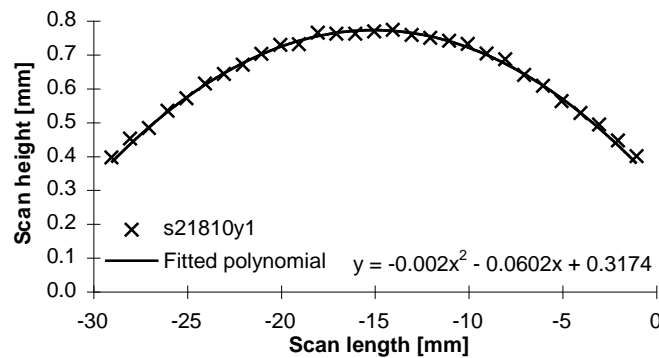


Figure 6-5: Fit of a point series in transverse direction of flow with a strong curvature (10 layers removed of specimen 2/18). The first and last three points indicate edge effects.

For smaller curvatures (i.e. when little material has been removed) the scatter of the points around the fit are larger. Also in this case a small edge effect can be seen in the outer points of the scans, which were thrown out for the calculations (see Figure 6-6 and Figure 6-7).

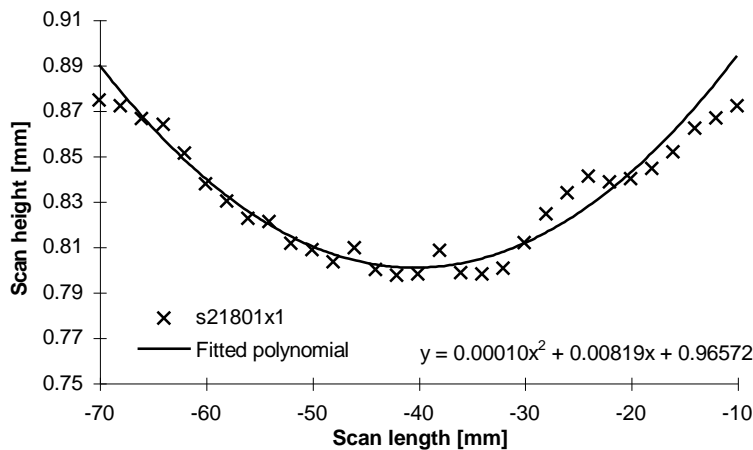


Figure 6-6: Scatter in a scan in flow direction for a very small curvature (1 layer removed of specimen 2/18). Note the amplification of the error by decreasing the scale.

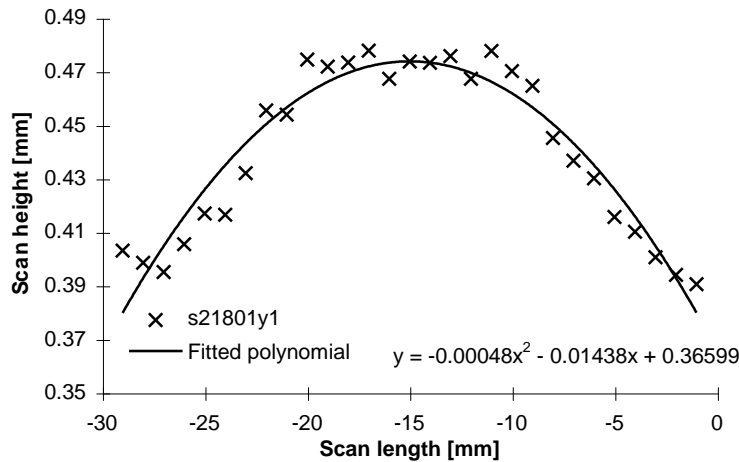


Figure 6-7: Scatter in a scan in transverse direction for a very small curvature (1 layer removed of specimen 2/18).

6.1.6 Strain measurement

Specimens 2/18, 2/19 and 8/16 were provided with strain gauges. For these specimens the strain readings were put to zero at the beginning of an experiment. Fifteen minutes after each layer removal the strain readings were taken in flow and transverse direction.

6.1.7 Calculation of the stresses from the moments

After the layer removal experiments the moments that induce the deformations were calculated for the specimens with mounted strain gauges. For this a minimisation technique of the potential energy was used as described in section 3.4. The material stiffness calculation for every layer was based upon the measured fibre orientation (section 5.1) and the material properties of chapter 4. A dedicated Mathematica program was written to perform the necessary calculations. The listing can be found in appendix E. The calculations after the measurements result in a moment profile as a function of thickness. This profile needs to be fitted with a correct function so that the stresses can be calculated from this function. There is no particular reason to assume any function on these moments data. For a compression moulded laminate the moment development is assumed to be linear, and therefore a linear fit is used for those calculations. For an injection moulded product, the shape of the moment profile as a function of removed material is unknown because the function prescribing the change in fibre orientation is unknown (in an exact way) and because other stress effects may be present. It is tried to find functions that can prescribe the moment data best. Three fitting techniques were considered to fit the moment data: polynomial approximation, spline approximation and moving window filtering, as discussed in subsection 3.4.3.

In appendix D the different types of fit are compared for specimen 8/16 in flow direction. The requirement that should be met by the fits are resumed here:

For the moment fit:

- the fitting line should be within the error of the data points
- because the error prediction is complicated, the fitting line should be as close to the data points as possible, so the R^2 value has to be minimised
- the shape of the line must be location independent because of unknown shape

For the resulting stress profile the demands are:

- symmetric in the core because product symmetry is assumed
- area under the graph should be zero for force equilibrium
- high resolution to obtain as much information as possible
- no oscillation between the data points

With these criteria in mind the can be concluded from different moment fits:

1. polynomials: Although not location independent, this type of function was used because of ease of use and interesting results. The moment points were fitted well with a fourth or sixth order polynomial. But particularly in the end points (at the surface and in the core) the polynomials behaved badly. For that reason the polynomial fit was rejected.
2. B-splines: Only for the B-spline approximation the symmetry and zero force conditions were used. This resulted in a bad fit at the core region of the moments points for splines of every degree. Interesting to note is that for a first order spline fit (which is a straight line from point to point) the stresses can be calculated for every measured layer so that the moment points are used optimally and edge errors are minimised. In the meanwhile the measured error is amplified maximally. So this is an approximation that gives an extreme indication of the average stress level in every removed layer when no error in the data is assumed.
3. moving window filtering: This method can smooth the graph so that random errors are eliminated. With higher order splines a similar effect can be reached. The advantage above the splines is that the stress equilibrium condition was not used. This resulted in a better fit in the core region.

There are two contradictory demands. First the resolution of the stress profile must be as high as possible. The best fit that accomplishes this requirement is the first order spline fit with as much intervals as possible (the maximum number of intervals is reached when the graph starts oscillating).

The second demand is based upon the assumption that the stress profile should not oscillate. Because it is assumed that the material properties do not change instantaneously across the thickness it is also expected that there are no local peaks in the stress profile. This has been used as a criterion to prevent oscillation.

The moment points are subject to measurement errors, and therefore it was supposed that the smoothness requirement was most important. For these reasons the window 2, 7 fit (7 points window size, fitted with second order polynomial) is used for comparison in this chapter.

As an indication of the error that may be possessed by a moment point, the maximum and the minimum moment was calculated, with the maximum and the minimum curvature that was measured with the scan lines x1 and x2. Figure 6-8 shows an example of the fit for specimen 2/18 with the error bars indicating this maximum and this minimum.

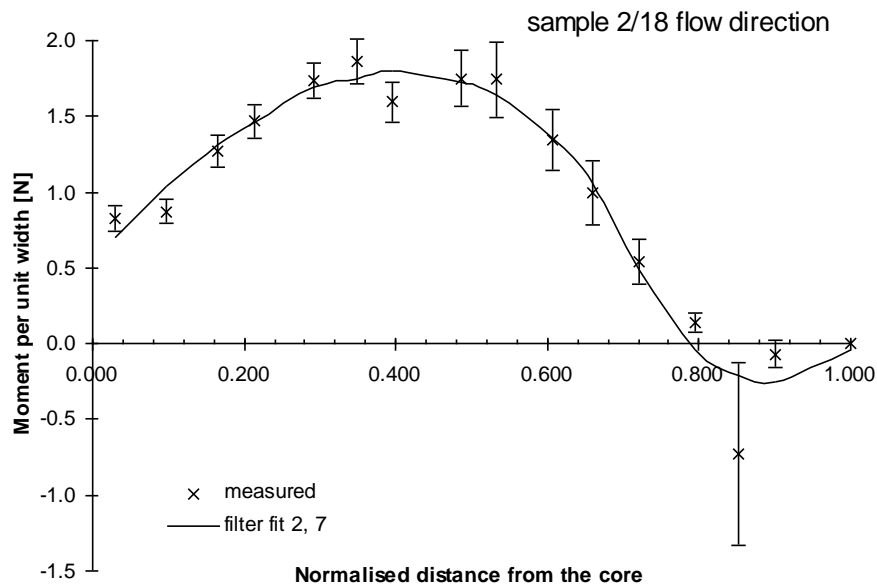


Figure 6-8: Example of a moment fit. The error bars indicate the maximum and the minimum value of the determined point calculated from the maximum and the minimum curvature that was measured.

It can be concluded that the error in curvature has a significant influence on the moment data. The difference between the fitting line and the data points can almost completely be explained by the error in curvature. The error is eventually larger because of errors in material data, thickness, transverse curvature and in strain measurement.

6.2 Validation of the measurements

In this section the following assumptions made for the plates are verified:

1. in-plane symmetry
2. no angle-ply behaviour → no twisting curvature
3. symmetry in thickness direction
4. negligible effects of the coating
5. no time dependant behaviour during the experiment

6.2.1 In-plane symmetry

In first instance specimens were used without strain gauges. This gave the possibility to make multiple scans over the surface of the plate, and so the curvature at several locations could be determined. Figure 6-9 shows the measured curvatures obtained from plate 5/24 in flow direction. The data points are connected with lines to indicate the trend.

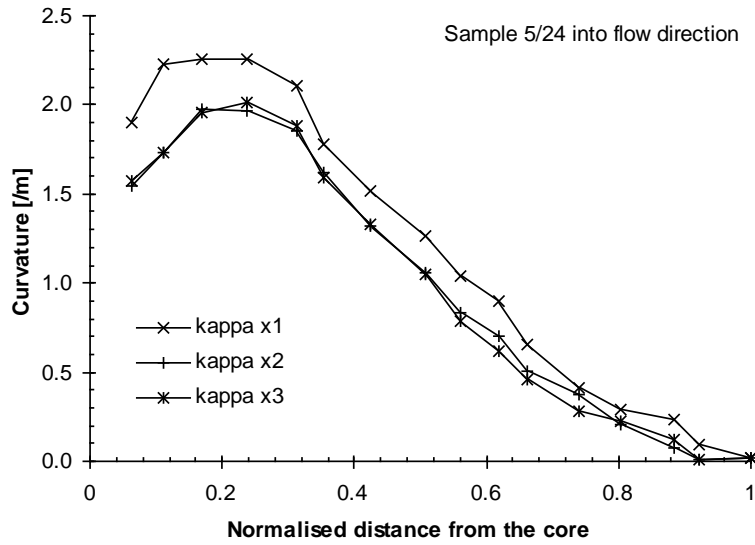


Figure 6-9: Curvatures of the three different scan lines as a function of thickness of specimen 5/24 in flow direction.

As can be seen in the graph the curvature at one side of the plate is consistently stronger than at the other side. A similar behaviour was found for every plate in flow- as well as in transverse direction. Most likely this effect is caused by the difference in plate thickness that had a consistent error after each milling cycle. One side of the plate was slightly thicker. Another explanation for this effect is that the fibre orientation would change in transverse direction. For the calculations of the moments always the average of the different curvatures was taken as was done for the thickness data.

6.2.2 Twisting curvature

In the calculations it is assumed that no twisting curvature is present after layer removal (no angle-ply behaviour). To verify whether any twisting curvature is present measurements were done from which the twist can be recovered. Twist can be determined by scanning the surface over different parallel lines.

Therefore specimens had to be used without strain gauges. Figure 6-10 shows the measured twist of specimen 2/20. The twist was calculated by fitting the measured series

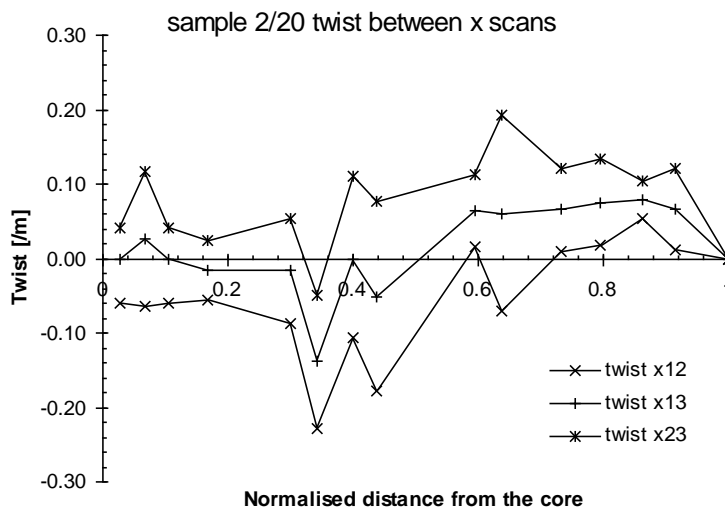


Figure 6-10: Twist as a function of thickness for specimen 2/20 for scans in x direction.

with a straight line. Then the difference in slope was taken, divided by the distance between the lines. In formula notation:

$$\kappa_{xy} = \frac{\frac{\Delta w_3}{\Delta x_3} - \frac{\Delta w_1}{\Delta x_1}}{y_3 - y_1} \quad \text{Eq. 6-2}$$

Because the specimen was scanned over three lines, the twist could be calculated between the 1-2, 2-3 and the 1-3 lines.

From the results the following can be concluded:

- the measured twisting curvature is generally smaller than 0.00020 /mm
- the twisting curvature is not constant across the plate
- the twisting curvature is relatively large when little material has been removed. In that case the twist is of similar magnitude as the curvatures. This indicates that depending on the actual values of the elements B_{16} , B_{26} , D_{16} and D_{26} from the ABD matrix the actual residual stress may contain extra error in the region near the surface.

6.2.3 Symmetry in thickness direction

To verify the symmetry of the plates the curvature profiles from two specimens of the same processing condition were compared. Specimen 2/18 was milled at the opposite side as specimen 2/19. Both specimens were not coated and no strain gauges were used. For the curvatures at every thickness the average of the curvatures for three different scans was used. The results in flow-direction are shown in Figure 6-11.

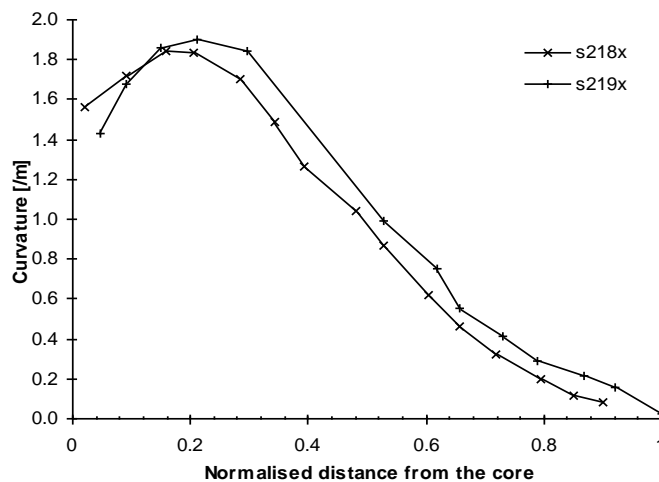


Figure 6-11: In-plane symmetry verification; Curvatures of plate 2/18 (upside down) and 2/19 into flow direction.

From this graph it can be concluded that the difference in symmetry is within the error that was measured between the different scan lines, as shown in the previous subsection. The difference in curvature into transverse direction was even smaller. Therefore it can be concluded that a difference in symmetry could not be measured for the plates of process condition 2 and the symmetry assumption is justified.

6.2.4 Effects of the coating

To verify whether the used coating had some influence on the residual stresses and/or the material stiffness, the curvature profiles of 2/19, 2/18 (both not coated) and 2/20 (coated)

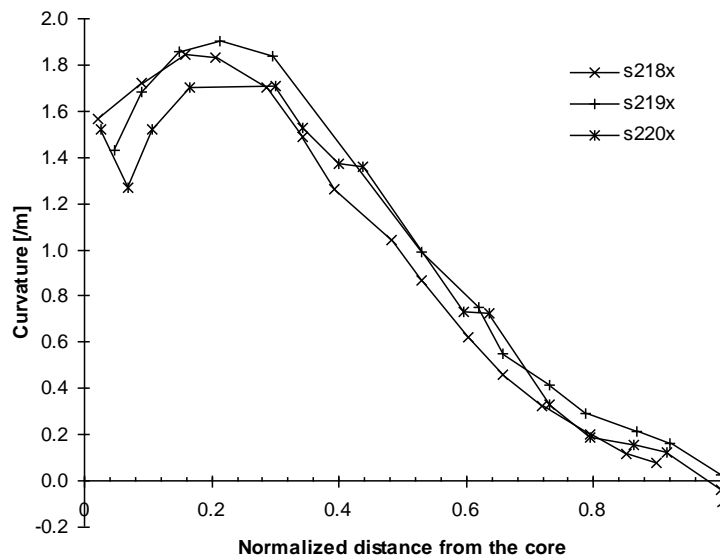


Figure 6-12: Comparison of specimens with (2/20) and without (2/19) coating.

were compared. The curvatures that were measured from the coated specimen 2/20 were all very close to the curvatures measured with the non-coated plates. Again the differences between the curvatures are so small that they are within the measurement error. As for the symmetry results, also for the coating the measurement differences are within this error and so no influence of the coating could be found.

Note that the coating improves the approximation of the small curvatures slightly, as can be seen in the R^2 values in the appendix data. For this reason it was chosen to do all measurements with coating.

6.2.5 Time and temperature effects

As mentioned before the unstable behaviour immediately after milling is contributed to the specimens temperature. There may be other effects that influence the unstable behaviour in the first ten minutes, like creep or relaxation. It is expected that these effects are negligible because the fibre reinforcement prevents the material to relax or to creep. It is difficult to make a quantitative prediction of the time dependant behaviour since both effects are related to each other and time dependant behaviour of the material is not known.

The most important thing to know is whether strain and stress change after layer removal in such an amount that the measurements are not reliable. Therefore the strain in a specimen that was used for layer removal was monitored during several weeks. With a fit on the data the strain can then be extrapolated and so that the strains could be recovered immediately after milling, when temperature effects would not be present.

From the experiment it was found that (the absolute value of) the strain increased with time. This suggests that creep behaviour dominates, since stress relaxation would have resulted in a strain decrease. It was tried to find a fit function for the measured data.. For this fit a generalisation of the Kelvin-Voigt model could be used:

$$D(t) = \int_0^{\infty} L(\tau) \cdot \left(1 - \exp\left(-\frac{t}{\tau}\right)\right) d\tau \quad \text{Eq. 6-3}$$

With $D(t)$ the time dependent compliance and $L(\tau)$ any function. This formula is in fact a (infinite) summation of all different Kelvin-Voigt elements in a spectrum. Unfortunately not enough data were available to fit this equation. Therefore a simplification with only one Kelvin-Voigt element is used, but also this type did not fit the data very well. A better fit was obtained with the empirical formula [40]:

$$D(t) = a + b \cdot t^{\frac{1}{3}} \quad \text{Eq. 6-4}$$

with a and b constants. Since only strains are available a relationship between the strain and the compliance is needed. For pure creep the residual stress is independent of time, so that can be written:

$$\varepsilon(t) = \sigma_0 \cdot D(t) \quad \text{Eq. 6-5}$$

with σ_0 a constant, and therefore:

$$\varepsilon(t) = \hat{a} + \hat{b} \cdot t^{\frac{1}{3}} \quad \text{Eq. 6-6}$$

Figure 6-13 and Figure 6-14 show the measured data and their fits. Note that only the time scale is logarithmic.

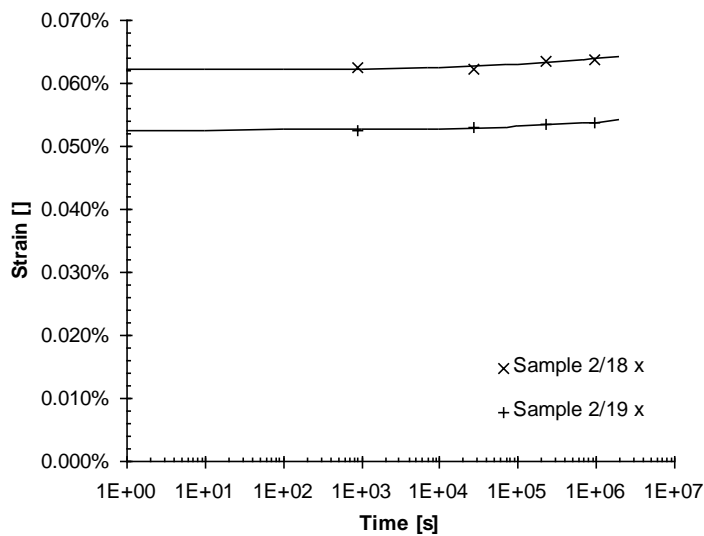


Figure 6-13: Change in strain in time of specimen 2/18 and 2/19 in flow direction.

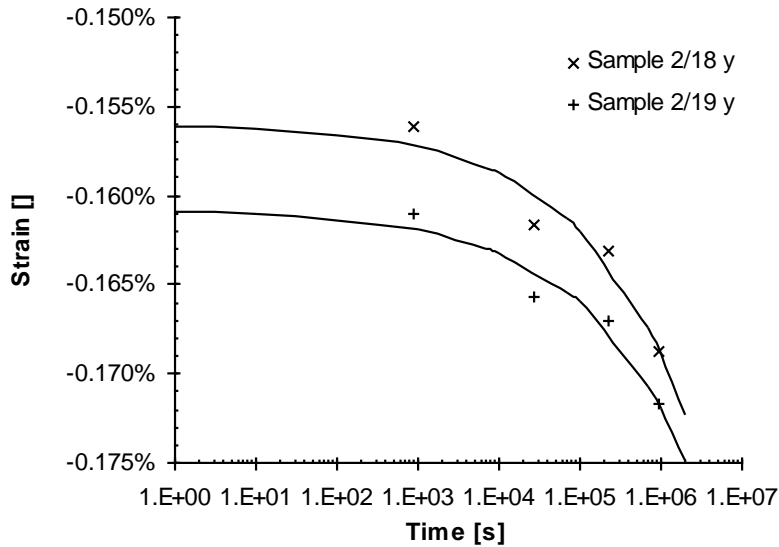


Figure 6-14: Change in strain in time of specimen 2/18 and 2/19 in flow direction.

It can be seen that the points can not be fitted perfectly. Apparently stress relaxation is also present in a smaller amount. Also the short term history of the strains may influence the strain measured at $t = 900$ s. (remember that before the measurement of the first point the specimen has been deformed several times during the layer removal experiment of about 8 hours).

Extrapolation of the graphs for $t \rightarrow 0$ gives an indication of the strain directly after milling if no temperature effects were present. From this information it can be concluded that the measured error due to creep and relaxation is negligible. A similar behaviour is assumed for the curvatures.

6.3 Discussion of the layer removal results

In this section the results of the layer removal method are discussed. First the obtained curvatures of the specimens are compared instead of the resulting stresses. This has been done because there is almost no theory introduced to obtain the curvature values. Beside some necessary assumptions (see section 6.1.5) the curvatures are the values that are most close to the real measurements.

6.3.1 Comparison of the curvatures from the different processing conditions

Measurements were done on plates of processing condition 2, 5 and 8. The process conditions of these series are listed in section 4.3. Figure 6-15 shows the obtained average curvature profiles as a function of removed material for the different specimens, in both directions. A complete overview of all measured (twisting) curvatures and strains can be found in appendix C.

In transverse direction no meaningful differences can be seen. All curvatures are within the error of measurement. In flow direction some differences can be seen. Although there is a difference between the maximum curvature for the plates of series 2 and 5 at 0.2, the

difference is too small to draw conclusions from. The curvatures of series 8 in flow direction are larger than the curvatures of series 2. For this reason a different stress profile can be expected for 8/16 in flow direction.

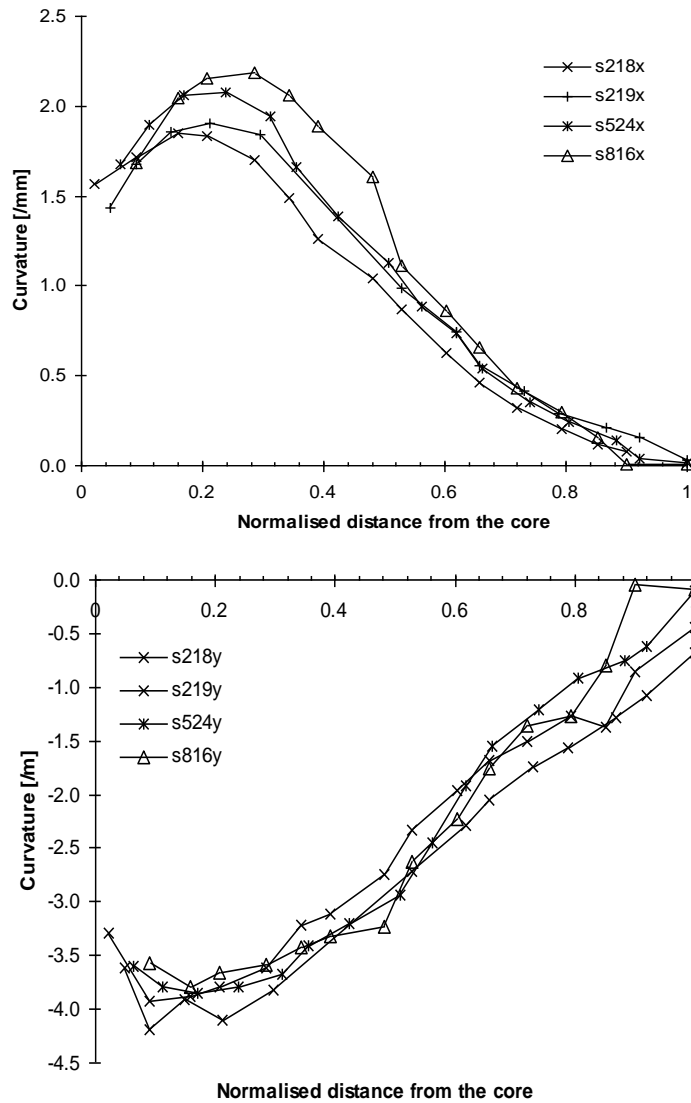


Figure 6-15: The average curvatures for the different process conditions (2, 5 and 8) in flow (above) and transverse direction (below).

6.3.2 Experimental stresses

From the curvature profiles and the measured strains the moments in the material for every plate thickness were calculated. For these calculations the material stiffness is needed as a function of thickness. This was done using the Halpin-Tsai equations and the Advani-Tucker tensor constants that were measured (see section 5.1). The orientation was interpolated between three points with a second order polynomial to get the orientation for every layer.

For the moment fits it was chosen to use the window 7, 2 window filtering technique to calculate the stresses. This results in smooth lines without too much loss of detail that can be compared. To have an indication of the stresses that can be obtained from the moments without smoothing, also the stress profiles were calculated using first order splines. The moment fits and stresses with both methods for all measurements can be found in appendix C.

Figure 6-16 shows the obtained stress profiles as a function of thickness for the specimens of process condition 2 and 8.

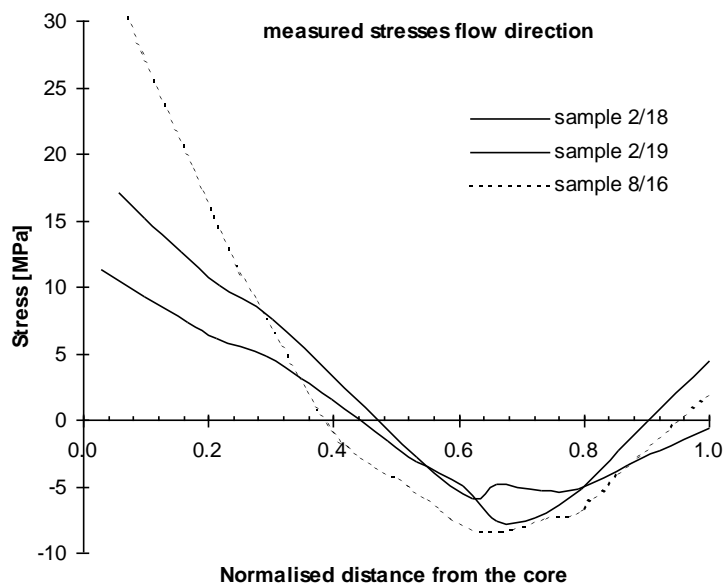


Figure 6-16: Measured stress profiles in flow direction for process condition 2 and 8.

In *flow direction* the stress profiles have similar shapes. In the core stresses are obviously positive. The maximum stress comes above 12 MPa here. This is a considerable amount of the total material strength (The documented value for material strength of the composite is 121 MPa). In the region of 0.4 (40% of half the thickness) the stress profiles change sign and become negative in the region between core and surface. A minimum stress of -8 MPa is measured. Just at the surface the stress tends to become slightly positive again. It was already seen that the fibre orientation changes also in this small region. Specimen 8/16 seems to have the largest stresses in the core region.

Figure 6-17 shows the obtained stresses in *transverse direction*. In the core region very high compressive stresses are found. They raise steadily and change sign at 0.4. In the surface region the stresses raise up to +25 MPa.

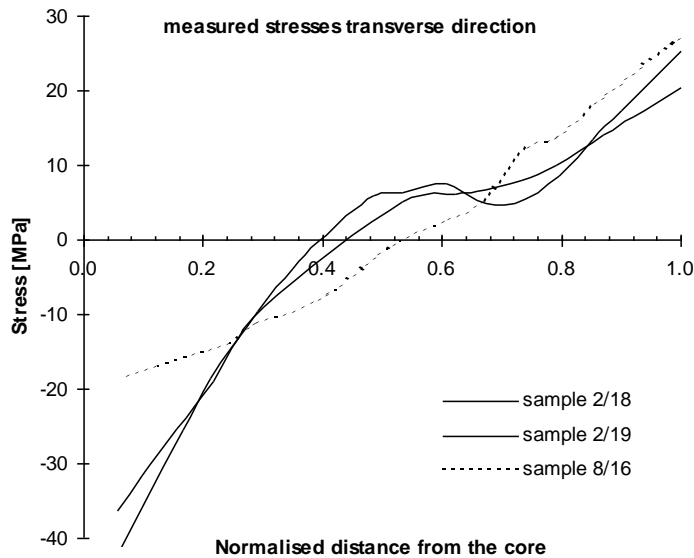


Figure 6-17: Measured stress profile in transverse direction for process condition 2 and 8.

Particularly for the stress profiles in transverse direction the lines of the specimens of processing condition 2 (2/18 and 2/19) are identical. For all profiles stress equilibrium is not met. In flow direction the integral of the stresses over the thickness are always positive, and in transverse direction they are always negative. Table 6-1 shows the results of the calculated integrals.

<i>specimen</i>	<i>flow direction</i>	<i>transverse direction</i>
2/18	0.90	-2,97
2/19	2.43	-2.66
8/16	3.36	-0.42

Table 6-1: Error in stress equilibrium for every specimen in both directions for the window 7,2 fit [MPa].

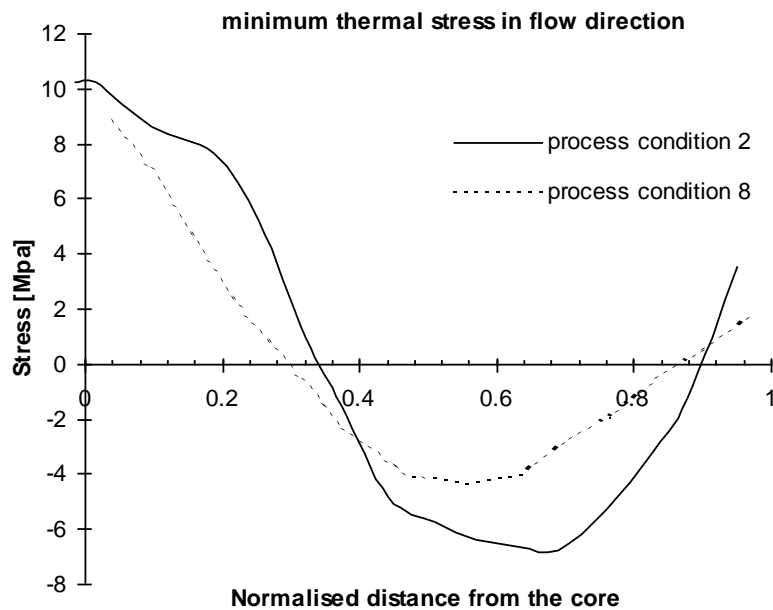
These values indicate that there is a structural error in the measurements. It seems that the error in one direction is always smaller when the error in the other direction is larger. If this is a structural behaviour, there may be a problem with the equilibrium of the anti-clastic deformation. If the curvature in flow direction is larger, the specimen in transverse direction is prevented from curving and vice versa. It may be that equilibrium in this state is not very stable. Another explanation can be that there is an error in the used material stiffness. The material stiffness in both directions is related to each other with the orientation tensor. When the used orientation in one direction is too high, the stiffness is calculated too high, and the obtained stress will be higher. In transverse direction the opposite will occur.

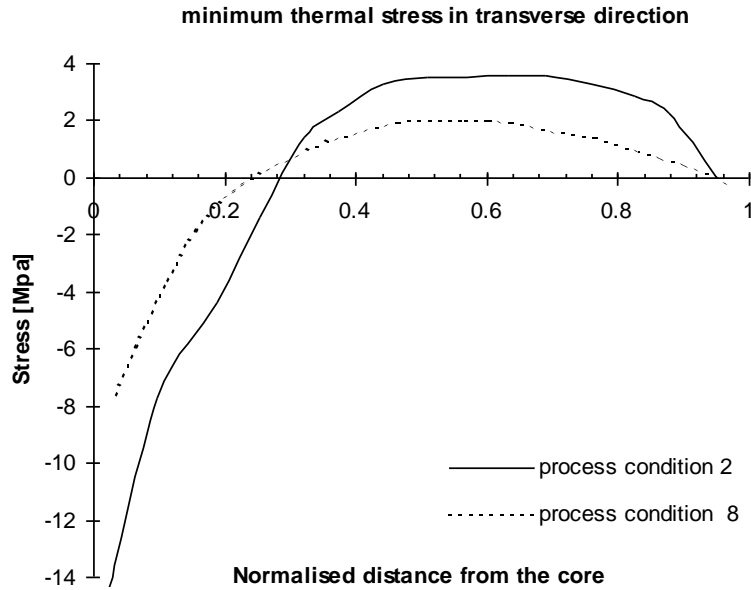
A final error-introducing problem that may be present is that the milling process influences the stresses in the newly obtained surface. It is suspected that during the milling process plastic deformations take place. This means that the stresses are disturbed up to a certain depth in the specimen. When it is assumed that this depth is independent of specimen thickness, which is reasonable, the influence of this disturbed region becomes relatively larger when more layers are removed. This means that particularly the obtained stresses in the core region are erroneous. If this is true, the difference in stress equilibrium can also be explained. For future work the milling process should be inspected and if there

is a consequent error with a certain depth, the relative error could be reduced for thicker specimens.

6.3.3 Theoretical stresses

Theoretical stresses were calculated with the CLT as explained in section 3.2. The used material stiffness was the same as used in the previous subsection for the stress measurements. The thermal expansion as a function of thickness was calculated from the measured orientation (section 5.1), the material properties of chapter 4 and the Schapery equations. It was found that the stress free temperature could not be determined (see section 5.4). Therefore the glass transition temperature was used as a minimum temperature from which stresses are built up. The calculated profiles are shown in Figures 6-18 for processing conditions 2 and 8.





Figures 6-18: Theoretical minimum stress profiles for process condition 2 and 8 in flow (above) and transverse direction (below).

In both the flow and the transverse direction the theoretical stresses are smaller for processing condition 8. This can be explained by the fact that the difference between the fibre orientation in the core and at the skin is smaller. Therefore the change in thermal expansion across the thickness is smaller and so stress build up is smaller.

The results of these calculations can be compared with the stress calculated with the stiffness obtained from the three point bending test as explained in section 5.2. Figure 6-19 shows the difference in profile that is obtained.

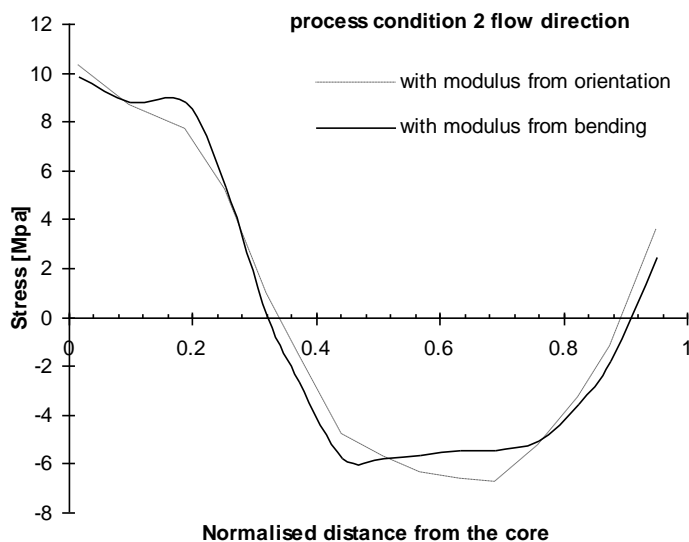


Figure 6-19: Theoretical stress profile calculated with material stiffness calculated from the fibre orientation and the stiffness obtained from the three point bending test for process condition two..

From the graph it can be seen that the shape of the stress profile becomes more squared with the measured modulus. The layered nature of the plate is more pronounced. It is clear that a good estimation of the material properties is important for a reliable stress calculation.

It is important to realise that the thermal expansion that was used in the calculations is still based on the fibre orientation for both cases.

6.3.4 Comparison of theory and experiment

The theoretical stress profiles have similar trends as the experimental profiles of Figure 6-16 and Figure 6-17. Similar to the measurements in flow direction the theoretical stresses are obviously positive in the core and negative at some distance from the surface. The opposite is the case for the transverse direction. In flow direction the fibre orientation tends to become positive again at the surface for both theory and experiment.

The theoretical profiles change sign closer to the core than the measured stresses. It is supposed that this is related to the equilibrium error in the experimental stresses. When equilibrium was reached better, the zero-stress axis might be shifted so that the axis is crossed more closely to the expected point.

In transverse direction the largest stress was found in the core region, being compressive. The stress in the core is somewhat smaller for specimen 8, similar to what was found in the experiments. The shape of the profile is different. In the experiments almost a straight line was found whereas theory shows stresses constant between the surface and core region and dropping at the surface. Apparently the model is not appropriate here. Possible explanation for this behaviour are:

- the fibre orientation is not completely known at the surface. The fibre orientation may change very quickly in this region because of complex (fountain) flow effects, or the fibre orientation in this region is not even planar, but has relatively much out of plane orientation.
- other types of stresses like thermally induced stresses at solidification may have significant influence in this region so that they can not be neglected

In flow direction the theoretical stress profiles resemble the measured profiles very well. In the core sample 8/16 becomes much more positive than expected from theory. There is no explanation for this line. From the orientation that was measured the opposite was expected. It is not clear whether an error was made in the orientation data or whether other stress effects are present.

It is difficult to make a quantitative comparison between the theory and experiment. The theoretical stresses should be higher because it is likely that stress will build up from higher temperatures. But even when the stress free temperature was known, the calculated stress could be smaller than the measured stress because of stress relaxation. For a temperature independent thermal expansion it can be shown that the theoretical stresses are proportional to the temperature difference. So a stress free temperature of 156° C would result in twice as high stresses as was calculated (88 °C) at a room temperature of 20 °C.

7. Conclusions and discussion

In this report a first step is made on the area of stress prediction in fibre reinforced injection mouldings. The goal was to model and measure the residual stresses in short fibre reinforced injection moulded plates. Therefore a model was introduced and the predictions were verified with the measurements that were done.

In section 7.1 the conclusions are summarised that can be drawn from the modelling and experiments discussed in this report. A practical consideration that can be made on the basis of these conclusions is discussed in section 7.2. Section 7.3 discusses recommendations that might be useful for future work.

7.1 Conclusions

From the aim of this report five questions were derived in the introduction. Here they are repeated and answered on the basis of this report:

1. What is known about residual stresses in injection moulded products and what stress effect is expected to be dominant in fibre reinforced ones? In literature three important effects that induce residual stresses are reported. The most important stress effect is caused by the change in material properties across the thickness.
2. How can the material properties be modelled? Methods have been found to describe the fibre orientation (Advani - Tucker). With the orientation tensor the material stiffness (Halpin - Tsai) and thermal expansion (Schapery) can be predicted. these properties are discussed in chapter three.
3. How can the stress in a plate be modelled? The plate is considered as a layered structure. For plates that are symmetric around the centre the Classical Laminate Theory can be used. For non-symmetric plates a minimisation of the potential energy can be used.
4. Are the models for material characterisation (i.e. the parameters in the stress predictions) accurate? Prediction of the fibre orientation with a computer simulation did not give accurate results. The prediction of the material stiffness was accurate compared to experiment, the thermal expansion prediction was not accurate.
5. Is the stress prediction in accordance with the theoretical predictions? Yes, the theoretically predicted stress profiles have similar trends with the experimental profiles.

Beside these main conclusions other conclusions that have been found during the project are listed in subsection 7.1.1 to 7.1.3.

7.1.1 Determination of the material properties

For a good calculation of thermal residual stresses and for a good interpretation of the layer removal measurements the material stiffness must be precisely known as a function of thickness. For the theoretical calculation also the thermal expansion and the stress free temperature are needed. For the determination of these properties the following is concluded:

- material stiffness as a function of thickness can also be determined with a three point bending test. The test should be done in two directions. This can be difficult to realise because the fibre orientation should not change in the plane of the used specimen.

7.1.2 Experimental determination of residual stresses

Concerning the layer removal method to determine the residual stresses the following is concluded:

- care should be taken that the fibre orientation is uniform in the considered area
- during experiment time dependant effects are negligible for the considered material
- for a qualitative comparison the comparison of curvatures saves a lot of time because no strain gauges have to be applied and no calculations have to be performed. The smoothness and the height of a curvature profile give a good first indication of the residual stress
- a minimisation of potential energy is found to be a good way to calculate the residual moments as a function of removed material
- the window filtering is found to be the best technique to fit the moment data in the stress determination after layer removal. In this report seven points per window and second order polynomials gave best results.
- although the window filtering technique is found to be best the results are still sensitive for errors in the edges of the profiles (at the surface and the core).
- accuracy of experimental results can be improved when curvatures can be obtained more accurately. This is related to the accuracy of the layer removal process
- residual stresses were present with an amount of up to one third of the documented material strength
- there is an error in stress equilibrium which suggests that the layer removal experiment is not accurate. Most likely this error is caused by plastic deformation during the milling process

7.1.3 Theoretical stress prediction

Concerning the modelling of the residual stresses the following is concluded:

- the coinciding trends of theoretical and experimental curves suggest that the stresses are mainly built up by the stress effects due to a change in material properties across the thickness (as was expected), although some stress peaks could not be explained on the basis of this effect
- for comparison in a quantitative way the stress free temperature must be known. This temperature is easier to find for amorphous polymers
- for a quantitative stress prediction creep and stress relaxation behaviour between moment of injection and experiment should be taken into account

7.2 Practical consideration

This report provides confidence for the assumption that the stress build up is largely caused by the change in fibre orientation across the thickness for fibre reinforced injection moulded products with high fibre content. Based upon this theory higher stresses occur when:

1. the difference between the maximum and the minimum value across the thickness of a_{11} becomes larger
2. the width of a peak in a_{11} becomes smaller

This suggests that lower stresses are obtained when the fibre orientation across the thickness is more constant. To achieve lower stresses one should try create an injection moulding with a more constant fibre orientation. In the shear layer the orientation is mainly directed in (shear-) flow direction. To get a fibre orientation in the core that is similar, a convergent flow should be present. For example for a plate with sides that are not a convergent flow can be created by choosing the right point and the right type of injection. Figure 7-1 shows a good and a bad possibility to inject the a tabulated plate.

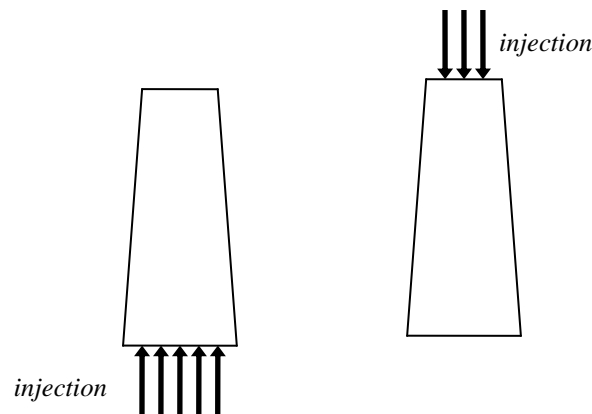


Figure 7-1: Choice of the right place of injection to optimise fibre orientation. Convergent flow must be achieved (left) and divergent flow must be avoided (left).

From this reasoning it can be concluded that a pin point should be avoided when minimising residual stresses.

7.3 Recommendations

For future work in the area of layer removal and residual stresses in fibre reinforced injection mouldings the following recommendations might be useful:

- a good analysis should be made of the influence of the milling process on the residual stresses at the milled surface
- to optimise measurement accuracy the milling machine must be more accurate so that the obtained specimen thickness is more uniform
- for the following reasons it might be useful to use thicker specimens for the layer removal experiment:
 - 1 better relative thickness accuracy which results in a better curvature profile (better in plane symmetry)
 - 2 when it is assumed that there is a certain surface layer in which the mill diminishes the residual stresses, this layer becomes relatively thin for thicker specimens
 - 3 relatively more layers can be removed which results in more data points for the fitting of the moment profile, particularly at the edges of the fit
- it would be useful to find a method to measure the thermal expansion as a function of thickness, so that the theoretical prediction can be verified

- for a more accurate profile of material properties across the thickness the fibre orientation should be known in more detail
- the bending test can be combined with the stress measurement as long as transverse curvature can be neglected. A possibility is to do the combined layer removal experiment with specimens of, say 10 mm width, so that transverse curvature can be neglected. The experiment can then be done with specimens for two directions. The results are combined later. In that case the Classical Laminate Theory might even be valid for the moments calculations in the non-symmetric specimens.

Literature

- [1] Cox, H.L.
'The elasticity and strength of paper and other fibrous materials', British Journal of Applied Physics, 1952, Vol. 3, pp. 72.
- [2] Powell, P.C.
Engineering with fibre-polymer laminates, Chapman & Hall, 1994, ISBN 0-412-49620-8.
- [3] Cristie, M.A., Darlington, M.W.
'Creep anisotropy in short fibre reinforced thermoplastics',
Proceedings of the third international conference on composite materials, Paris, 26-29 August 1980, Pergamon Press.
- [4] Folkes, M. J.
Short fibre reinforced thermoplastics, Research Studies Press, 1982, ISBN 0-471-10209-1.
- [5] Advani, S. G., Tucker, C. L.
'The use of tensors to describe and predict fiber orientation in short fiber composites',
Journal of rheology, 1987, 31, p 751.
- [6] Halpin, J. C.
'Stiffness and expansion estimates for oriented short fibre composites',
Journal of composite materials, 1969, Vol. 3, pp. 732.
- [7] Halpin, J. C. and Kardos, J. L.
'The Halpin-Tsai equations: a review',
Polymer engineering and science, 1976, Vol. 16, No. 5, pp. 344.
- [8] Halpin, J. C. and Pagano, N. J.
'The laminate approximation for randomly oriented fibrous materials',
Journal of composite materials, 1969, Vol. 3, pp. 720.
- [9] Halpin, J. C., Jerine, K. and Whitney, J. M.
'The laminate analogy for 2 and 3 dimensional composite materials',
Journal of composite materials, 1971, Vol. 5, pp. 36.
- [10] Verbeek, D. C.
De layer removal methode voor vezelversterkte kunststoffen,
Afstudeerverslag Universiteit Twente, 1994.
- [11] Eijpe, M. P. I. M. and Powell, P. C.
'A modified layer removal analysis for the determination of internal stresses in polymer composites',
accepted for publication in Journal of thermoplastic composite materials, 1995.
- [12] Hamberg, M. J. J.
Interne spanningen in vezelversterkte kunststof platen,
Afstudeerverslag Universiteit Twente, August 1995.
- [13] Treuting, R. G. and Read, W. T.
'A mechanical determination of biaxial residual stress in sheet materials',
Journal of applied physics, 1951, Vol. 22, pp. 130.
- [14] Peeters, L. J. B.
Design and manufacture of curved composite panels using flat moulds, University of Twente, 1994
- [15] Hindle, C. S. and White, J. R.
'Internal stress, molecular orientation and distortion in injection moldings: polypropylene and glass fiber filled polypropylene'

- Polymer engineering and science, 1992, vol32, no. 3.
- [16] O'Donnell, B. and White, J. R.
 'Young's modulus variations within short glass fibre reinforced nylon 6,6 injection mouldings'
Plastics, rubber and composites processing and applications, 1994, vol. 22, no. 2.
- [17] Yu, Z., Brisson, J. and A. Ait-Kadi
 'Prediction of mechanical properties of short kevlar fiber nylon 6,6 composites'
Polymer composites, 1994, Vol. 15, No. 1.
- [18] 'Fiber orientation and the mechanical properties of SFRP parts'
 ANTEC 1994, pp. 374.
- [19] Doshi, S. R. and Charrier, J. M.
 'A simple illustration of structure properties relationships for short fiber reinforced thermoplastics'
Polymer composites, 1989, Vol. 10, No. 1.
- [20] Denault, J., Vu-Khanh, T. and Foster, B.
 'Tensile properties of injection molded long fiber thermoplastic composites'
Polymer composites, 1989, Vol. 10, No. 5.
- [21] Nairn, J., Zoller, P.
 'The development of residual thermal stresses in amorphous and semicrystalline thermoplastic matrix composites'
Toughened composites, ASTM STP 937, Philadelphia, pp. 328
- [22] Sirkis, J. S., Cheng, A. and Dasgupta, A.
 'Image processing based method of predicting stiffness characteristics of short fibre reinforced injection molded parts'
Journal of composite materials, 1994, Vol. 28, No. 9.
- [23] Hashin, Z.
 'Analysis of properties of fiber composites with anisotropic constituents'
Journal of applied physics, 1979, Vol. 46, pp. 543.
- [24] Bader, M. G., Tsu-Wei Chou and Quigley, J. J.
 'On the strength of discontinuous fibre composites with polymeric matrices'
 University of Surrey, Guildford, Surrey, UK.
- [25] Gupta, M. and Wang, K.K.
 'Fiber orientation and mechanical properties of short fiber reinforced injection molded composites: simulated and experimental results'
Polymer composites, 1993, Vol. 14, No. 5.
- [26] Brady, D. G.
 'The crystallinity of poly(phenylene sulfide) and its effect on polymer properties'
Journal of applied polymer science, 1976, Vol. 20, pp. 2541.
- [27] Gardner, J. W. and Boeke, P. J.
Handbook of plastic materials and technology, John Wiley and Sons, New York, 1990.
- [28] Advanced CAE Technology, Inc.,
C-MOLD v4.0 Reference manual, USA, 1995.
- [29] Advanced CAE Technology, Inc.
C-MOLD Filling and post-filling user's guide, USA, 1995.
- [30] Jun W.J. and Hong, C.S.
 'Cured shape of unsymmetric laminates with arbitrary lay-up angles',
Journal of reinforced plastics and composites, Vol. II, p1352-1366, 1992.
- [31] Jun W.J. and Hong, C.S.

- ‘Effect of residual shear strain on the cured shape of unsymmetric cross-ply thin laminates’
Composite science and technology, Vol. 38, p55-67, 1990.
- [32] O’Donnel, B. and White, J.R.
 ‘Young’s modulus variations in Polystyrene injection moldings’
 University of Newcastle-upon-Tyne, UK.
- [33] Peeters, L.J.B.
Stiffness of laminated beams, University of Twente, The Netherlands.
- [34] Paterson, M. W. A.
Origins of distortion in injection moulded nylon 6,6, part of Ph. D. Thesis at the department of metallurgy and engineering materials, university of Newcastle upon Tyne, UK.
- [35] Timoshenko S. P. and Gere, J. M.
Mechanics of materials, PWS-KENT publishing company, Wadsworth, USA, 1990
- [36] Slutrapport 1989-1994, Center for plastbaserede kompositmaterialer,
 Internal report, edited by Torben Knudsen, university of Aalborg, Denmark, May 1995.
- [37] Ole Kjær,
Fiberorientering, Målemethode, databehandling og anvendelse,
 Internal report university of Aalborg, Denmark, October 1993.
- [38] Report for midway evaluation of Centre activities,
 Centre for Polymer Composites, development programme for materials technology, University of Aalborg, Denmark, May 1991.
- [39] Ashton, J. E., Halpin, J. C. and Petit, P.H.
Primer on composite materials: Analysis,
 Technomic Publishing & Co., Stamford, USA, 1969.
- [40] Vegt, A.K., van der
Polymeren van keten tot kunststof,
 Delftse Uitgevers Maatschappij, Delft, The Netherlands, 1991, ISBN 90-6562-130-X.
- [41] Klarenbeek, M.
Residual stresses in flat injection moulded polystyrene plates,
 Afstudeerverslag Universiteit Twente, November 1995.
- [42] Chapman, T. J., Gillespie, J. W. and Pipes, R. B.
 ‘Prediction of process induced residual stresses in thermoplastic composites’,
 Center for composite materials, Department of Mechanical Engineering, University of Delaware, Delaware, USA, 1989.

Appendix (recovered)

ature and they are just mentioned here for completeness.

Transformation of the stiffness matrix

When a stiffness matrix [Q] has been calculated for the main direction, the transformed stiffness matrix [Q*] becomes:

$$\text{Eq. } _ \text{ SEQ Eq. } \backslash * \text{ ARABIC } _ 1 _$$

with

$$\text{Eq. } _ \text{ SEQ Eq. } \backslash * \text{ ARABIC } _ 2 _ \text{ and } \text{Eq. } _ \text{ SEQ Eq. } \backslash * \text{ ARABIC } _ 3 _$$

where (is the angle over which the [Q] matrix should be transformed.

Calculation of the [A], [B] and [D] components in the stiffness matrix of the CLT

When the stiffness matrices [Q*]_n and the z coordinates of the several layers are known, the ABD matrix can be calculated using:

$$\text{Eq. } _ \text{ SEQ Eq. } \backslash * \text{ ARABIC } _ 3 _$$

$$\text{Eq. } _ \text{ SEQ Eq. } \backslash * \text{ ARABIC } _ 4 _$$

$$\text{Eq. } _ \text{ SEQ Eq. } \backslash * \text{ ARABIC } _ 5 _$$

where h_n is the z-coordinate of the upper side of the nth ply. For short fibre reinforced materials with a fibre orientation distribution the matrix [Q*]_n is replaced by the orientation averaged matrix [⟨Q*⟩]_n.

Constants in the Advani -Tucker model

The constants that are used in the Advani - Tucker model to construct the orientation averaged stiffness matrix:

$$B1 = Q11 + Q22 - 2Q12 - 4Q66 \quad \text{Eq. } _ \text{ SEQ Eq. } \backslash * \text{ ARABIC } _ 4 _$$

$$B2 = Q12 - Q23$$

$$B3 = Q66 + (Q23 - Q22) / 2$$

$$B4 = Q23$$

$$B5 = (Q22 - Q23) / 2$$

where Q_{ij} are the constants in the stiffness matrix, which are derived from the properties for entirely oriented material, using the Halpin - Tsai equations.

The matiral stiffness (Halpin and Tsai)

The Halpin-Tsai model gives a prediction of the material constants E1, E2, G12 and (12 for completely oriented material. The model corrects for the fibre length.

It is assumed that the fibres have a constant, circular cross-section, that the fibres are of uniform length, and that the modulus of the matrix material, E_m , has a unique value, despite of possible differences because of molecular orientation and/or cristallisation.

$\frac{E_c}{E_m} = \frac{V_f E_f}{E_m} + V_m$ with $\frac{E_c}{E_m} = \frac{V_f E_f}{E_m} + V_m$ Eq. 5

$\frac{E_c}{E_m} = \frac{V_f E_f}{E_m} + V_m$ with $\frac{E_c}{E_m} = \frac{V_f E_f}{E_m} + V_m$

$\frac{E_c}{E_m} = \frac{V_f E_f}{E_m} + V_m$ with $\frac{E_c}{E_m} = \frac{V_f E_f}{E_m} + V_m$

$\frac{E_c}{E_m} = \frac{V_f E_f}{E_m} + V_m$

The thermal expansion (Schapery equations)

The Schapery equations give an estimation of the thermal expansion coefficient in the main and transverse direction for fully aligned material.

$\alpha_c = \frac{V_f \alpha_f E_f}{E_c} + V_m \alpha_m$ Eq. 6

$\alpha_c = \frac{V_f \alpha_f E_f}{E_c} + V_m \alpha_m$

In this model the mechanical and thermal properties of the matrix material and the fibre material is used. The value ν_c is the poisson's ratio of the composite, obtained using the equation of Halpin - Tsai.

Closure approximations to solve the equation of change (Advani and Tucker)

To solve the equation of change three different equations can be used. The linear equation is exact for random orientation, the quadratic equation is exact for completely aligned fibres. The hybrid closure is a mix of the two, giving an acceptable estimate in most of the cases (i.e. fibres generally do not align completely with injection moulding)

linear (for planar orientation; for 3D the numerical factors are $-1/34$ and $1/7$):

$\frac{E_c}{E_m} = \frac{V_f E_f}{E_m} + V_m$ Eq. 7

quadratic:

$\frac{E_c}{E_m} = \frac{V_f E_f}{E_m} + V_m$ Eq. 8

hybrid:

$\frac{E_c}{E_m} = \frac{V_f E_f}{E_m} + V_m$ Eq. 9

where f is a generalisation of the Hermans factor, obtained with:

$\frac{E_c}{E_m} = \frac{V_f E_f}{E_m} + V_m$ Eq. 10

$A=2$ and $B=1$ for planar orientation and $A=3/2$ and $B=1/2$ for 3D.

Computer simulation

The input files of CmolD for the injection simulation to assess the fibre orientation are listed on the following pages.

the .prc file. This file contains the information about the process conditions. This file was varied for the three different cases.

the .mtl file. This file contains the information about the material behaviour.

the .par file. This file contains some parameters for the calculation.

the finite element mesh is given graphically.

then the orientation results are listed.

The output of this version of CmolD for the fibre orientation is not very clear. To describe the orientation of the fibres, two parameters are required for the Advani Tucker model: the angle and the first element of the orientation tensor. The other elements of the tensor a_{ij} are zero for $j \neq i$ (because data is given into the main direction of orientation) and a_{33} is assumed to be 0.005. With the normalisation condition ($a_{11} + a_{22} + a_{33} = 1$) we can then recover all elements of the orientation tensor.

In every finite element CmolD gives the angle as follows:

in the .oo2 file the orientation angles are obtained between the main fibre direction and the first principle axis (in degrees) at a certain time and depth instant during second pressure for every element.

in the .fem (Finite Element Mesh) file the node numbers of the elements and their coordinates can be found. The angle of the first principle axis can then be calculated by taking the inverse tangent of the line between the first two elements, so

$$\text{atan}((x_2-x_1)/(y_2-y_1)) \text{ Eq. } _ \text{ SEQ Eq. } \backslash * \text{ ARABIC } _ 11 _$$

the average orientation angle is the sum of these two angles.

Subsequently the parameters of the orientation tensor can be obtained:

in the .oo2 file for every element at a certain time instant a measure for orientation is presented (here called delta) using equation 12:

$$_ \text{ EMBED Equation.2 } _ _ _ \text{ Eq. } _ \text{ SEQ Eq. } \backslash * \text{ ARABIC } _ 12 _$$

$a_{11} + a_{22} + a_{33} = 1$ and a_{33} is assumed to be 0.005 so that a_{11} can be calculated using:

$$_ \text{ EMBED Equation.2 } _ _ _ \text{ Eq. } _ \text{ SEQ Eq. } \backslash * \text{ ARABIC } _ 13 _$$

The .PRC file

Input file with the processing conditions (.prc). The values in this file are for the plates of processing condition 5.

---- Beginning of title

TITL filmplaat2.prc : Productivity Solution

FILE 04/11/96 17:18:44 C-MOLD v4.0

---- Beginning of << C-MOLD Process Conditions - Version 4.0 >>

PROC 1 17 Description of TCODE

---- Machine description: Ludwig Engel ES 700/175-AH

10000 1 Max machine clamp force

1.71569E+06

```

10001  1  Max machine injection volume
        0.000475146
10002  1  Max machine injection pressure
        2E+08
10005  1  Max machine injection rate
        0.000225348
10006  1  Machine hydraulic response time
        0.2
10100  1  Fill time
        1
10102  1  Post-fill time
        25
10104  1  Mold-open time
        3
10300  1  F/P switch over by % volume
        99
10602  22  Ram speed profile (rel)
         0      60      10      100
         20     100      30     100
         40     100      60    80.53
         60    80.42      70    80.44
         80    80.35      80    80.36
        100      70
10702  4  Pack/hold pressure profile (rel)
         0      75     100      75
11000  1  Ambient temperature
        297.15
11002  1  Inlet melt temperature
        613.15
11100  10  Coolant manifold control
         1    413.15  0.000333333    1E+06
         1      2    413.15  0.000333333
        1E+06      1
11200  6  Hot runner manifold control
         1    413.15    0.01      2
        413.15    0.01
14004  2  Min/max melt temperature
        563.15    638.15
14006  2  Min/max coolant temperature
        277.444    423.15
---- End of file
ENDF

```

The .MTL file

Input file with the material properties (.mtl). The material properties were used like presented in chapter 4.

```

---- Beginning of title
TITL    filmplaat2.mtl : Performance (filled)

```



```

FILE    04/11/96    12:23:05    C-MOLD v4.0
---- Beginning of << C-MOLD Material Properties - Version 4.0 >>
MTRL   1   23   Description of TCODE ....
 1004   13   2-domain mod Tait polymer den
           518.15   2.05E-07   0.0006403   2.01E-07
           6.44E+08   0.00357   0.0006101   2.46E-08
           9.95E+08   0.0001   3.02E-05   0.030736
           6.21E-09
 1100   1   Constant polymer specific heat
           1510
 1200   1   Const polymer thermal conduct
           0.44
 1303   5   Cross-exp polymer viscosity
           0.37218   69958   0.0082317   7259.9
           0
 1313   7   Cross-WLF polymer viscosity
           0.37479   68006   1.67E+14   373.15
           0   31.218   51.6
 1500   1   Transition temperature
           533.15
 1702   2   Trans-iso thermal expan coeff
           2.5E-05   4.4E-05
 1999   0   PPS/PHILLIPS 66/RYTON R-4XTHV
 3000   1   Constant fiber density
           2560
 3600   2   Fiber iso elastic tensor
           7.24E+10   0.22
 3700   1   Fiber iso thermal expan coeff
           5E-06
 3900   1   Fiber weight fraction
           0.427
 3910   1   Fiber aspect ratio
           19
 3999   0   GF
 6000   1   Constant coolant density
           988
 6100   1   Constant coolant specific heat
           4180
 6200   1   Constant coolant thermal conduct
           0.643002
 6302   3   Coolant viscosity w/ exp temp
           2.861E-05   783.8   396.8
 6999   0   -
 8000   1   Constant mold density
           7850
 8100   1   Constant mold specific heat
           434
 8200   1   Constant mold thermal conduct
           60.4999
 8999   0   TOOL STEEL P-3

```

---- End of file
ENDF

The .PAR file

Input file with the calculation parameters (.par).

---- Beginning of title

TITL filmplaat2.par : Injection Molding

FILE 04/11/96 16:05:40 C-MOLD v4.0

---- Beginning of << C-MOLD Parameters - Version 4.0 >>

```
PRMT 1 36 Description of TCODE ....
100 1 # of layers across full-gap
      20
200 1 # design outputs in filling
      2
201 1 # detail outputs in filling
      2
202 1 # design outputs in post-filling
      2
203 1 # detail outputs in post-filling
      2
204 1 # design outputs in mold-opening
      0
205 1 # detail outputs in mold-opening
      0
300 1 Pressure convergence criterion
      0.5
301 1 Flow-rate convergence criterion
      0.5
302 1 Melt-temp convergence criterion
      0.2
305 1 Orientation convergence criterion
      0.5
307 1 Balancing convergence criterion
      5
310 1 Mold-melt heat-transfer coeff
      25000
313 1 Mold temp convergence criterion
      0.05
314 1 Cooling time convergence criterion
      1
400 1 Max # of pressure iterations
      8
401 1 Max # of flow-rate iterations
      125
402 1 Max # of melt-temp iterations
      100
405 1 Max # of orientation iterations
      100
```

```

407 1 Max # of balancing iterations
      10
413 1 Max # of cooling iterations
      50
514 1 Pressure work
      0
516 1 Juncture losses
      0
520 1 Save restart file (COOL)
      1
522 1 Age of the mold (COOL)
      3.16456E+07
542 1 Runner diameter increment (RB)
      0.0001
544 1 Max vol ratio of runner vs part
      25
600 1 Residual stress analysis (W)
      0
602 1 Option for structural package (W)
      0
604 1 Isolate mechanism for warpage (W)
      1
606 1 Stress analysis w/o C-COOL (W)
      0
620 1 Fiber orientation analysis (W)
      1
622 1 Fiber interaction coefficient (W)
      0.00288
624 1 Fiber shape factor (W)
      1
626 1 Orientation BC option
      1
627 1 Fiber orientation during post-filling
      1
---- End of file

```

The .FEM file

Instead of presenting the Finite Elements input-file (.fem) that has been used for the computer simulations the mesh is plot here graphically.

—

Fibre orientations

Fibre orientations as a function of the normalised distance from the core. As a measure of alignment the a11 tensor element of Advani and Tucker is used. For the processing conditions 2, 5 and 8 respectively the results of the measurements, the Moldflow computer simulation and the Cmolde computer simulation are compared. In all cases it is

supposed that the main fibre direction is in flow direction. The data points are connected with lines to indicate the trend.

_ LINK Excel.Sheet.5 ""\\UTWOU5\\VOERMAN\\rik\\orienta.xls" "orientatie
vergelijking![orienta.xls]orientatie vergelijking Chart 2" \a \p ____ LINK Excel.Sheet.5
""\\UTWOU5\\VOERMAN\\rik\\orienta.xls" "orientatie
vergelijking![orienta.xls]orientatie vergelijking Chart 3" \a \p ____
_ LINK Excel.Sheet.5 ""\\UTWOU5\\VOERMAN\\rik\\orienta.xls" "orientatie
vergelijking![orienta.xls]orientatie vergelijking Chart 4" \a \p ____

Experimental results

Processing conditions

For the measurements three series of different processing conditions were used. The numbers of every plate were taken from the supplier, the University of Aalborg, Denmark. In _ REF _Ref358878125 * MERGEFORMAT _Table C-1_ the used processing conditions are listed.

processing condition nr. 2 5 8 melt temperature [°C]

mould temperature [°C]

injection time [s]

second pressure [MPa] 320

140

2

40 340

140

1

20 360

140

3

60 Table _ STYLEREF 1 \n _C_-_ SEQ Table * ARABIC \r 1 _1_: The process conditions of the used plates.

Measurements program

From the PPS GF 40 material 15 plates were available, with which the experiments were done. In _ REF _Ref359204815 * MERGEFORMAT _Table C-2_ the measurements for which every plate has been used are listed.

processing condition 2 processing condition 5 processing condition 8 2/18 layer

removal with strain gauges, coated, upside down 5/24 - 8/14 thermal expansion in

flow and transverse direction 2/19 layer removal with strain gauges, coated 5/25

- 8/15 layer removal 2/20 layer removal without strain gauges, not coated 5/26

thermal expansion flow direction 8/16 layer removal, with strain gauges,

coated 2/21 modulus with bending test 5/27 - 8/17 - 2/22 thermal expansion in

flow and transverse direction 5/28 modulus with bending test 8/18 modulus with

bending test Table _ STYLEREF 1 \n _C_-_ SEQ Table * ARABIC _2_: Specimen

usage of precessing confition 2, 5 and 8.

Tensile measurements

To assess the tensile properties of the material, the specimen was clamped in all four possible positions to compensate for dimensional errors. The specimens were loaded first

to the maximum load. After this the specimens were tested four times in each position. The stress-strain curve was fitted, and the R2 value of this fit is reported as well. In all cases the stress-strain curve was fitted very well ($R2 \geq 0.9997$).

First the Carbon/PEI measurements are listed. On the next page the measurements of the PPS-GF40 are given.

```
_ LINK Excel.Sheet.5 "////UTWOU5\\VOERMAN\\rik\\modulus.xls" "tensile
udcp!R1C1:R31C6" \a \r \* MERGEFORMAT _
Tensile measurements of the Carbon/PEI laminates UD, 12 layers CP (0,90)s 12
layers date 12/2/96 12/2/96 v 0.16 mm/min (1) 0.16 mm/min (1) Fmax 1000 N 1000
N Fv 2 N 2 N clamp length 65 mm 65 mm width 10.65 mm 10.2 mm thickness 1.85
mm 1.85 mm E [GPa] R2 E [GPa] R2 clamp1 114.3 1.0000 60.9 1.0000 112.3
0.9998 60.9 0.9999 112.6 0.9998 61.0 1.0000 clamp2 120.2 1.0000 62.0 1.0000
120.4 1.0000 61.9 0.9999 121.2 0.9999 61.6 1.0000 clamp3 124.0 0.9999 63.1 1.0000
125.4 1.0000 63.8 1.0000 124.3 1.0000 63.2 1.0000 clamp4 120.3 0.9999 63.4 0.9999
120.6 0.9997 62.8 0.9999 121.4 0.9999 63.0 0.9999 average 119.7 62.3 stdev 4.4
1.1 Measurements using GFLA 6.350.50 strain gauges (1) strain rate is 4.1
E-5 m/ms _
```

```
_ LINK Excel.Sheet.5 "////UTWOU5\\VOERMAN\\rik\\modulus.xls" "tensile
258!R1C1:R27C7" \a \r \* MERGEFORMAT _
Tensile measurements of series 2, 5 and 8 sample 2/21 sample 5/28 sample
8/18 date 21/2/96 16/2/96 21/2/96 v 0.16 mm/min (1) 0.16 mm/min (1) 0.16 mm/min
(1) Fmax 500 N 500 N 500 N Fv 50 N 50 N 50 N clamp length 65 mm 65 mm 65 mm
width 9.2 mm 9.65 mm 10.05 mm thickness 1.895 mm 1.90 mm 2.00 mm E [GPa]
R2 E [GPa] R2 E [GPa] R2 clamp1 13.89 1.0000 14.04 0.9999 14.0 1.0000 13.89
1.0000 14.04 0.9999 14.2 1.0000 13.90 1.0000 14.01 0.9999 14.3 1.0000 clamp2 13.77
1.0000 14.45 0.9999 14.2 1.0000 13.82 1.0000 14.48 0.9999 14.2 1.0000 13.82 1.0000
14.42 0.9999 14.3 1.0000 clamp3 15.90 1.0000 14.42 0.9999 15.5 0.9998 15.93 1.0000
14.39 0.9999 15.6 0.9998 15.93 1.0000 14.42 0.9999 15.5 0.9998 clamp4 15.77 1.0000
14.64 0.9998 15.6 0.9999 15.77 0.9999 14.58 0.9998 15.7 0.9999 15.80 0.9999 14.52
0.9998 15.7 0.9999 average 14.85 14.37 14.9 stdev 1.0 0.2 0.7 _
```

Three point bending tests

After the tensile tests the specimens were tested using a three point bending test. Each time a layer of 0.1 mm was removed, new bending tests were done. The bending test was performed three times for every plate thickness. Then calculations were performed to recover the material stiffness for every removed layer. For more details see the Mathematica listings in appendix E.

On the next pages the modulus for every layer calculated by Mathematica are listed. After this the results are shown graphically.

Results from three point bending test for Carbon/PEI laminates

Unidirectional laminate (UD)		Cross-ply laminate (CP)	
testing date	13/2/96	testing date	13/2/96
testing speed [mm/min]	1	testing speed [mm/min]	1
testing depth [mm]	1	testing depth [mm]	1
span width [mm]	59,6	span width [mm]	59,6

plate width [mm]	10,65					10,2				
thickness	normalized location	modulus (bending)	expected modulus (1)	error	E*h	thickness	normalized location	modulus (bending)	expected modulus (1)	
1,850						1,820				
1,725	0,966	116813	119700	-2,4%	14602	1,720	0,973	106270	119700	
1,615	0,903	100147	119700	16,3%	11016	1,615	0,916	99391	119700	
1,520	0,847	113275	119700	-5,4%	10761	1,525	0,863	108539	119700	
1,415	0,793	107669	119700	10,1%	11305	1,410	0,806	100048	119700	
1,330	0,742	118736	119700	-0,8%	10093	1,330	0,753	108663	119700	
1,235	0,693	121729	119700	1,7%	11564	1,250	0,709	9656	7849	
1,125	0,638	123530	119700	3,2%	13588	1,145	0,658	5953	7849	
1,005	0,576	128019	119700	6,9%	15362	1,010	0,592	8141	7849	
0,925	0,522	118531	119700	-1,0%	9482	0,910	0,527	5645	7849	
Average modulus:			119700		116512				63775	

	sample 2/21			sample 5/28		
testing date	21/2/1996			16/2/1996		
testing speed [mm/min]	1	2 mm/min for layers 5-8		1	2 mm/min for layers 6-7	
testing depth [mm]	1	2 mm for layers 5-8		1	2 mm for layers 6-7	
span width [mm]	59,7			59,55		
plate width [mm]	9,2			9,65		

values from bending test

layer nr.	measured thickness [mm]	normalized location []	modulus (bending) [MPa]	E*h	measured thickness	normalized location	modulus (bending) [MPa]	E*h
0	1,895				1,900			
1	1,815	0,979	14186	1135	1,825	0,981	10134	76
2	1,725	0,935	15368	1383	1,735	0,937	16621	149
3	1,510	0,857	13782	2963	1,635	0,888	14803	148
4	1,325	0,751	16876	3122	1,535	0,835	15709	157
5	1,225	0,674	17818	1782	1,440	0,784	15715	149
6	1,120	0,620	15869	1666	1,345	0,734	16096	152
7	1,030	0,568	11807	1063	1,240	0,681	13219	138
8	0,948	0,523	10368	855	0,913	0,579	8920	292
9								
modulus average				14743	138			

_ LINK Excel.Sheet.5 "////UTWOU5\\VOERMAN\\rik\\modulus.xls" "bending udcp![modulus.xls]bending udcp Chart 2" \a \p _____ LINK Excel.Sheet.5 "////UTWOU5\\VOERMAN\\rik\\modulus.xls" "bending udcp![modulus.xls]bending udcp Chart 1" \a \p _____

Figure _ STYLEREF 1 \n _C_- SEQ Figure * ARABIC \r 1 _1_: Obtained modulus for unidirectional (left) and cross-ply (right) Carbon/PEI laminate.

LINK Excel.Sheet.5 ":///UTWOU5\VOERMAN\rik\modulus.xls" "grafieken![modulus.xls]grafieken Chart 2" \a \p LINK Excel.Sheet.5 ":///UTWOU5\VOERMAN\rik\modulus.xls" "grafieken![modulus.xls]grafieken Chart 3" \a \p

LINK Excel.Sheet.5 ":///UTWOU5\VOERMAN\rik\modulus.xls" "grafieken![modulus.xls]grafieken Chart 4" \a \p
Figure _ STYLEREF 1 \n _C_- SEQ Figure * ARABIC _2_: Obtained modulus in flow direction from orientation and bending measurements of series 2, 5 and 8.

Thermal expansion measurements

The thermal expansion was measured for a specimen of each processing condition. A specimen was measured three times. The thermal expansion was calculated for heating and cooling separately, including their root square error. From this the average was calculated.

For every measurement the cooling speed and the maximum temperature is given.

LINK Excel.Sheet.5 ":///UTWOU5\VOERMAN\rik\alfa_ave.xls" "alfas!R1C1:R28C10" \a \p

To analyse the difference in thermal expansion above and below Tg, the thermal expansion has been calculated in both temperature intervals, resulting in:

LINK Excel.Sheet.5 ":///UTWOU5\VOERMAN\rik\alfa_ave.xls" "alfas cool!R1C1:R16C10" \a \p

Layer removal curvatures and strains

The results of the layer removal measurements are listed on the following pages. First the measurements data is listed in tables for every specimen. The quadratic fit error is given as an indication of the accuracy of the fit.

Then the data is presented graphically. The following graphs are given:

the curvatures of every specimen, grouped by flow and transverse to flow direction, are presented in a table and then graphically

the twisting curvatures for the specimens without strain gauges. The scans were fit with a straight line and then the difference in steepness was divided by the distance between the scan-lines

the measured mid-plane strains, These were calculated by measuring the strains at the surface and then correcting them for the curvature to get the mid-plane strain, using equation 14:

EMBED Equation.2 Eq. _ SEQ Eq. * ARABIC _14_

so there was not made any correction for shear strains.

the moment profiles, calculated from the measurements including their fits

the stress profiles, calculated from the fitted moment data

The names for the several scans that were used are built up as follows:

Ssssllxn

which means that all series start with an S, followed by the specimen number which is the series number plus the plate number. The ll indicate the layer number, x the x or y direction and n the number of the scan line, which can be 1, 2 or 3.

Fit error

For every curvature fit the R-squared value was calculated to have an indication of the accuracy of the fit. This value was calculated using equation 15:

$$\frac{\sum_{i=1}^n (Y_i - \hat{Y}_i)^2}{\sum_{i=1}^n Y_i^2} \quad \text{Eq. 15}$$

where n is the number of points to be fit, Y_i is the measured value of point i, i is the index number of the points, ranging from 1 to n, and \hat{Y}_i is the approximated value of point i.

[LINK](#) Excel.Sheet.5 "\\\\UTWOU5\\VOERMAN\\rik\\curvatures.xls"
"s218curv!R1C1:R24C10" \a \p

[LINK](#) Excel.Sheet.5 "\\\\UTWOU5\\VOERMAN\\rik\\curvatures.xls"
"s219curv!R1C1:R21C10" \a \p

[LINK](#) Excel.Sheet.5 "\\\\UTWOU5\\VOERMAN\\rik\\curvatures.xls"
"s816curv!R1C1:R23C10" \a \p

[LINK](#) Excel.Sheet.5 "\\\\UTWOU5\\VOERMAN\\rik\\curvatures.xls"
"s524curv!R1C1:R24C20" \a \p

Curvatures from the layer removal measurements

Curvature profiles as a function of the normalised distance from the core.

[LINK](#) Excel.Sheet.5 "\\\\UTWOU5\\VOERMAN\\rik\\curvatures.xls"
"s218curv![curvatures.xls]s218curv Chart 2" \a \p [LINK](#) Excel.Sheet.5

"\\\\UTWOU5\\VOERMAN\\rik\\curvatures.xls" "s219curv![curvatures.xls]s219curv
Chart 2" \\a \\p ____
_ LINK Excel.Sheet.5 "\\\\UTWOU5\\VOERMAN\\rik\\curvatures.xls"
"s220curv![curvatures.xls]s220curv Chart 2" \\a \\p ____ LINK Excel.Sheet.5
"\\\\UTWOU5\\VOERMAN\\rik\\curvatures.xls" "s524curv![curvatures.xls]s524curv
Chart 2" \\a \\p ____

_ LINK Excel.Sheet.5 "\\\\UTWOU5\\VOERMAN\\rik\\curvatures.xls"
"s816curv![curvatures.xls]s816curv Chart 2" \\a \\p ____

_ LINK Excel.Sheet.5 "\\\\UTWOU5\\VOERMAN\\rik\\curvatures.xls"
"s218curv![curvatures.xls]s218curv Chart 4" \\a \\p ____ LINK Excel.Sheet.5
"\\\\UTWOU5\\VOERMAN\\rik\\curvatures.xls" "s219curv![curvatures.xls]s219curv
Chart 4" \\a \\p ____
_ LINK Excel.Sheet.5 "\\\\UTWOU5\\VOERMAN\\rik\\curvatures.xls"
"s220curv![curvatures.xls]s220curv Chart 4" \\a \\p ____ LINK Excel.Sheet.5
"\\\\UTWOU5\\VOERMAN\\rik\\curvatures.xls" "s524curv![curvatures.xls]s524curv
Chart 4" \\a \\p ____

_ LINK Excel.Sheet.5 "\\\\UTWOU5\\VOERMAN\\rik\\curvatures.xls"
"s816curv![curvatures.xls]s816curv Chart 4" \\a \\p ____
Twisting curvatures

_ LINK Excel.Sheet.5 "\\\\UTWOU5\\VOERMAN\\rik\\curvatures.xls"
"s220curv![curvatures.xls]s220curv Chart 6" \\a \\p ____ LINK Excel.Sheet.5
"\\\\UTWOU5\\VOERMAN\\rik\\curvatures.xls" "s220curv![curvatures.xls]s220curv
Chart 7" \\a \\p ____
_ LINK Excel.Sheet.5 "\\\\UTWOU5\\VOERMAN\\rik\\curvatures.xls"
"s524curv![curvatures.xls]s524curv Chart 6" \\a \\p ____ LINK Excel.Sheet.5
"\\\\UTWOU5\\VOERMAN\\rik\\curvatures.xls" "s524curv![curvatures.xls]s524curv
Chart 7" \\a \\p ____
Mid-plane strains

_ LINK Excel.Sheet.5 "\\\\UTWOU5\\VOERMAN\\rik\\curvatures.xls"
"strains![curvatures.xls]strains Chart 1" \\a \\p ____ LINK Excel.Sheet.5
"\\\\UTWOU5\\VOERMAN\\rik\\curvatures.xls" "strains![curvatures.xls]strains Chart 2"
\\a \\p ____

Calculated moments with fit and resulting stresses

For the fit of the moment lines first order splines were used, with a number of intervals depending on the amount of available points. The result is a step-wise stress profile, that indicates the average stress level in each layer. This technique does not filter any errors in the moment profiles. A sixth order polynomial was fit on the stress profile to indicate the smoothed stress profile, being symmetric. For a direct smooth fit the moving window technique was used, the results of which are shown on the next pages.

_ LINK Excel.Sheet.5 "\\\\UTWOU5\\VOERMAN\\layrem\\stresses.xls"
"s218mx130![stresses.xls]s218mx130 Chart 1" \\a \\p ____ LINK Excel.Sheet.5

""\\UTWOU5\\VOERMAN\\layrem\\stresses.xls" "s218mx130![stresses.xls]s218mx130
 Chart 2" \a \p ____
 _ LINK Excel.Sheet.5 ""\\UTWOU5\\VOERMAN\\layrem\\stresses.xls"
 "s219mx124![stresses.xls]s219mx124 Chart 1" \a \p ____ LINK Excel.Sheet.5
 ""\\UTWOU5\\VOERMAN\\layrem\\stresses.xls" "s219mx124![stresses.xls]s219mx124
 Chart 2" \a \p ____
 _ LINK Excel.Sheet.5 ""\\UTWOU5\\VOERMAN\\layrem\\stresses.xls"
 "s816mx128![stresses.xls]s816mx128 Chart 1" \a \p ____ LINK Excel.Sheet.5
 ""\\UTWOU5\\VOERMAN\\layrem\\stresses.xls" "s816mx128![stresses.xls]s816mx128
 Chart 2" \a \p ____
 _ LINK Excel.Sheet.5 ""\\UTWOU5\\VOERMAN\\layrem\\stresses.xls"
 "s218my130![stresses.xls]s218my130 Chart 1" \a \p ____ LINK Excel.Sheet.5
 ""\\UTWOU5\\VOERMAN\\layrem\\stresses.xls" "s218my130![stresses.xls]s218my130
 Chart 2" \a \p ____

 _ LINK Excel.Sheet.5 ""\\UTWOU5\\VOERMAN\\layrem\\stresses.xls"
 "s219my124![stresses.xls]s219my124 Chart 1" \a \p ____ LINK Excel.Sheet.5
 ""\\UTWOU5\\VOERMAN\\layrem\\stresses.xls" "s219my124![stresses.xls]s219my124
 Chart 2" \a \p ____
 _ LINK Excel.Sheet.5 ""\\UTWOU5\\VOERMAN\\layrem\\stresses.xls"
 "s816my128![stresses.xls]s816my128 Chart 1" \a \p ____ LINK Excel.Sheet.5
 ""\\UTWOU5\\VOERMAN\\layrem\\stresses.xls" "s816my128![stresses.xls]s816my128
 Chart 2" \a \p ____
 _ LINK Excel.Sheet.5 ""\\UTWOU5\\VOERMAN\\rik\\samples\\s219\\stresses.xls"
 "s218x![stresses.xls]s218x Chart 2" \a \p ____ LINK Excel.Sheet.5
 ""\\UTWOU5\\VOERMAN\\rik\\samples\\s219\\stresses.xls" "s218x![stresses.xls]s218x
 Chart 4" \a \p ____
 _ LINK Excel.Sheet.5 ""\\UTWOU5\\VOERMAN\\rik\\samples\\s219\\stresses.xls"
 "s219x![stresses.xls]s219x Chart 2" \a \p ____ LINK Excel.Sheet.5
 ""\\UTWOU5\\VOERMAN\\rik\\samples\\s219\\stresses.xls" "s219x![stresses.xls]s219x
 Chart 4" \a \p ____

 _ LINK Excel.Sheet.5 ""\\UTWOU5\\VOERMAN\\rik\\samples\\s219\\stresses.xls"
 "s816x![stresses.xls]s816x Chart 2" \a \p ____ LINK Excel.Sheet.5
 ""\\UTWOU5\\VOERMAN\\rik\\samples\\s219\\stresses.xls" "s816x![stresses.xls]s816x
 Chart 4" \a \p ____
 _ LINK Excel.Sheet.5 ""\\UTWOU5\\VOERMAN\\rik\\samples\\s219\\stresses.xls"
 "s218y![stresses.xls]s218y Chart 2" \a \p ____ LINK Excel.Sheet.5
 ""\\UTWOU5\\VOERMAN\\rik\\samples\\s219\\stresses.xls" "s218y![stresses.xls]s218y
 Chart 4" \a \p ____

 _ LINK Excel.Sheet.5 ""\\UTWOU5\\VOERMAN\\rik\\samples\\s219\\stresses.xls"
 "s219y![stresses.xls]s219y Chart 2" \a \p ____ LINK Excel.Sheet.5
 ""\\UTWOU5\\VOERMAN\\rik\\samples\\s219\\stresses.xls" "s219y![stresses.xls]s219y
 Chart 4" \a \p ____
 _ LINK Excel.Sheet.5 ""\\UTWOU5\\VOERMAN\\rik\\samples\\s219\\stresses.xls"
 "s816y![stresses.xls]s816y Chart 2" \a \p ____ LINK Excel.Sheet.5
 ""\\UTWOU5\\VOERMAN\\rik\\samples\\s219\\stresses.xls" "s816y![stresses.xls]s816y
 Chart 4" \a \p ____

Fit of the obtained moments

In this appendix three techniques are discussed to fit the moments line obtained from the layer removal results. To compare the results the data of only one specimen (8/16 into flow direction) is used.

Each technique uses its own set of functions that is fitted using the least squares method. Note that the R2 value is not the only thing that should be considered. See subsection 3.4.3 and 6.3.2 for a detailed consideration of the fitting techniques.

On the following pages the most interesting examples of each fitting technique are shown. The fitting techniques that are considered are:

splines; splines were used by Klarenbeek [41] to recover stresses from unfilled material using the layer removal technique. This fit uses B-splines as trial functions. The graph is divided into a given number of intervals. The splines have a local support depending on the size of the intervals. Therefore a local error will not be transferred throughout the complete domain. A higher resolution is obtained by using smaller intervals. The graphs show the order of the splines and the number of intervals. First, second and third order splines are considered.

polynomials; to fit the moments a polynomial function of the form: $y = \sum_{i=0}^n a_i x^i$ was used on the entire domain, where n is the order of the polynomial and a_i are constants. In the graphs polynomials of several degrees are plot.

moving window using polynomials; to fit the moments a polynomial function of order n is used within a certain window of the moments data. The window width is the number of data points that is used within the window. These points are fit with a polynomial and then the window is shifted.

Splines fit

[LINK](#) Excel.Sheet.5 ":///UTWOU5\\VOERMAN\\layrem\\stresses.xls" "Sheet1![stresses.xls]Sheet1 Chart 2" \a \p ____

[LINK](#) Excel.Sheet.5 ":///UTWOU5\\VOERMAN\\layrem\\stresses.xls" "Sheet1![stresses.xls]Sheet1 Chart 3" \a \p ____

Moment (above) and stress (below) profiles of first order splines with 15, 25 and 28 intervals. With more than 28 intervals the fit oscillates for this data. With fewer intervals the approximation becomes less refined.

The number of intervals can be increased when more data points are available and when the distance between the data points is more uniform.

[LINK](#) Excel.Sheet.5 ":///UTWOU5\\VOERMAN\\rik\\report\\fittest.xls" "splines 2![fittest.xls]splines 2 Chart 2" \a \p ____

[LINK](#) Excel.Sheet.5 ":///UTWOU5\\VOERMAN\\rik\\report\\fittest.xls" "splines 2![fittest.xls]splines 2 Chart 4" \a \p ____

Moment (above) and stress (below) profiles of second order splines with 10, 24, 27 and 28 intervals. With more than 27 intervals the fit oscillates. With fewer intervals the approximation becomes less refined.

_ LINK Excel.Sheet.5 "\\UTWOU5\\VOERMAN\\rik\\report\\fittest.xls" "splines 3![fittest.xls]splines 3 Chart 2" \a \p ____
 _ LINK Excel.Sheet.5 "\\UTWOU5\\VOERMAN\\rik\\report\\fittest.xls" "splines 3![fittest.xls]splines 3 Chart 4" \a \p ____

Moment (above) and stress (below) profiles of third order splines with 10, 24 and 27 intervals. With more than 27 intervals the fit oscillates. With fewer intervals the approximation becomes less refined. At the core the moment fit is changing because of the stress equilibrium condition.

Polynomial fit

_ LINK Excel.Sheet.5 "\\UTWOU5\\VOERMAN\\rik\\report\\fittest.xls" "polynomials![fittest.xls]polynomials Chart 2" \a \p ____
 _ LINK Excel.Sheet.5 "\\UTWOU5\\VOERMAN\\rik\\report\\fittest.xls" "polynomials![fittest.xls]polynomials Chart 4" \a \p ____

Moment (above) and stress (below) profiles of polynomials of order 4, 6, 8 and 10. With a lower order the approximation becomes less refined. Especially in the edges (near the surface at 1 and in the core at 0) the approximation becomes erroneous. The stress profile is not in equilibrium, because the surface under the graphs is positive for all fits.

Moving window fit

_ LINK Excel.Sheet.5 "\\UTWOU5\\VOERMAN\\rik\\report\\fittest.xls" "filter check![fittest.xls]filter check Chart 2" \a \p ____
 _ LINK Excel.Sheet.5 "\\UTWOU5\\VOERMAN\\rik\\report\\fittest.xls" "filter check![fittest.xls]filter check Chart 4" \a \p ____

Moment (above) and stress (below) profiles of second order polynomials with window sizes 2, 5 and 7. With larger intervals the fit becomes less refined.

_ LINK Excel.Sheet.5 "\\UTWOU5\\VOERMAN\\rik\\report\\fittest.xls" "filter check![fittest.xls]filter check Chart 1" \a \p ____
 _ LINK Excel.Sheet.5 "\\UTWOU5\\VOERMAN\\rik\\report\\fittest.xls" "filter check![fittest.xls]filter check Chart 3" \a \p ____

Moment (above) and stress (below) profiles of third order polynomials with window sizes 2, 5 and 7. With larger intervals the fit becomes less refined. The stress profile is not in equilibrium, because the surface under the graphs is positive for all fits, like with the polynomial fits.

Mathematica Calculations

In this appendix the listings of the Mathematica calculations are given. The calculations for the material stiffness of the bending test and the moments calculations of the layer removal measurements both use the LRSUB package that contains some reusable Modules.

Listing of the package containing the Modules

```
(*** LRSUB.M      Package file containing the modules used for the three point
bending
```

```
calculations and the stress calculations for fibre reinforced injection
moulded plates.
```

```
*** University of Twente, 1996      ***
*** by Rik Voerman                  ***
*****)
```

```
BeginPackage["LRsub`"];
```

```
Inlezen::usage = " reads measurements data";
ModulusInterpolation::usage = "interpolates to get modulus values";
ABDMatrices::usage = "calculates the ABD matrices for every layer";
Curvatures::usage = "calculates curvatures of measured lines";
EpsXNul::usage = "calculates the midplane strains";
IntegralPiece::usage = "energy integral of a part of the plate";
Write2Data::usage = "writes one- or two dimensional arrays to disc";
Filter::usage = "filters the obtained moment points to obtain the stresses";
```

```
Begin ["`Private`"];
```

```

                (**** read in data files, first row as x and third as z data ****)
Inlezen[nomeasurements_, thickn_, bestand_, b2_] :=
                Module [{i,dummy,lxcoorfile,eerste,tweede,lxcoor},

                (*** reading coordinates of measured points (dimension is mm)
                ***)
eerste = 48; (* counters for layer numbers *)
tweede = 48;
lxcoor={ };

For[i = 0,i < nomeasurements,i++,

                (* read x *)
                lxcoorfile = OpenRead[bestand <> FromCharCode[eerste] <>
FromCharCode[tweede]<> b2 <> ".dat"];
                Skip[lxcoorfile,Record,6];
                dummy = ReadList[lxcoorfile, {Number,Number,Number}];
                (* neglect first and last 3 points*)
                AppendTo [lxcoor,
Table[{dummy[[w,1]],dummy[[w,3]]},{w,4,Length[dummy]}]-3];
                Close[lxcoorfile];
                tweede++;
                If [tweede==58, tweede=48;eerste++]; (* werkt voor nummers tot 99 *)

                ]; (* next *)
lxcoor
```

```
]; (* end inlezen *)
```

```
ModulusInterpolation[nomeasurements_,thickn_,zvalue_,xmodulus_] :=  
Module [{p,j,xmodulusz,half,zv,xfit,xm,help,help2},
```

```
(* construct the modulus in the several thicknesses from the given points, using  
polynomial interpolation between the different modulus values *)  
(* x-direction is flow direction *)
```

```
(* find modulus modulus list at moduluslist *)
```

```
half=thickn[[1]]/2;
```

```
xmodulusz={};
```

```
For[j=1,j<=nomeasurements,j++,
```

```
zv=(thickn[[j]]-half)/half;
```

```
(* find closest point *)
```

```
help=Length[zvalue]-1;
```

```
p=2;
```

```
While [p<help,
```

```
help2=(zvalue[[p]]+zvalue[[p+1]])/2;
```

```
If [zv<=help2, Break[;
```

```
];
```

```
p=p+1];
```

```
(* next p *)
```

```
(* 2e graads interpolatie *)
```

```
xm=Table[{zvalue[[w]],xmodulus[[w]]},{w,p-1,p+1}];
```

```
xfit[z_]=InterpolatingPolynomial[xm,z];
```

```
AppendTo [xmodulusz,(xfit[zv])];
```

```
]; (* next j *)
```

```
xmodulusz
```

```
]; (***) end ModulusInterpolation (***)
```

```
(* construct the Q matrix and the A, B and D matrices for the different layers *)
```

```
ABDMatrices[nomeasurements_,dikte_,xmodulusz_,ymodulusz_,nu12_,G12_] :=
```

```
Module [{i,j,Amlist,Bmlist,Dmlist,hh,dif,Q,Qstardummy},
```

```
Abase,Bbase,Dbase,Aext,Bext,Dext,thickn,xmod,ymod,nu21},
```

```
(* calculate the Q matrices in the first half of the material *)
```

```
Q={};
```

```
For [i=1,i<nomeasurements,i++,
```

```
(* ymod = (ymodulusz[[i]]+ymodulusz[[i+1]])/2;
```

```
xmod = (xmodulusz[[i]]+xmodulusz[[i+1]])/2; *)
```

```
ymod = ymodulusz[[i];
```

```
xmod = xmodulusz[[i];
```

```
nu21 = ymod*nu12[[i]]/xmod;
```

```

j = 1 - (nu12[[i]]*nu21);
AppendTo [Q,{{ xmod/j,nu12[[i]]*ymod/j,0},
            {nu12[[i]]*ymod/j,ymod/j,0},
            {0,0,G12}}];
];      (* next i *)
AppendTo [Q,{{ xmodulusz[[i]]/j,nu12[[i]]*ymodulusz[[i]]/j,0},
            {nu12[[i]]*ymodulusz[[i]]/j,ymodulusz[[i]]/j,0},
            {0,0,G12}}];

(* Q star not rotated because of symmetry -> main direction is x
direction!!*)
Qstardummy = Table[Q[[i]],{i,nomeasurements}];

Amlist = {};
Bmlist = {};
Dmlist = {};
thickn=dikte;
AppendTo[thickn,thickn[[1]]/2];
For[i=1,i<=nomeasurements,i++,
    (* the ABD matrix after i layers being removed *)
    dif=thickn[[1]]-thickn[[i]]/2;
    Abase=Sum[Qstardummy[[w]]*(thickn[[w]]-
thickn[[w+1]]),{w,1,nomeasurements}];
    Bbase=Sum[Qstardummy[[w]]*(1/2)*((thickn[[w]]-dif)^2-(thickn[[w+1]]-
dif)^2),{w,1,nomeasurements}];
    Dbase=Sum[Qstardummy[[w]]*(1/3)*((thickn[[w]]-dif)^3-(thickn[[w+1]]-
dif)^3),{w,1,nomeasurements}];

    hh=thickn[[i]]/2;
    Aext=Sum[Qstardummy[[w]]*(thickn[[w]]-
thickn[[w+1]]),{w,i,nomeasurements}];
    Bext=Sum[Qstardummy[[w]]*(1/2)*((thickn[[w+1]]-hh)^2-(thickn[[w]]-
hh)^2),{w,i,nomeasurements}];
    Dext=Sum[Qstardummy[[w]]*(1/3)*((thickn[[w]]-hh)^3-(thickn[[w+1]]-
hh)^3),{w,i,nomeasurements}];
    (* the total ABD after i layers being removed *)
    AppendTo[Amlist,Abase+Aext];
    AppendTo[Bmlist,Bbase+Bext];
    AppendTo[Dmlist,Dbase+Dext];

];
{Amlist,Bmlist,Dmlist}
];      (***) end ABDMatrices  (***)

(**** Calculation of curvature ****)
Curvatures[nomeas_, punten_] :=
Module[{i,klist,kwadfout,foutelaag,kf,somkwadafwc,somkwadafwp,
kappac,kappap,c1,c2,c3,th,pf,pssum,psum,rsv},

```

```

klist={ }; (* calculation of kappa *)
rsv={ }; (* root square values *)
kwadfout=0;
foutelaag=0;

For [i=1,i<=nomeas,i++, (* i is meetreeksnummer *)
(* parabolische fit *)
pf[x_] = Fit[(punten[[i]]),{1,x,x^2},x];
kappap = D[pf[x],{x,2}];
somkwadafwp = Sum[(punten[[i]][[w]][[2]] - pf[punten[[i]][[w]][[1]])^2
, {w,Length[punten[[i]]}]];

cirfitlist =
Table[{punten[[i]][[w]][[1]],punten[[i]][[w]][[2]],(punten[[i]][[w]][[1]])^2
+(punten[[i]][[w]][[2]])^2},{w,Length[punten[[i]]}]];
th[x_,y_] = Fit[cirfitlist, {1, x, y}, {x, y}];
c1 = th[0,0];
c2 = (th[1,0] - c1)/2; (* cirkel middelpunt x-coordinaat *)
c3 = (th[0,1] - c1)/2; (* cirkel middelpunt y-coordinaat *)
kappac = 1/Sqrt[c1 + c2^2 + c3^2];
If [c3<punten[[i]][[1]][[2]],
kappac=-kappac; (* negatieve kromming *)
somkwadafwc = Sum[(punten[[i]][[w]][[2]]-(1/kappac^2
(punten[[i]][[w]][[1]])^2
+ 2*(punten[[i]][[w]][[1])*c2 - c2^2)^(1/2)
+ c3))^2,{w,Length[punten[[i]]}],
(* else *)
somkwadafwc = Sum[(punten[[i]][[w]][[2]]-(-(1/kappac^2
(punten[[i]][[w]][[1]])^2
+ 2*(punten[[i]][[w]][[1])*c2 - c2^2)^(1/2)
+ c3))^2,{w,Length[punten[[i]]}]];
];
pssum=Sum[punten[[i]][[w]][[2]]^2,{w,Length[punten[[i]]}]];
psum=Sum[punten[[i]][[w]][[2]],{w,Length[punten[[i]]}]]^2;
If[somkwadafwc >= somkwadafwp, (* gebruik fit met kleinste fout *)
(* THEN *) AppendTo[klist,kappap];
AppendTo [rsv,1-somkwadafwp/(pssum-psum/Length[punten[[i]])];
kf=somkwadafwp,
(* ELSE *) AppendTo[klist,kappac];
AppendTo [rsv,1-somkwadafwp/(pssum-psum/Length[punten[[i]])];
kf=somkwadafwc;
];
If[kf>kwadfout,
kwadfout=kf;
foutelaag=i-1;
];

]; (* next i *)
{klist, {kwadfout},{foutelaag},rsv}

```



```

]; (* end Curvature *)

      (***) calculate the midplane strain ***)
EpsXNul [nomeasurements_,thickn_,strainx_,kxlist_,strainxfactor_] :=
      Module [{},
      epsnulletje=(strainx*strainxfactor) - (kxlist * 0.5 * thickn)
];      (***) end EpsXNul ***)

      (***) calculate the moments into x direction using CLT ***)
Xmoments [nomeasurements_,Bmlist_,Dmlist_,epsxnullist_,epsynullist_,kxlist_,kylist_]
:=
      Module [{},

      Table[- Bmlist[[i,1,1]] epsxnullist[[i]] -
      Bmlist[[i,1,2]] epsynullist[[i]] -
      Dmlist[[i,1,1]] (kxlist[[i]]-kxlist[[1]]) -
      Dmlist[[i,1,2]] (kylist[[i]]-kylist[[1]]),{i,nomeasurements }

];      (***) end Xmoments ***)

      (***) calculate the moments into y direction using CLT ***)
Ymoments [nomeasurements_,Bmlist_,Dmlist_,epsxnullist_,epsynullist_,kxlist_,kylist_]
:=
      Module [{},

      Table[ -Bmlist[[i,2,1]] epsxnullist[[i]] -
      Bmlist[[i,2,2]] epsynullist[[i]] -
      Dmlist[[i,2,1]] (kxlist[[i]]-kxlist[[1]]) -
      Dmlist[[i,2,2]] (kylist[[i]]-kylist[[1]]),{i,nomeasurements }

];      (***) end Ymoments ***)

Stress[nomeasurements_,thickn_,mlist_] :=
      Module[{i,j,onder,boven,fp,spx,mx,Sigma},
      (* Sigma will contain pointseries with a distance of 0.01 mm *)
Sigma={};
For [i=2,i<nomeasurements,i++,      (* grenzen anders voor polynoom fit *)
      onder=(thickn[[i+1]]+thickn[[i]])/2;
      boven=(thickn[[i]]+thickn[[i-1]])/2;
      If [i==2, boven=thickn[[1]] ];
      If [i==(nomeasurements-1),onder=thickn[[1]]/2 ];
      mx=Table[{thickn[[w]],mlist[[w]]},{w,i-1,i+1}];
      fp[z1_]=InterpolatingPolynomial[mx,z1];
      spx[z1_]= 2/z1^2*(fp[z1])-4*Integrate[fp[t]/(t^3),{t,z1,thickn[[1]]}] +
      2/z1*D[fp[z1],z1];

```

```

For [j=boven,j>onder,j=j-0.01,
    AppendTo[Sigma,{j,(spX[j])}];
    ]; (* next j *)
]; (* next i *)
Sigma
]; (*** end Stress ***)

SumStress [Sigmax_]:= (* check integral under stress = 0? *)
Module [{sumx},
sumx=0;
For [i=1,i<Length[Sigmax],i++, (* trapezium rule *)
    sumx=sumx+((Sigmax[[i+1]][[1]]-
Sigmax[[i]][[1]])*0.5*(Sigmax[[i]][[2]]+Sigmax[[i+1]][[2]]));
    ];

sumx
]; (*** end SumStress ***)

(* calculate piece of integral for constant plate thickness *)
IntegralPiece
[x_,y_,width_,left_,right_,Ar_,Br_,Dr_,h1_,h2_,h3_,h4_,h5_,h6_,h7_,h9_,h10_,h12_]:=
Module [{EP1,EP2,EP3,EP4,EP5,EP6,EP7,EP8,EP9,EP10,total},

EP1 = Integrate[ 1/2 Ar[[1,1]] h1, {x, left, right}, {y, -width/2, width/2}];
EP2 = Integrate[ 1/2 Ar[[2,2]] h4, {x, left, right}, {y, -width/2, width/2}];
EP3 = Integrate[ Ar[[1,2]] h10, {x, left, right}, {y, -width/2, width/2}];
EP4 = Integrate[ 2 Ar[[3,3]] h7, {x, left, right}, {y, -width/2, width/2}];
EP5 = Integrate[ 1/2 Br[[1,1]] h2, {x, left, right}, {y, -width/2, width/2}];
EP6 = Integrate[ 1/2 Br[[2,2]] h5, {x, left, right}, {y, -width/2, width/2}];
EP7 = Integrate[ 1/2 Dr[[1,1]] h3, {x, left, right}, {y, -width/2, width/2}];
EP8 = Integrate[ 1/2 Dr[[2,2]] h6, {x, left, right}, {y, -width/2, width/2}];
EP9 = Integrate[ Dr[[1,2]] h12, {x, left, right}, {y, -width/2, width/2}];
EP10 = Integrate[ 2 Dr[[3,3]] h9, {x, left, right}, {y, -width/2, width/2}];
total=EP1+EP2+EP3+EP4+EP5+EP6+EP7+EP8+EP9+EP10;
total

]; (*** end IntegralPiece ***)

(* write one and two dimensional data to disc *)
Write2Data [filen_,tbw_]:=
Module [{fn,i,j,values,h},
fn=OpenWrite [filen];
For [i=1,i<=Length [tbw],i++,
    If [AtomQ[tbw[[i]]],
        values=ToString [tbw[[i]]],
        values="";
        For [j=1,j<=Length[tbw[[i]]],j++,

```

```

                                h=tbw[[i]][[j]];
                                If [Sqrt[h*h]<0.00001, h=0];
                                values=values <> ToString [h]<>" ";
                                ];                                (* next j *)
                                ];                                (* If *)
                                WriteString [filen,values<>"\n"];
                                ];                                (* next i *)
                                Close [fn];
];                                (***) end Write2Data (***)

                                (***) filters the moments points to obtain stresses (***)
Filter[data_,windowwidth_,degree_]:=
Module[{powerlist,windowpoints,Ntot,j,k,m,jstart,x,ww},
  Ntot=Length[data];
  powerlist=Table[x^k,{k,0,degree}];
  If[windowwidth>Ntot, ww=Ntot, ww=windowwidth ];
  If[ EvenQ[ww], ww=ww-1];
  m=Quotient[ww,2];
  Transpose[
  Table[
    jstart=Which[j<=m, m+1,
                j>Ntot-m,Ntot-m,
                True, j];
    windowpoints=Take[data,{jstart-m,jstart+m}];
    yjFit=Fit[windowpoints,powerlist,x];
    yjfil=yjFit /. x->data[[j,1]];
    d1yj =D[yjFit,{x,1}] /. x->data[[j,1]];
    d2yj =D[yjFit,{x,2}] /. x->data[[j,1]];
    {yjfil,d1yj,d2yj},
    {j,1,Ntot}
  ]
];                                (***) end filter (***)

End [];
Protect [Inlezen,ModulusInterpolation,ABDMatrices,
          Curvatures,EpsXNul,IntegralPiece,Write2Data,Filter];

EndPackage [];

```

Listing of the calculation for the three point bending test

(***) BENDING.MA file to calculate the material stiffness in different layers, based upon the three point bending test results.

```

*** University of Twente, 1996    ***
*** by Rik Voerman              ***
*****

```

Stiffness calculations of three point bending test

Input of data

```

(***) plate dimensions (***)
thickn={ 1.895,1.815,1.725,1.51,1.325,1.225,1.12,1.03}; (* thickness of every layer *)
width=9.65; (* width of the plate [mm] *)
platelength=59.55; (* length of the support span [mm] *)
G12=3050; (* shear modulus [MPa] *)

ldzwick1={}; (* series initialisation *)
ldzwick2={};
ldzwick3={};
nomeasurements=Length[thickn];

(***) input of load-displacement files; three for every thickness (***)
eerste=48;
tweede=48;
For [layer=0,layer<nomeasurements+3,layer++,
  If [layer!=0 && layer !=4 && layer!=6,
    coorfile = OpenRead["c:\\users\\rik\\specimens\\s221\\b221"<>
      FromCharacterCode[eerste] <>FromCharacterCode[tweede]
    <>"m1.dat"];
    Skip[coorfile,Record,6];
    cp = ReadList[coorfile, {Word,Number,Number,Number}];
    Close[coorfile];
    AppendTo [ldzwick1,Table[{cp[[i,3]],cp[[i,2]]},{i,Length[cp]-5}]];

    coorfile = OpenRead["c:\\users\\rik\\specimens\\s221\\b221"<>
      FromCharacterCode[eerste] <>FromCharacterCode[tweede]
    <>"m2.dat"];
    Skip[coorfile,Record,6];
    cp = ReadList[coorfile, {Word,Number,Number,Number}];
    Close[coorfile];
    AppendTo [ldzwick2,Table[{cp[[i,3]],cp[[i,2]]},{i,Length[cp]-5}]];

    coorfile = OpenRead["c:\\users\\rik\\specimens\\s221\\b221"<>
      FromCharacterCode[eerste] <>FromCharacterCode[tweede]
    <>"m3.dat"];
    Skip[coorfile,Record,6];
    cp = ReadList[coorfile, {Word,Number,Number,Number}];
    Close[coorfile];
    AppendTo [ldzwick3,Table[{cp[[i,3]],cp[[i,2]]},{i,Length[cp]-5}]];

  ];
  tweede++;
  If [tweede==58, tweede=48;eerste++];
];
(* next layer *)

(* fit all the load-deflection series with a straight line *)
zwickseries={};
```

```

For [layer = 1, layer <= nomeasurements, layer ++,
    fp[x_] = Fit[lidzwick1[[layer]], {1, x}, x];
    zw1 = D[fp[x], x];
    fp[x_] = Fit[lidzwick2[[layer]], {1, x}, x];
    zw2 = D[fp[x], x];
    fp[x_] = Fit[lidzwick3[[layer]], {1, x}, x];
    zw3 = D[fp[x], x];
    AppendTo [zwickseries, {thickn[[layer]], -
((platelength^3)*(zw1+zw2+zw3)/3)/48}];
]; (* next layer *)

```

Calculation of moduli

```

d11 = {}; (* calculation of d11 for every thickness, with shear correction *)
For [layer = 1, layer <= nomeasurements, layer ++,
    shearterm = 24 / ((platelength^2) * width * thickn[[layer]] * G12);
    AppendTo [d11, width * (1 / zwickseries[[layer]][[2]] - shearterm)];
]; (* next layer *)

```

(* estimation values for the transverse direction *)

```

E1est = 14000;
E2est = 9000;
<<LRsub`

```

(* lp are going to contain the retrieved modulus in layer p *)

```

Clear [l0, l1, l2, l3, l4, l5, l6, l7, l8, l9];
xmodulusz = {l0, l1, l2, l3, l4, l5, l6, l7, l8, l9};
ymodulusz = {E2est, E2est, E2est, E2est, E2est, E2est, E2est, E2est, E2est, E2est};
nu12 = {0.418, 0.418, 0.418, 0.418, 0.418, 0.418, 0.418, 0.418, 0.418, 0.418};
(* calculate the stiffness matrices for every layer *)
ABDset = ABDMatrices[nomeasurements, thickn, xmodulusz, ymodulusz, nu12, G12];
Amlist = ABDset[[1]];
Bmlist = ABDset[[2]];
Dmlist = ABDset[[3]];

```

d11list = {}; (* calculate d11 elements for every layer *)

```

For [layer = 1, layer <= nomeasurements, layer ++,
    A = Amlist[[layer]];
    B = Bmlist[[layer]];
    P = Dmlist[[layer]]; (* d11 is element 4,4 of inverse ABD matrix *)

    hulp = -(A[[2,2]] B[[1,2]]^2) + 2 A[[1,2]] B[[1,2]] B[[2,2]] - A[[1,1]] B[[2,2]]^2 -
A[[1,2]]^2 P[[2,2]]
    + A[[1,1]] A[[2,2]] P[[2,2]]) / (B[[1,2]]^4 - 2 B[[1,1]] B[[1,2]]^2 B[[2,2]] +
B[[1,1]]^2 B[[2,2]]^2
    - A[[2,2]] B[[1,2]]^2 P[[1,1]] + 2 A[[1,2]] B[[1,2]] B[[2,2]] P[[1,1]] - A[[1,1]]
B[[2,2]]^2 P[[1,1]]
    + 2 A[[2,2]] B[[1,1]] B[[1,2]] P[[1,2]] - 2 A[[1,2]] B[[1,2]]^2 P[[1,2]] - 2 A[[1,2]]
B[[1,1]] B[[2,2]] P[[1,2]]

```

```

+ 2 A[[1,1]] B[[1,2]] B[[2,2]] P[[1,2]] + A[[1,2]]^2 P[[1,2]]^2 - A[[1,1]] A[[2,2]]
P[[1,2]]^2
- A[[2,2]] B[[1,1]]^2 P[[2,2]] + 2 A[[1,2]] B[[1,1]] B[[1,2]] P[[2,2]] - A[[1,1]]
B[[1,2]]^2 P[[2,2]]
- A[[1,2]]^2 P[[1,1]] P[[2,2]] + A[[1,1]] A[[2,2]] P[[1,1]] P[[2,2]]);

```

```

AppendTo [d11list,hulp];
]; (* next layer*)

```

```

(* initialize layer values *)
l0=l1=l2=l3=l4=l5=E1est;
l6=l7=l8=l9=l10=E2est;

```

```

(* pass loop several times to optimize the layer values *)
For [counter=1,counter<10,counter++,
(* calculate the modulus of every layer, assuming the other ones at
the initialized values after this the new value has become the
guess value; findroot cannot solve for all equations together *)
For [i=1,i<=nomeasurements,i++,
layer=nomeasurements-i+1;
If [layer==1,
Clear [l0];
f=d11list[[layer]]-d11[[layer]];
r = FindRoot[{f==0},{l0,E1est},
AccuracyGoal -> 6, MaxIterations ->1250];
l0=l0/.r;
];
If [layer==2,
Clear [l1];
f=d11list[[layer]]-d11[[layer]];
r = FindRoot[{f==0},{l1,E1est},
AccuracyGoal -> 6, MaxIterations ->1250];
l1=l1/.r;
];
If [layer==3,
Clear [l2];
f=d11list[[layer]]-d11[[layer]];
r = FindRoot[{f==0},{l2,E1est},
AccuracyGoal -> 6, MaxIterations ->1250];
l2=l2/.r;
];
If [layer==4,
Clear [l3];
f=d11list[[layer]]-d11[[layer]];
r = FindRoot[{f==0},{l3,E1est},
AccuracyGoal -> 6, MaxIterations ->1250];
l3=l3/.r;
];
If [layer==5,
Clear [l4];

```

```

f=d11list[[layer]]-d11[[layer]];
r = FindRoot[{f==0},{14,E1est},
AccuracyGoal -> 6, MaxIterations ->1250];
l4=l4/.r;
];
If [layer==6,
Clear [15];
f=d11list[[layer]]-d11[[layer]];
r = FindRoot[{f==0},{15,E1est},
AccuracyGoal -> 6, MaxIterations ->1250];
l5=l5/.r;
];
If [layer==7,
Clear [16];
f=d11list[[layer]]-d11[[layer]];
r = FindRoot[{f==0},{16,E1est},
AccuracyGoal -> 6, MaxIterations ->1250];
l6=l6/.r;
];
If [layer==8,
Clear [17];
f=d11list[[layer]]-d11[[layer]];
r = FindRoot[{f==0},{17,E1est},
AccuracyGoal -> 6, MaxIterations ->1250];
l7=l7/.r;
];
If [layer==9,
Clear [18];
f=d11list[[layer]]-d11[[layer]];
r = FindRoot[{f==0},{18,E1est},
AccuracyGoal -> 6, MaxIterations ->1250];
l8=l8/.r;
];
If [layer==10,
Clear [19];
f=d11list[[layer]]-d11[[layer]];
r = FindRoot[{f==0},{19,E1est},
AccuracyGoal -> 4, MaxIterations ->1250];
l9=l9/.r;
];

]; (* next i*)

(*Print ["Kwadfout: ",Sum[(d11list[[t]]-d11[[t]])^2,{t,1,9}]]; *)

]; (* next counter *)

```

Graphs

```

AppendTo[thickn,thickn[[1]]/2];
f3 = ListPlot[zwickseries, DisplayFunction -> Identity,PlotJoined->True];
solv={ };
AppendTo [solv,10];
AppendTo [solv,11];
AppendTo [solv,12];
AppendTo [solv,13];
AppendTo [solv,14];
AppendTo [solv,15];
AppendTo [solv,16];
AppendTo [solv,17];
AppendTo [solv,18];
AppendTo [solv,19];
f4 = ListPlot[Table [ {(thickn[[i]]+thickn[[i+1]])/2,solv[[i]]},{i,nomeasurements}],
DisplayFunction -> Identity,PlotJoined->True];

Show[f3,Frame -> True,
      FrameLabel -> {"thickness [mm]","stiffness [N.mm^2]"},
      DefaultFont -> {"Arial",10},
      PlotLabel -> "depth dependant stiffness",
      DisplayFunction -> $DisplayFunction];
Show[f4,Frame -> True,
      FrameLabel -> {"thickness [mm]","modulus"},
      DefaultFont -> {"Arial",10},
      PlotLabel -> "depth dependant modulus",
      DisplayFunction -> $DisplayFunction];

Print ["Specimen 2/21"];
Print ["Retrieved modulus array: "];
solv
-

```

Listing of the calculation for the layer removal experiment

(*** LR.MA file to calculate the residual moments based upon the surface scans of the layer removal experiment.

```

*** University of Twente, 1996      ***
*** by Rik Voerman                ***
*****

```

Layer Removal analysis Glass Filled PPS, specimen 2-18

```

(* program initialisation *)
Off [General::spell1];
Off [General::spell];
Off [Integrate::gener];
Off [SetDelayed::write];
AppendTo [$Path,"u:\\rik\\math\\"]; (* pathname of the packages *)

```


Input of data

```

                (**** xyz measurement data *)
bestand="u:\\rik\\specimens\\s218\\s218";          (* pathname plus specimen name *)
                (* filename structure: SSSSLXX (Specimen name, Layer number,
X1/x2/x3/y1/y2/y3 *)

                (**** thickness after each layer removal, starting at total thickness, mm *)
thickn={ 1.92,1.825,1.78,1.725,1.655,1.595,1.545,1.475,1.43,1.345,1.3,1.245,1.17,1.125,1
.06,0.995};
                (**** display values of strains in x and y direction *)
strainy = {0,-0.7,-1.19,-1.58,-2.06,-2.65,-3.21,-3.9,-4.64,-5.36,-5.89,-6.49,-6.89,-7.17,-
7.16,-6.69};          (* mV *)
strainx = {0,0.48,0.47,0.7,0.96,1.24,1.58,1.95,2.21,2.45,2.68,2.8,2.83,2.83,2.70,2.68};
                (**** plate dimensions ****)
width = 30.5;
L = 80.2;
rrb = 2.5;
lrb = 2.4;
deltax = 7.1;          (* distance of y-gauge from middle of specimen in
mm*)
deltay = 0;          (* distance of x-gauge from middle of specimen in
mm*)

paintthickn=0.015;          (* correction for coating thickness *)
thickn=thickn-paintthickn;
strainxfactor = 0.000233645; (* = display*0.01*0.1/(kfactor*calibrationvalue) to get
strains *)
strainyfactor = 0.000233645;
                (**** Get material properties for this specimen
****)
<<Materia2`
dummy=Specimen2 [thickn[[1]]];
xmodulus=dummy[[1]];
ymodulus=dummy[[2]];
zval=dummy[[3]];
nu12=dummy[[4]];
G12=dummy[[5]];

nomeasurements=Length[thickn]; (* check length of arrays as a cross- check *)
If [(Length[strainx]) != nomeasurements,
    Print ["Aantal x rekken klopt niet!!"];];
If [(Length[strainy]) != nomeasurements,
    Print ["Aantal y rekken klopt niet!!"];];
If [Length[xmodulus] != Length[zval] || Length[ymodulus] != Length[zval],
    Print ["modulusgegevens kloppen niet!!"];];
<<LRsub`          (* open package with modules *)
                (* read in surface scans, edge effects are eliminated
*)
```

```

xreeks1=Inlezen [nomeasurements,thickn,bestand,"x1"];
xreeks3=Inlezen [nomeasurements,thickn,bestand,"x3"];
yreeks=Inlezen [nomeasurements,t=hickn,bestand,"y1"];
(* interpolate material stiffness for every layer *)
xmodulusz = ModulusInterpolation[nomeasurements,thickn,zval,xmodulus];
ymodulusz = ModulusInterpolation[nomeasurements,thickn,zval,ymodulus];
nu12z = ModulusInterpolation[nomeasurements,thickn,zval,nu12];
(* calculate ABD matrices for every plate thickness *)
ABDset=ABDMatrices[nomeasurements,thickn,xmodulusz,ymodulusz,nu12z,G12];
Amlist=ABDset[[1]];
Bmlist=ABDset[[2]];
Dmlist=ABDset[[3]];
(* get curvatures in x-direction *)
dummy1=Curvatures [nomeasurements,xreeks1];
dummy3=Curvatures [nomeasurements,xreeks3];
kxlist=(dummy1[[1]]+dummy3[[1]])/2; (* average of left and right curvatures *)
kxlist=kxlist-kxlist[[1]]; (* subtract initial curvature *)
kwadfoutx=dummy1[[2]][[1]];
foutelaagx=dummy1[[3]][[1]];
(* get curvatures in y-direction *)
dummy=Curvatures [nomeasurements,yreeks];
kylist=dummy[[1]];
kylist=kylist-kylist[[1]]; (* subtract initial curvature *)
kwadfouty=dummy[[2]][[1]];
foutelaagy=dummy[[3]][[1]];
(* write curvature and root square error data *)
curvinfo=Table[{thickn[[i]],dummy1[[1,i]],dummy1[[4,i]],dummy3[[1,i]],dummy3[[4,i]],
dummy[[1,i]],dummy[[4,i]]},{i,nomeasurements}];
Write2Data [bestand <> "curv",curvinfo];
(* calculate midplane strains *)
epsxnullist = EpsXNul [nomeasurements,thickn,strainx,kxlist,strainxfactor];
epsynullist = EpsYNul [nomeasurements,thickn,strainy,kylist,strainyfactor];
a1list = epsxnullist - a3*deltay^2;
b1list = epsynullist - b3*deltax^2; (* write midplane strains *)
strinfo=Table[{thickn[[i]],epsxnullist[[i]],epsynullist[[i]]},{i,nomeasurements}];
Write2Data [bestand <> "str",strinfo];

```

Minimisation of potential energy

```

(* displacement and strain equations *)
u = x (a1 - a^2/6 x^2 + a3 y^2);
v = y (b1 - b^2/6 y^2 + b3 x^2);
w = 1/2 a x^2 + 1/2 b y^2;
e1 = D[u, x] + 1/2 (D[w, x])^2 + z D[w, {x, 2}];
e2 = D[v, y] + 1/2 (D[w, y])^2 + z D[w, {y, 2}];
e12 = 1/2 (D[u, y] + D[v, x] + D[w, x] D[w, y] + 2 z D[w, x, y]);
(* calculate parts of the equations symbolically *)

```

```

(*e1 x e1*)
h1 = (D[u, x] + 1/2 (D[w, x])^2)^2;
h2 = 2 ((D[u, x] + 1/2 (D[w, x])^2) (D[w, {x, 2}]));
h3 = (D[w, {x, 2}])^2;
(*e2 x e2*)
h4 = (D[v, y] + 1/2 (D[w, y])^2)^2;
h5 = 2 ((D[v, y] + 1/2 (D[w, y])^2) (D[w, {y, 2}]));
h6 = (D[w, {y, 2}])^2;
(*e12 x e12*)
h7 = (1/2 (D[u, y] + D[v, x] + D[w, x] D[w, y]))^2;
(* h8 = - (D[u, y] + D[v, x] + D[w, x] D[w, y]) (D[w, x, y]); *)
h9 = (D[w, x, y])^2;
(*e1 x e2*)
h10 = (D[u, x] + 1/2 (D[w, x])^2) (D[v, y] + 1/2 (D[w, y])^2);
(* h11 = - (D[u, x] + 1/2 (D[w, x])^2) (D[w, {y, 2}]) -(D[v, y] + 1/2 (D[w, y])^2) (D[w,
{x, 2}]); *)
h12 = ((D[w, {x, 2}]) (D[w, {y, 2}]));

```

```

Ar=Amlist[[1]]; (* A,B and D matrices of edges *)
Br=Bmlist[[1]];
Dr=Dmlist[[1]];

```

```

(* integral parts of edges *)
Ipiece = IntegralPiece [x,y,width,-(L/2)+lrb,-
(L/2),Ar,Br,Dr,h1,h2,h3,h4,h5,h6,h7,h9,h10,h12];
rpiece = IntegralPiece [x,y,width, (L/2)-rrb,
(L/2),Ar,Br,Dr,h1,h2,h3,h4,h5,h6,h7,h9,h10,h12];

```

```

(*e1*)
h13 = D[u, x] + 1/2 (D[w, x])^2;
h14 = (*-*) D[w, {x, 2}];
(*e2*)
h15 = D[v, y] + 1/2 (D[w, y])^2;
h16 = (*-*) D[w, {y, 2}];

```

```

mxlist={}; mylist={}; nxlist={}; nylist={}; (* initialize arrays to be calculated *)
shearx={}; sheary={}; estrainx={}; estrainy={};
Mt1i = -0.002; (* estimation values to start with*)
Mt2i = 0.002;
Nt1i = Nt2i = -0.002;
a3i = b3i = -1 10^-8;

```

```

For [n=1,n<=nomeasurements,n++,
Clear [a,b];
Clear [a1,b1];
Clear [a3,b3];
Ar=Amlist[[n]]; (* A,B and D matrices of milled plate, layer
n *)
Br=Bmlist[[n]];
Dr=Dmlist[[n]];

```

```

Mt = {Mt1,Mt2,0};          (* unknown moments and forces *)
Nt = {Nt1,Nt2,0};

EP11 = Integrate[- Nt[[1]] h13 - Nt[[2]] h15, {x, -L/2, L/2}, {y, -width/2,
width/2}];
EP12 = Integrate[- Mt[[1]] h14 - Mt[[2]] h16, {x, -L/2, L/2}, {y, -width/2,
width/2}];
mid = IntegralPiece [x,y,width,-(L/2)+lrb,(L/2)-
lrb,Ar,Br,Dr,h1,h2,h3,h4,h5,h6,h7,h9,h10,h12];
EP = Simplify [(lpiece + mid + rpiece + EP11 + EP12)/(L*width)];
(* non-linear algebraic equations for minimising potential energy *)
f1 = Simplify[D[EP,a]];
f2 = Simplify[D[EP,b]];
f3 = Simplify[D[EP,a1]];
f4 = Simplify[D[EP,b1]];
f5 = Simplify[D[EP,a3]];
f6 = Simplify[D[EP,b3]];

a = kxlist[[n]];          (* use measured curvatures and strains *)
b = kylist[[n]];
a1 = a1list[[n]];
b1 = b1list[[n]];

(* Newton-Raphson procedure to solve the problem *)
r = FindRoot[{f1==0,f2==0,f3==0,f4==0,f5==0,f6==0},
{Mt1, Mt1i},{Mt2, Mt2i},{Nt1, Nt1i},{Nt2, Nt2i},{a3, a3i},{b3, b3i},
AccuracyGoal -> 6, MaxIterations ->2000];

Mt1i=Mt1/.r; Mt2i=Mt2/.r; Nt1i=Nt1/.r; Nt2i=Nt2/.r; a3i=a3/.r; b3i=b3/.r;

AppendTo [shearx, a3i];   (* found shear strains *)
AppendTo [sheary, b3i];
a3=a3i;
b3=b3i;
AppendTo [estrainx ,a1list[[n]]]; (* found strains *)
AppendTo [estrainy ,b1list[[n]]];
AppendTo [mxlist, Mt1i];  (* found moments *)
AppendTo [mylist, Mt2i];
AppendTo [nxlist, Nt1i]; (* found in plane forces *)
AppendTo [nylist, Nt2i];

Print [Mt1i];
]; (* next n *)

Polynomial fit of the moment data and calculation of stresses

mxfit[th_]=Fit
[{{thickn[[w]],mxlist[[w]]},{w,nomeasurements}},{1,th,th^2,th^3,th^4},th];
myfit[th_]=Fit
[{{thickn[[w]],mylist[[w]]},{w,nomeasurements}},{1,th,th^2,th^3,th^4},th];

```

[Table

[Table

```

sxfit[th_]=(2/th)*D[mxfit[th],th]+2*mxfit[th]/(th^2)-
4*Integrate[mxfit[t]/(t^3),{t,th,thickn[[1]]}];
syfit[th_]=(2/th)*D[myfit[th],th]+2*myfit[th]/(th^2)-
4*Integrate[myfit[t]/(t^3),{t,th,thickn[[1]]}];

```

```

sumx=2*SumStress[Sigmax]/thickn[[1]];
sumy=2*SumStress[Sigmay]/thickn[[1]];
Filter fit of the moment data and calculation of stresses

```

```

<<NumericalMath`ListIntegrate`
nomeasurements=Length[thickn]-1;
thickness = Table[thickn[[i]]-0.5thickn[[1]],{i,nomeasurements}];
poldegree = 3; (* polynomial degree generally 2 or 3 *)
filterwindow = 7;
z0=thickness[[1]]; (* original upper surface *)
(* filter fit *)
mxnlist=Table[{thickness[[i]],mxlist[[i]]},{i,nomeasurements}];
filfitresultx = Filter[mxnlist,filterwindow,poldegree];
mynlist=Table[{thickness[[i]],mylist[[i]]},{i,nomeasurements}];
filfitresulty = Filter[mynlist,filterwindow,poldegree];

(* treatment of data for x direction *)
fmxdata = filfitresultx[[1]];
dfmxdata = filfitresultx[[2]];
d2fmxdata = filfitresultx[[3]];
fmxlist = Table[{thickness[[i]],fmxdata[[i]]},{i,nomeasurements}];
fmxintgrlist=Table[{thickness[[i]],fmxdata[[i]]/(thickness[[1]]+thickness[[i]])^3},{i,nomeasurements}];
(* Treuting and Reed moment - sigma calculation *)
sigmaxlist=Simplify[Table[If[i==1,intgral=0,If[i<3,intgral=ListIntegrate[Take[fmxintgrlist,i],1],
intgral=ListIntegrate[Take[fmxintgrlist,i],2]]];
{thickness[[i]],(2/(z0+thickness[[i]])^2 fmxdata[[i]] - 4 intgral +
2/(z0+thickness[[i]]) dfmxdata[[i]])},{i,nomeasurements}]];

ne=-ListIntegrate[sigmaxlist]
+(sigmaxlist[[nomeasurements,1]]*sigmaxlist[[nomeasurements,2]]);
Print["Non-equilibrium in x direction is: ",ne];
(* output calculations to disc *)
dd=Table
[{thickness[[i]]/thickness[[1]],fmxlist[[i,2]],sigmaxlist[[i,2]]},{i,nomeasurements}];
AppendTo [dd,ne];
Write2Data [bestand<>"fx"<>FromCharacterCode[poldegree+48]<>FromCharacterCode
[filterwindow+48]<> ".dat",dd];
Non-equilibrium in x direction is: 0.00257414

(* treatment of data for y direction *)
fmydata = filfitresulty[[1]];
dfmydata = filfitresulty[[2]];
d2fmydata = filfitresulty[[3]];

```

```

fmylist = Table[{thickness[[i]],fmydata[[i]]},{i,nomeasurements}];
fmyintgrlist=Table[{thickness[[i]],fmydata[[i]]/(thickness[[1]]+thickness[[i]]^3},{i,nomeasurements}];

(* Treuting and Reed moment - sigma calculation *)
sigmaylist = Simplify[
Table[If[i==1,intgral=0,If[i<3,intgral=ListIntegrate[Take[fmyintgrlist,i],1],
intgral=ListIntegrate[Take[fmyintgrlist,i],2]]];
{thickness[[i]],(2/(z0+thickness[[i]])^2 fmydata[[i]] - 4 intgral +
2/(z0+thickness[[i]]) dfmydata[[i]])},{i,nomeasurements}]];

ne=-ListIntegrate[sigmaylist]
+(sigmaylist[[nomeasurements,1]]*sigmaylist[[nomeasurements,2]]);
Print["Non-equilibrium in y direction is: ",ne];

(* output calculations to disc *)
dd=Table
[{{thickness[[i]]/thickness[[1]],fmylist[[i,2]],sigmaylist[[i,2]]},{i,nomeasurements}];
AppendTo [dd,ne];
Write2Data [bestand<>"fy"<>FromCharacterCode[poldegree+48]<>FromCharacterCode
[filterwindow+48]<> ".dat",dd]

```